

https://dspace.org/

Evaluating PLGA Encapsulated Recombinant LRP as a Treatment for Cardiovascular Disease

Gqeba, Sichumiso Zimi

2024-09

University of the Witwatersrand, Johannesburg

https://hdl.handle.net/10539/47647

Gqeba, Sichumiso Zimi. (2024). Evaluating PLGA Encapsulated Recombinant LRP as a Treatment for Cardiovascular Disease. [Master's dissertation, University of the Witwatersrand, Johannesburg]. WIReDSpace. https://hdl.handle.net/10539/47647

Downloaded from a DSpace repository. https://dspace.org/



Evaluating PLGA Encapsulated Recombinant LRP as a Treatment for Cardiovascular Disease

by

Sichumiso Zimi Gqeba

(1843413)

Dissertation

Submitted in fulfilment of the requirements for the degree

Master of science

in

Molecular and Cell Biology

in the Faculty of Science, University of the Witwatersrand, Johannesburg, South Africa

Supervisor: Dr Eloise van der Merwe

Co-supervisor: Dr Tyrone C. Otgaar

September 2024

Declaration

I, Sichumiso Gqeba (1843413), declare that this dissertation is my own work, unaided work. It is being submitted for the degree of Master of Science at the University of the Witwatersrand, Johannesburg. It has not been submitted before for any degree or examination at any other university.



30th day of September 2024 at Johannesburg

Abstract

Cardiovascular diseases are a classification of heart disorders that affect the heart and/or blood vessels with an estimated 523 million prevalent cases and 18.56 million deaths worldwide. In South Africa, CVD is the leading cause of death and accounts for 17.3% of yearly deaths. A frequent cause of most cardiovascular diseases is atherosclerosis, a disease characterized by chronic inflammation and the accumulation of fats and cholesterol that lead to plaque formation. When the plaques rupture, this leads to life threatening coronary syndromes. The most prescribed therapeutic intervention for atherosclerosis is statins. However, mortality rates are still high, nationally, and globally. Therefore, we could benefit from investigating other potential therapeutic biomolecules such as the 37/67 kDa laminin receptor precursor/laminin receptor (LRP/LR). LRP/LR is a multi-localized and multi-functional receptor that has also been shown to mediate cardioprotective effects in atherosclerosis. Hence, this study focused on investigating LRP/LR delivery into cells as a potential treatment for atherosclerosis. Firstly, recombinant LRP was overexpressed, purified, and characterized. The LRP protein was successfully overexpressed using *E. coli* and purified using affinity chromatography. The secondary structure and folding of the protein were characterized using circular dichroism and intrinsic tryptophan fluorescence spectroscopy, respectively. The protein was confirmed to be predominantly α-helical and correctly folded. Thereafter, functional characterization of the protein was performed indicating that the purified protein was active. The second aim of this project was to encapsulate the protein into PLGA nanoparticles to develop an *in vitro* delivery system. Characterization of the nanoparticles was performed using scanning electron microscopy and dynamic light scattering which showed that the nanoparticles have spherical morphology with a narrow size distribution of 221 nm, respectively. The release profile of LRP from the nanoparticles showed sustained release. Therefore, the successful encapsulation and release of LRP indicated that the therapeutic was successfully developed and it could be assessed as a possible treatment for CVD. The atherosclerotic cell culture model was successfully produced using 25 nM and 100 µg/ml of oxidized LDL. Effective doses of PLGA encapsulated LRP were determined on U937 cells and atherosclerotic cell models using an MTT assay and 75 µg/ml of encapsulated LRP was shown to exhibit therapeutic effects on the cells possibly through reverse cholesterol transport which led to regression of foam cells.

In loving memory of

My grandmother, Mapaseka Caroline Gqeba

1946 - 2023

My mother, Nosicelo Gqeba

1975 - 2024

Do not be anxious about anything, but in every situation, by prayer and petition, with thanksgiving, present your requests to God – Philippians 4:16

Acknowledgements

I would like to express my sincerest gratitude to;

My supervisor, Dr Eloise van der Merwe. I would like to thank you for the support and guidance that you have provided over the years. The advice and knowledge have been an invaluable contribution to my project. Thank you for providing me with the opportunity to work in your lab and creating a great and friendly environment to work in.

My co-supervisor, Dr Tyrone Otgaar. Thank you for checking in and offering a helping hand and advice to help with my research project. I appreciate the support you have provided during my academic journey. It means the world to me.

Professor S. F. T. Weiss (*in memoriam* - 2023), for the lab and his wonderful protein.

My colleagues and friends at the Cell Biology and Signalling Research Lab. Thank you for laughs, advice, and heartfelt conversations.

Dr Martin Bernert. For your invaluable knowledge and help.

Members of the PSFRU. Thank you for all the advice and assistance you provided with the protein biochemistry part of my research.

To my people; family and friends. Thank you for the encouragement, support, and love.

Financial aid:

National Research Foundation (NRF) – Postgraduate Scholarship (2022-2023)

Technology Innovation Agency (TIA) Seed Fund (2022-2023)

Research outputs

14th Cross-Faculty Postgraduate Symposium

Oral Presentation

Title: Evaluating PLGA encapsulated recombinant LRP as a treatment for cardiovascular disease

Sichumiso Gqeba, Dr Eloise van der Merwe and Dr Tyrone Otgaar

University of the Witwatersrand, Johannesburg, South Africa

6 – 8 September 2023

Molecular Biosciences Research Thrust Symposium 2023

Poster Presentation

Title: Evaluating PLGA encapsulated recombinant LRP as a treatment for cardiovascular disease

Sichumiso Gqeba, Dr Eloise van der Merwe and Dr Tyrone Otgaar

University of the Witwatersrand, Johannesburg, South Africa

7 December 2023

Bernert M., Bignoux M.J., Madhav C., **Gqeba S.,** Otgaar T. C., Morris G., Weiss S.F.T., Ferreira E. PLGA nanocapsules as a delivery system for a recombinant LRP-based therapeutic. FEBS Open Bio, 14(7): 1072-1086.

Table of contents

Declaration 2

Abstract 3

Dedication 4

Acknowledgements 5

Research outputs 6

Table of contents 7

List of abbreviations 10

List of figures 13

List of symbols 14

1. Introduction 16

1.1 Cardiovascular disease epidemiology 16

1.2 Atherosclerosis pathophysiology and molecular mechanisms 17

1.2.1 Atherosclerosis pathogenesis 18

1.2.2 Statins 21

1.3 37 kDa laminin receptor precursor/ 67 kDa laminin receptor 22

1.3.1 LRP structure and function 23

1.3.2 LRP/LR in pathological processes 25

1.3.3 Role of LRP/LR in aging 26

1.3.4 Role of LRP/LR in atherosclerosis 27

1.4 Poly (lactic-co-glycolic) acid nanoparticles as a delivery system 27

2. Rationale 30

3. Aims and Objectives 32

3.1 Aims 32

3.2 Objectives 32

1. Overexpress, purify, and characterize human LRP. 32

2. Encapsulate LRP and characterize encapsulated protein. 32

3. Evaluate PLGA nanoparticle encapsulated recombinant LRP as a treatment for cardiovascular disease. 32

4. Methods and Materials 34

4.1 Expression and purification of LRP 34
4.1.1 Constructed plasmid 34
4.1.2 Transformation 35
4.1.3 Protein expression 36
4.1.4 Sodium dodecyl sulphate–polyacrylamide gel electrophoresis 37
4.1.5 Protein solubilization and extraction 38
4.1.6 Immobilized metal-ion affinity chromatography 38
4.1.7 Western blotting 39
4.1.8 Protein characterization 40
4.2 Encapsulation of LRP and characterization of the encapsulated protein 44
4.2.1 PLGA nanoparticle synthesis and recombinant LRP encapsulation. 44
4.2.2 PLGA nanoparticle encapsulated LRP characterisation 45
4.3 Cell culture and PMA-induced differentiation 47
4.4 Oxidized LDL treatment and lipid (Oil Red O) staining 48
4.5 3-(4, 5-Dimethylthiazol-2-yl)-2, 5-Diphenyltetrazolium Bromide (MTT) assay to assess cell viability after encapsulated LRP treatment 48
4.6 Statistical analysis 49
5. Results 50
5.1 37 kDa LRP overexpression, purification, and characterization 50
5.1.1 Plasmid sequencing 50
5.1.2 Protein overexpression trials 51
5.1.3 Solubilization of LRP using Triton X-100 detergent 53
5.1.4 Protein purification using immobilized metal-ion affinity chromatography 55
5.1.5 Western blotting 59
5.1.6 Protein purity and concentration assessment using absorbance spectroscopy 59
5.6.1 Structural characterization of LRP 61
5.1.7 Functional characterization of LRP 63
5.2 Encapsulation of LRP into PLGA nanoparticles and characterization of the nanoparticles 64
5.2.1 Morphology and size distribution of the nanoparticles 64
5.2.2 Release profile of LRP from nanoparticles 66
5.3 Assessing encapsulated LRP as a treatment for cardiovascular disease 68

5.3.1 Cell culture models 68
5.3.2 Atherosclerotic cell culture model 69
5.3.3 Cell viability after encapsulated LRP treatment 70
6. Discussion 73
6.1 37 kDa LRP overexpression, purification, and characterization 73
6.1.1 Expression and purification of LRP 73
6.1.2 Protein purity and concentration 76
6.1.3 Structural characterization of LRP 77
6.1.4 Functional characterization of LRP 78
6.2 Encapsulation of LRP into PLGA nanoparticles and characterization of the nanoparticles 79
6.2.1 Scanning electron microscopy and dynamic light scattering 79
6.2.2 Release profile of LRP from nanoparticles 81
6.3 Assessing encapsulated LRP as treatment for cardiovascular disease 82
6.3.1 Cell culture models 82
6.3.2 Cell viability after encapsulated LRP treatment 83
7. Conclusion 85
7.1 Future studies 86
7.2 Study limitations 87
8. References 88
9. Appendices 99
Appendix 1: Reagents and materials 99
Appendix 2: Calculations 99
Appendix 3: Additional data 100

List of abbreviations

AB_{42}	Amyloid beta 42
ABC	ATP-binding cassette
APS	Ammonium persulphate
AU	Absorbance unit
AuPd	Gold palladium
BMI	Body mass index
BRCA1	Breast cancer gene 1
BSA	Bovine serum albumin
CD	Circular dichroism
cDNA	Complementary DNA
CME	Clathrin-mediated endocytosis
Co^{2+}	Cobalt ion
Cu^{2+}	Copper ion
$CuSO_4$	Copper sulphate
CVD	Cardiovascular disease
dH_2O	Distilled water
DLS	Dynamic light scattering
DMSO	Dimethyl sulfoxide
DNA	Deoxyribonucleic acid
ECM	Extracellular matrix
EDTA	Ethylenediaminetetraacetic acid
EGCG	Epigallocatechin-3-gallate
FBS	Fetal bovine serum
HIV/AIDS	Human immunodeficiency virus/ acquired immunodeficiency syndrome
HMG-CoA	3-hydroxy-3-methylglutaryl coenzyme A
HMGCR	HMG-CoA reductase
HSPG	Heparan sulphate proteoglycan

IgG1-Is18	anti-LRP/LR specific antibody
IHD	Ischemic heart disease
IL-1β	Interleukine-1β
IL-6	Interleukin-6
IMAC	Immobilized metal-ion affinity chromatography
IPTG	Isopropyl β-D-1-thiogalactopyranoside
ITF	Intrinsic tryptophan fluorescence
Kbp	Kilo base pairs
KCl	Potassium chloride
KDa	Kilo Dalton
KH_2PO_4	Potassium phosphate monobasic
LB-agar	Luria-Bertani agar
LDL	Low density lipoprotein
LRP/LR	37kDa/67 kDa laminin receptor precursor/ laminin receptor
LXR	Liver X protein
MCP-1	Monocyte chemo-attractant protein-1
$MgCl_2$	Magnesium chloride
miRNA	Micro RNA
MMP	Matrix metalloproteinase
mRNA	Messenger RNA
MTT	3-(4, 5-Dimethylthiazol-2-yl)-2, 5-Diphenyltetrazolium Bromide
MVA	Mevalonate
M0	Naïve
NaCl	Sodium chloride
Na_2HPO_4	Sodium phosphate dibasic
NaN_3	Sodium azide
NF-κB	Nuclear factor kappa B
Ni^{2+}	Nickel ion
OD	Optical density
PBS	Phosphate buffered saline

PBST	PBS Tween
PCA	Protocatechuic acid
PDGF	Platelet-derived growth factor
PdI	Polydispersity index
PEG	Polyethylene glycol
PKC	Protein Kinase C
PLGA	Poly-lactic-co-glycolic acid
PMA	Phorbol-12-myristate-13-acetate
PMSF	Phenylmethylsulphonyl fluoride
PrP^{C}	Cellular prion proteins
PVDF	Polyvinylidene difluoride
R_f	Relative migration distance
RhoA/ROCK	RhoA/Rho-associated protein kinase
RIPA	Radioimmunoprecipitation assay
RNA	Ribonucleic acid
RNAi	RNA interference
RPMI	Roswell Park Memorial Institute
rRNA	Ribosomal RNA
SDS-PAGE	Sodium dodecyl sulphate–polyacrylamide gel electrophoresis
SEC	Size exclusion chromatography
SEM	Scanning electron microscopy
siRNA	Small interfering RNA
SOC	Super Optimal broth with Catabolite repression
SR-B1	Scavenger receptor class B type 1
SUMO	Small ubiquitin-like modifier
TEMED	Tetramethyl ethylenediamine
TERT	Telomerase reverse transcriptase
TNF-α	Tumour necrosis factor α
TPGS	D- α- Tocopherol polyethylene glycol succinate
Tris-HCl	Tris(hydroxymethyl)aminomethane

UV-Vis	Ultraviolet-visible
U937	Human myeloid leukaemia cell line
VCAM-1	Vascular cell adhesion molecule 1
VSMC	Vascular smooth muscle cell
Zn^{2+}	Zinc ion
γH2AX	Phosphorylated H2AX

List of figures

Figure 1: Number of deaths caused by different diseases in 2019.

Figure 2: Atherosclerosis pathogenesis from lesion initiation to thrombosis.

Figure 3: The mevalonate pathway and statin inhibition.

Figure 4: The partial theoretical ribbon secondary structure of LRP/LR (amino acid residues 1-220).

Figure 5: Schematic presentation of PLGA nanoparticle surface charge and coating.

Figure 6: Protein sequence alignment of query and reference sequencing.

Figure 7: Overexpression trials of human LRP at different IPTG concentrations and time intervals.

Figure 8: Linear regression model constructed from the standards of known molecular weight.

Figure 9: Supernatant fractions of scale-up solubilization of insoluble LRP fractions using Triton X-100.

Figure 10: Purification of LRP using nickel immobilized metal-ion affinity chromatography.

Figure 11: Purification of LRP using cobalt immobilized metal-ion affinity chromatography.

Figure 12: Confirmation of LRP protein in elution fractions from cobalt IMAC using western blotting.

Figure 13: Absorbance spectrum of LRP.

Figure 14: Circular dichroism spectra of LRP to determine secondary structure of the protein.

Figure 15: Intrinsic tryptophan fluorescence spectra of LRP in the absence and presence of 8M urea denaturant used to determine tertiary structure.

Figure 16: Functional assay to determine the binding affinity of purified LRP for laminin-1.

Figure 17: Scanning electron microscope image of PLGA nanoparticles with encapsulated recombinant LRP.

Figure 18: Polydispersity index of PLGA encapsulated LRP and empty PLGA nanoparticles.

Figure 19: Release profile of encapsulated LRP nanoparticles at a concentration of 100 µg/ml.

Figure 20: Microscopy image showing the morphology of human myeloid leukaemia cell line (U937) and M0 macrophages under an inverted light microscope (40x).

Figure 21: Inverted light microscopy (100x) image of foam cells stained using Oil Red O staining at 100 µg/ml oxidized LDL concentration.

Figure 22: Cell viability of U937 cells and foam cells of LRP encapsulated nanoparticles (75 µg/ml, 100 µg/ml, and 150 µg/ml) and empty nanoparticles.

List of symbols

AU	Absorbance units
α	Alpha
β	Beta
c	centi
°C	Degree Celsius
g	Gram
≤	Greater/Lesser or equal to
k	Kilo
l	Litre
µ	Micro
m	Milli

M	Molar
n	Nano
rpm	Resolution per minute
%	Percentage
π	Pi
±	Plus-minus
xg	Times gravity
V	Volt
v/v	Volume/volume
w/v	Weight/volume

1. Introduction

1.1 Cardiovascular disease epidemiology

Cardiovascular diseases (CVDs) are a group of heart disorders that affect the heart and/or blood vessels with an estimated 523 million prevalent cases worldwide. In 2019, CVD-related deaths were 18.56 million therefore accounting for 32% of deaths globally (Ritchie and Rosie, 2019; World Health Organization, 2020). Furthermore, CVD was the leading cause of death, and its mortality rate was almost double that of cancer, one of the world's leading causes of death (Figure 1). About 80% of these CVD-related deaths occur in low to medium income countries due to inaccessibility to health care services and programs for early detection and secondary disease prevention (World Heart Federation, 2017). Mortality rates associated with CVD negatively affect economies because patients die in their most productive years leading to the loss of people that contribute to the growth of the economy. Moreover, governments allocate a large budget to deal with the cardiovascular disease burden due to its morbidity and mortality. In 2010 alone, worldwide CVD costs were estimated at 863 million US dollars and these costs are expected to exceed 1 trillion US dollars by the year 2030 (Wang *et al.*, 2015). These statistics highlight the need for alternative therapies to treat cardiovascular diseases.

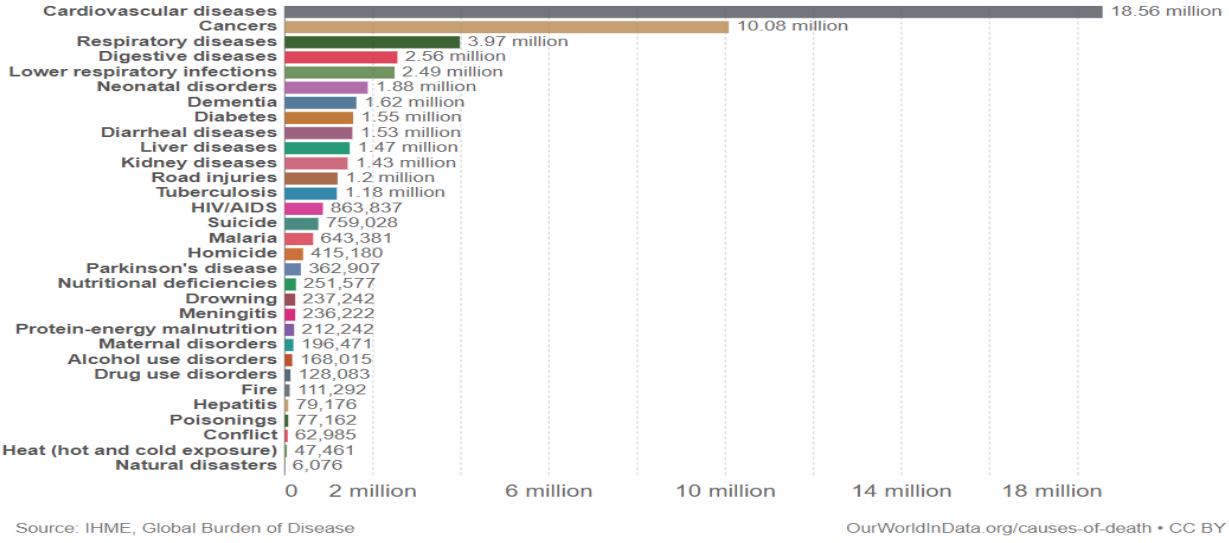

Figure 1: Number of deaths caused by different diseases in 2019. This figure shows the number of deaths that occurred globally in 2019 caused by different diseases. Cardiovascular diseases were the leading cause of death accounting for 18.56 million deaths, almost doubling cancer cases. Adopted from (Ritchie and Roser, 2019).

Furthermore, CVD has an increasing prevalence in sub-Saharan Africa and it is one of the leading causes of death in the South African population being responsible for 17.3% of deaths (Jardim *et al.*, 2017). The disease is especially inadequately managed in rural areas of South Africa which further contributes to the prevalence and mortality rates (Jardim *et al.*, 2017). However, different strategies and treatments have been implemented to mitigate cardiovascular diseases and associated risk factors.

In South Africa, broad-based prevention strategies were introduced by the government to manage the growing prevalence of the disease. In 2013, a legislation was signed by the Minister of Health to reduce sodium in the food industry as a primary prevention for cardiovascular diseases. Furthermore, in 2016 the government introduced a tax on sugar-sweetened drinks to combat risk factors associated with cardiovascular diseases (World Heart Federation, 2017). These in addition to physical activity and quitting smoking are heart-healthy lifestyle changes recommended to manage cardiovascular diseases. Current therapies that are recommended and prescribed for cardiovascular conditions include statins for ischemic heart diseases (IHD) and atherosclerosis, aspirin, and isosorbide dinitrate for myocardial infarctions, amlodipine for hypertension and amoxicillin for rheumatic fever (Department of health, 2018). Furthermore, other therapeutic interventions focus on the prevention of risk factors which include: hypertension, high body mass index (BMI), hyperglycaemia, and hypercholesterolemia which are a major causes of death but most importantly they are responsible for the underlying causes of most cardiovascular diseases (Keates *et al.*, 2017). Regardless of these treatments and preventative interventions cardiovascular diseases still account for the highest mortality rate globally. Therefore, we need to develop alternative therapies that contribute to the management of this disease.

1.1 Atherosclerosis pathophysiology and molecular mechanisms

Cardiovascular diseases affect the cardiac muscle and vascular system. Moreover, they are associated with damages to the arteries that supply vital organs such as the heart, kidneys, and the brain (Gaziano *et al.*, 2006). Different pathophysiological and molecular mechanisms are associated with CVD pathogenesis, however, many risk factors are shared amongst the different types of cardiovascular diseases. The four main types of CVDs are: ischemic heart disease also known as coronary artery disease, stroke, peripheral arterial disease, and aortic disease (NHS Inform, 2020). The most prevalent CVD type is IHD which affects 126 million individuals

globally and atherosclerosis is the primary pathological mechanism that leads to IHD (Khan *et al.*, 2020). In addition, atherosclerosis is also the most frequent underlying cause of peripheral arterial disease and stroke (Falk, 2006; Markin *et al.*, 2020). Atherosclerosis can also lead to other complications such as disabilities from strokes and death thus it is imperative to understand the molecular mechanism of atherogenesis to improve treatment interventions and decrease prevalence of atherosclerosis-linked diseases.

Atherosclerosis is a disease characterized by chronic inflammation and an accumulation of cholesterol and fats accompanied by smooth muscle cell proliferation and fibrous matrix protein agglomeration inside the walls of the arteries (Zhu *et al.*, 2018; Khan *et al.*, 2020). The build-up develops into an atherosclerotic plaque which causes arterial stenosis therefore the supply of oxygen-rich blood to vital organs is reduced as the disease progresses (Markin *et al.*, 2020). If the atherosclerotic plaque ruptures, platelet aggregation and thrombosis causes occlusion of arteries which leads to life threatening cardiovascular diseases (Falk, 2006; Zhu *et al.*, 2018). Atherogenic etiologic factors include: age, hyperlipidaemia, endothelial dysfunction associated with hypertension, smoking, diabetes mellitus and hemodynamic damage (Zhu *et al.*, 2018). These factors initiate and promote inflammation, which plays an important role in atherogenesis (Zhu *et al.*, 2018). Hyperlipidaemia and diabetes contribute to dysregulating cholesterol levels. This occurs through the increase of blood concentration of low-density lipoprotein (LDL) cholesterol and the decrease of high-density lipoprotein (HDL) cholesterol blood concentration to lead to the cardiovascular disease phenotype by blocking and narrowing the arteries.

1.1.1 Atherosclerosis pathogenesis

Reduction of HDL concentration and increased LDLs is the initial pathophysiological stimulus required for oxidative stress-mediated atherosclerosis. Additionally, etiologic factors such as hypertension and hemodynamic damage will induce endothelial cell modifications that cause leaky junctions causing LDLs to enter the intima (Dabagh *et al.*, 2009). The LDLs are deposited into the sub-endothelial layer (intima) and undergo lipid peroxidation modifications to form oxidized LDL (Singh *et al.*, 2002). This is an important step in lesion initiation (Figure 2) and causes endothelial activation which is important for atherogenesis (Steinl and Kaufmann, 2015). Thereafter, endothelial cells are stimulated by oxidized LDLs to increase expression of adhesion molecules (E-selectin, P-selectin, vascular cell adhesion molecule-1 (VCAM-1)) and

intercellular adhesion molecule-1 on their surfaces through the activation of nuclear factor kappa B (NF-κB) transcription factor (Douglas and Channon, 2014; Steinl and Kaufmann, 2015). Aside from stimulating adhesion molecule expression, NF- κB regulates inflammatory responses and its function in atherosclerosis is to mediate the induction of pro-inflammatory cytokines (Liu *et al.*, 2017). In order to express inflammatory cytokines, NF- κB mediates expression using monocytes recruited from the lumen by VCAM-1 expression (Crowther, 2005). Furthermore, the expression of VCAM-1 also results in recruitment of T-cells that accumulate in the sub-endothelial space (Crowther, 2005). Additionally, monocytes in the sub-endothelial space release monocyte chemo-attractant protein 1 (MCP-1) chemokines to accelerate inflammation by attracting more monocytes that secrete inflammatory cytokines and cause the proliferation of vascular smooth muscle cells (VSMCs) (Crowther, 2005). The local inflammatory environment activates the accumulated monocytes to differentiate into macrophages (Steinl and Kaufmann, 2015).

This is followed by the earliest visible lesion of atherosclerosis in the intima, the intimal xanthomas also known as the fatty streak (Figure 2) (Basatemur *et al.*, 2019). Atherogenic macrophages bind and scavenge residual oxidized LDL using scavenger receptors to further activate the endothelium, recruit leukocytes by secreting interleukin-1β (IL-1β), tumour necrosis factor α (TNF-α), and IL-6 cytokines as well as secrete platelet-derived growth factor (PDGF) (Singh *et al.*, 2002; Douglas and Channon, 2014). Continual oxidized LDL endocytosis by macrophages and monocyte recruitment leads to foam cell (lipid-laden macrophages) formation and intimal thickening, respectively (Steinl and Kaufmann, 2015). This accelerates plaque progression and potentiates the inflammatory response leading to the formation of fatty streaks (Douglas and Channon, 2014).

Cytokines and PDGF from macrophages contribute significantly to VSMC recruitment to the site of lesion. In response to the inflammatory cascade, VSMCs will migrate from the medial layer to the intima to synthesize and secrete extracellular matrix (ECM) proteins (collagen and elastin) (Douglas and Channon, 2014), and cytokines (Bennett *et al.*, 2016) which contributes to narrowing of the lumen via atherogenesis progression (Douglas and Channon, 2014). Furthermore, VSMCs stabilize the atherosclerotic plaque by forming an atheromatous fibrous cap (Figure 2) in the subendothelial space to reduce circumferential stress and prevent contact

between the blood and necrotic core (Singh *et al.*, 2002; Martos-Rodríguez *et al.*, 2021). As the atherosclerotic plaque increases during atherogenesis, when the intima becomes thicker than 500 µm this can cause hypoxia, due to inadequate supply of oxygenated blood, in the local tissues which results in neovascularization that further develops the lesion (Moreno *et al.*, 2006). The neovascularization micro-vessels become leaky, fragile and express VCAM-1 thus neovascularization is used to characterize high-risk plaques (Falk, 2006). Furthermore, as a hallmark of matured atheroma, excess accumulation of oxidized LDLs in lipid-laden foam cells leads to excessive accumulation of cholesterol resulting in the deposition of cholesterol crystals (Varsano *et al.*, 2018). The last step of atherosclerosis, thrombosis, is promoted by secretion of platelet adhesion protein von Willebrand factor (vWF) and tissue factor (a primary cellular initiator of blood coagulation) by the endothelium (Mackman, 2004; Crowther, 2005). Tissue factor and vWF recruit and deposit fibrin and platelets on the endothelium by the lumen causing erosion of endothelium thus creating a pro-thrombotic environment (Steinl and Kaufmann, 2015).

For the most part, atherosclerotic plaques are mostly stable, quiescent, and asymptomatic provided that the fibrous cap and endothelium are not impaired (Douglas and Channon, 2014). In the plaque, when foam cells undergo cell death, apoptosis and necrosis, they release lipids, lipid crystals and cell-debris forming a lipid (necrotic) core (Steinl and Kaufmann, 2015). Extrinsic and intrinsic signals trigger apoptosis of foam cells, intracellular signals that trigger apoptosis include: prolonged endoplasmic reticulum stress, deoxyribonucleic acid (DNA) damage and oxidative damage (Brophy *et al.*, 2017). Moreover, foam cells also release matrix metalloproteinases (MMPs) alongside the endothelial cells (Singh *et al.*, 2002) and smooth muscle cells (Laxton *et al.*, 2009). MMP-2 and MMP-9 degrade the endothelial cell membrane and ECM collagen in the fibrous cap thus mechanically weakening the cap (Douglas and Channon, 2014; Zhu *et al.*, 2018). As a result, the large necrotic core, thin fibrous cap and shear stress on endothelial cells predisposes the atherosclerotic plaque to rupture (Falk *et al.*, 1995). When the plaque ruptures or erodes, the thrombogenic core comes into contact with flowing blood in the lumen resulting in platelet aggregation to mediate thrombosis (Figure 1d) (Falk *et al.*, 1995; Douglas and Channon, 2014). Fatal thrombosis results in thrombotic occlusions causing acute coronary syndrome which is life-threatening (Douglas and Channon, 2014).

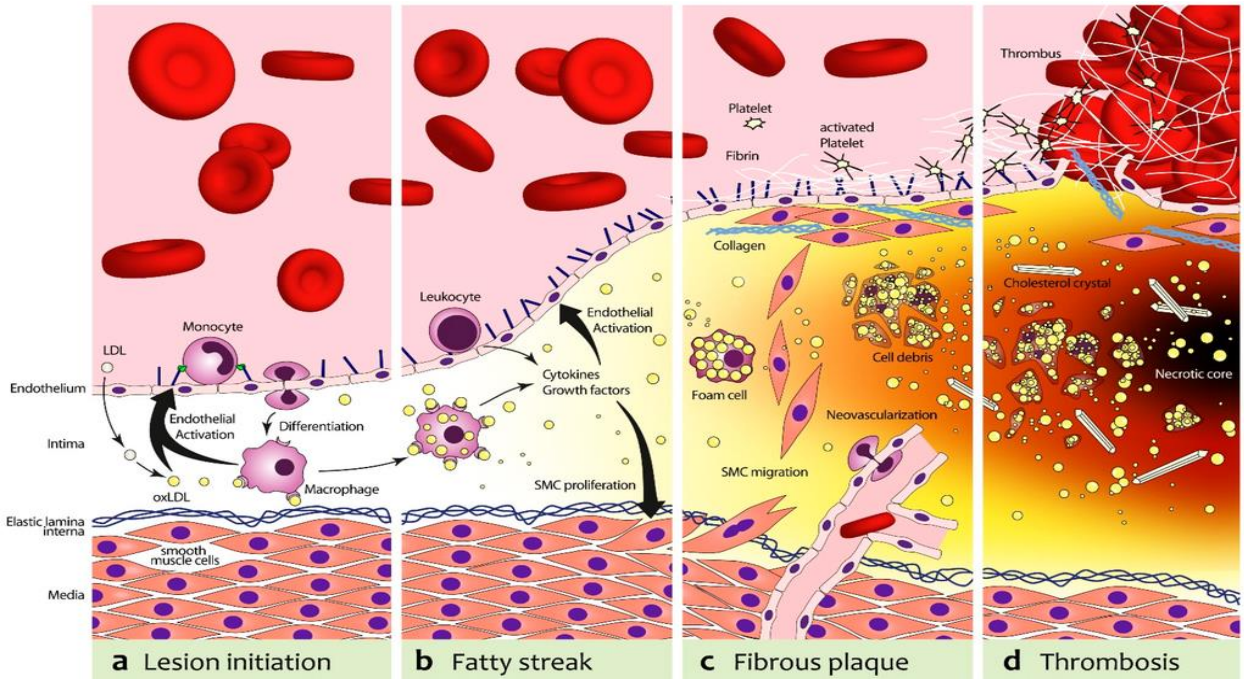

Figure 2: Atherosclerosis pathogenesis from lesion initiation to thrombosis. The schematic diagram shows atherogenesis from (a) lesion initiation where a pathophysiologic stimulus such as increased LDL cholesterol concentration and endothelial activation result in macrophages and inflammatory responses. A (b) fatty streak is formed from foam cells as the plaque gradually progresses. Thereafter, a (c) fibrous plaque is formed from VSMCs and ECM proteins to stabilize the plaque. However, (d) thrombosis occurs when the fibrous cap weakens and the plaque ruptures causing the necrotic core to encounter flowing blood. This causes arterial occlusions that lead to life threatening cardiovascular diseases. Adopted from (Steinl and Kaufmann, 2015).

1.1.2 Statins

Statins are the most prescribed drugs for regulating dyslipidaemia to reduce the risks of mortality and morbidity associated with cardiovascular diseases. Statins, also known as 3-hydroxy-3-methylglutaryl coenzyme A (HMG-CoA) reductase inhibitors, inhibit the cholesterol producing pathway also known as the mevalonate (MVA) pathway by inhibiting the lactone ring and side chains of HMG-CoA reductase (HMGCR) (Almeida and Budoff, 2019; Fracassi *et al.*, 2019). HMGCR is the rate-limiting enzyme therefore statin inhibition prevents the conversion of HMG-CoA to MVA and in turn cholesterol production.

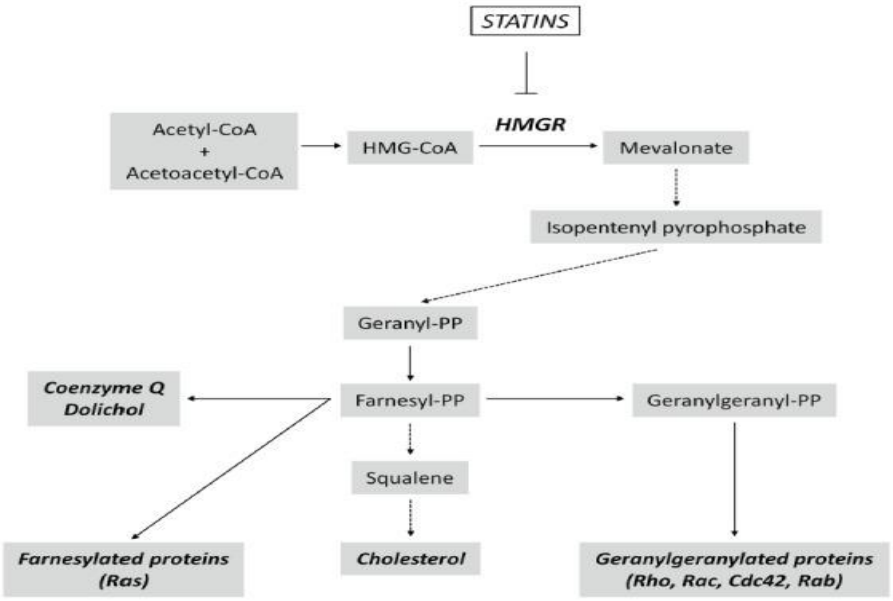

Figure 3: The mevalonate pathway and statin inhibition. The mevalonate pathway is the main pathway responsible for cholesterol production. Therefore, statins act by inhibiting the rate-limiting enzyme, HMGCR, to lower cholesterol in cardiovascular diseases. Adopted from (Fracassi *et al.*, 2019).

The MVA pathway is responsible mainly for producing cholesterol. However, Figure 3 shows that it is also responsible for producing other physiologically important metabolites, such as geranylnyl pyrophosphate and farnesyl pyrophosphate, necessary for normal cell metabolism, growth, and survival (Longo *et al.*, 2021). Hence statin therapy can have adverse pharmacological effects on the patients (Fracassi *et al.*, 2019). The risks associated with statin therapy include intracranial haemorrhage, hepatotoxicity and myopathy and new onset diabetes in patients (Horodinschi *et al.*, 2019; Zhao *et al.*, 2019). In addition to these negative effects, cardiovascular diseases are still the worlds' leading cause of death. Therefore, we could benefit from investigating other biomolecules such as the 37 kDa laminin receptor precursor / 67 kDa laminin receptor (LRP/LR) that plays a role in cardiovascular disease pathophysiology as a potential therapeutic intervention (DiGiacomo and Meruelo, 2016).

1.2 37 kDa laminin receptor precursor/ 67 kDa laminin receptor

LRP/LR, also known as p40, laminin receptor 1 and ribosomal protein SA, is a non-integrin transmembrane glycoprotein receptor. The protein is located in the cytosol, nucleus and primarily on the surface of cells (Khumalo *et al.*, 2013). Due to this, LRP/LR is a multi-

functional protein, and it interacts with ECM proteins, but its primary ligand is laminin-1. Laminin receptor and laminin-1 interactions, amongst other functions, are used to mediate adhesion, cell growth, differentiation, and migration (Omar *et al.*, 2012). However, LRP/LR is also involved in several pathological processes including cancer progression, aging, binding and internalizing amyloid beta-42 ($A\beta_{42}$) peptide, bacteria, prion proteins and viruses (Gauczynski *et al.*, 2001; Omar *et al.*, 2012). Due to its multi-localization, LRP/LR has also been shown to mediate cardioprotective effects in atherosclerosis.

1.2.1 LRP structure and function

The structure and localization of LRP determine the protein's functions. In the genetic material, the LRP/LR coding region is positioned on chromosome 3, on the short p-arm (chromosome 3p22.2) (Yun *et al.*, 2011). The open reading frame of the LRP/LR gene is 888 base pairs in length and encodes for a 295 amino acid protein that is 37 kDa in molecular weight (Yun *et al.*, 2011). The receptor is assumed to arise from a 37 kDa laminin receptor precursor protein to a molecular weight of 67 kDa through post-translational modifications such as fatty acid acylation that occur on the 37 kDa laminin receptor precursor (Landowski *et al.*, 1995). Following transcription and translation, the 37 kDa protein formed is predominantly alpha helical with beta strands (**Figure 4**) (Jamieson *et al.*, 2008). The central β sheet of the protein is composed of five parallel β strands (β3-β7). Three α helices border on one side (αB, αC, and αE) and a single α helix (αD) on the other side (Jamieson *et al.*, 2008). An N-terminal α helix (αA) and two anti-parallel β strands (β1-β2) pack against the α/β core of the protein (Jamieson *et al.*, 2008). Lastly, amino acid residues 1–8 and 206–220 of laminin receptor protein are disordered in the structure (Jamieson *et al.*, 2008).

Thereafter, the protein is translocated predominantly to the membrane where it serves as a receptor composed of an N-terminal domain, a transmembrane domain, and a C-terminal domain (Figure 2). The transmembrane domain spans between residues 86-105 (Rao *et al.*, 1983). The C-terminus has two laminin-binding domains, the peptide G sequence located between 161-180 amino acid residues and a direct binding region site located between amino acid residues 205-229 (Mbazima *et al.*, 2010). These binding domains also serve as binding sites for heparan sulphate proteoglycans (HSPGs) and the cellular prion proteins (PrP^C). The third binding domain

is an epitope that is located between 272-280 amino acids, and it is recognized and bound by IgG antibodies (Jovanovic *et al.*, 2015).

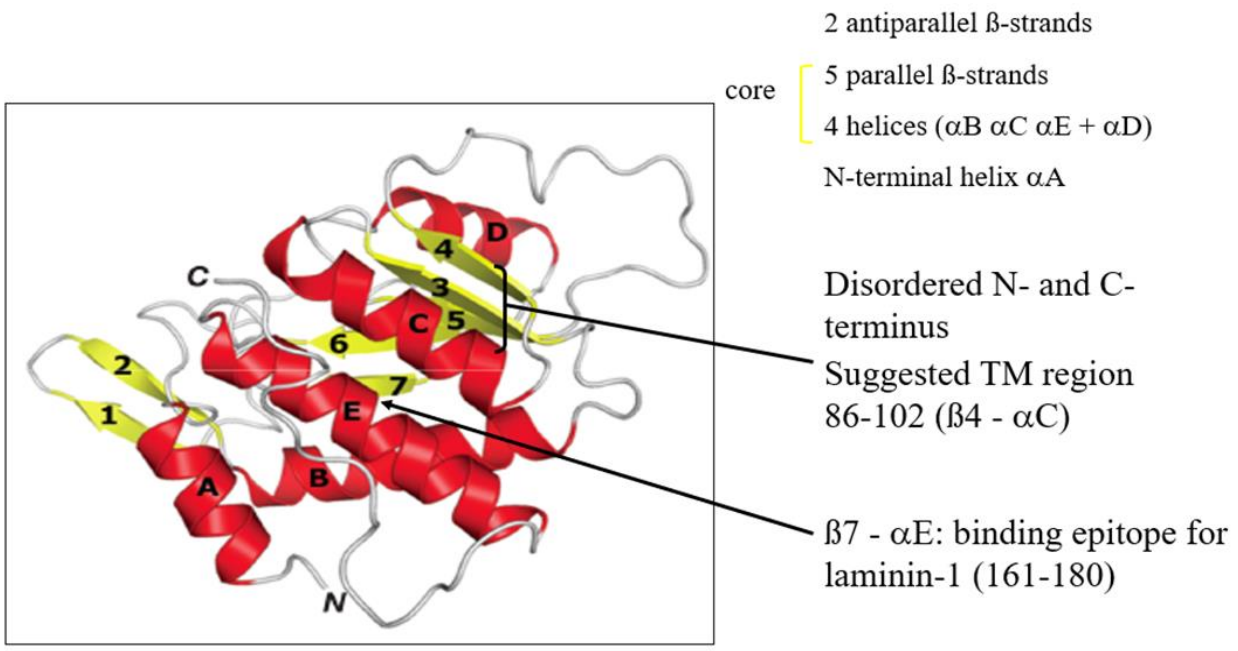

Figure 4: The partial theoretical ribbon secondary structure of LRP/LR (amino acid residues 1-220). The ribbon structure above shows LRP is predominantly α-helical with β strands and disordered regions. The central β sheet of the protein is composed of five parallel β strands (β3-β7). Three α helices border on one side (αB, αC, and αE) and a single α helix (αD) on the other side. An N-terminal α helix (αA) and two anti-parallel β strands (β1-β2) pack against the α/β core of the. Lastly, amino acid residues 1–8 and 206–220 of laminin receptor protein are disordered in the structure. The C-terminus has two laminin-binding domains, the peptide G sequence located between 161-180 amino acid residues and a direct binding region site located between amino acid residues 205-229 (not shown). Adopted from (Jamieson *et al.*, 2008).

The protein is localized in the cytosol, perinuclear component of the nucleus and predominantly on the cell surface. Thus this localization contributes towards LRP/LR's multi-functionality in biological processes (Khumalo *et al.*, 2013; Moodley and Weiss, 2013). LRP/LR localized in the nucleus plays a role in maintaining and stabilizing nuclear structures and forms a reserve of DNA damage repair proteins (Sato *et al.*, 1996). Furthermore, LRP/LR interacts with protein and nucleic acid components of the nucleosome to stabilize the chromatin (Kinoshita *et al.*, 1998). LRP/LR has also been found to isolate DNA damage repair proteins ring finger protein 8 and

breast cancer gene 1 (BRCA1) to the nucleolus to form a waiting reserve (DiGiacomo and Meruelo, 2016). Whereas the LRP/LR localized within the cytoplasm participates in protein synthesis and ribosomal biogenesis (Sato *et al.*, 1996). Here, the N-terminal domain of LRP/LR associates with the small 40S ribosomal subunit to mediate translation and the C-terminal domain stabilizes LRP/LR and ribosomal binding, by binding additional proteins or interacting with rRNA (Scheiman *et al.*, 2010; DiGiacomo and Meruelo, 2016). For LRP/LR ribosomal biogenesis function, it is involved in 21S pre-rRNA processing into the mature 18S rRNA (DiGiacomo and Meruelo, 2016). Lastly, LRP/LR located on the cell surface serves as an extracellular receptor for ECM molecules such as carbohydrates, elastin, HSPGs, and its high affinity ligand, laminin-1 (Mbazima *et al.*, 2010; Jovanovic *et al.*, 2015). LRP/LR and laminin-1 interaction mediates different biological processes including: cell adhesion, proliferation, angiogenesis, migration, and differentiation (Khumalo *et al.*, 2013). Therefore, due to the LRP/LR protein's ability to serve as a receptor for various biomolecules this has resulted in the protein playing a role in different pathological processes.

1.2.2 LRP/LR in pathological processes

Pathological agents have been shown to exploit LRP/LR to internalize into cells to promote disease progression. This is due to the protein's ability to bind various biomolecules as a surface receptor and its widespread cellular localization. LRP/LR participates in the progression of the following: cancer, aging, Alzheimer's disease (AD), prion disorders, viral and bacterial infections.

In bacterial and viral infections, bacteria and viruses use the cell surface LRP/LR receptor to internalize into the cells to enhance disease progression. Viral pathological agents that interact with LR/LR include: alphaviruses, Adeno-associated viruses (Akache *et al.*, 2006), Dengue virus (Nelson *et al.*, 2008), swine fever virus (Chen *et al.*, 2015), and Sindbis virus (Wang *et al.*, 1992). LRP/LR enhances internalization of viruses into host cells, alongside their primary receptor, to use the host cell's replication machinery to complete their viral cycles (Chen *et al.*, 2015). In bacterial infections such as bacterial meningitis, LRP/LR mediates endocytosis of *Streptococcus pneumoniae*, *Haemophilus influenzae* and *Neisseria meningitidis* through the endothelial blood brain barrier into the cerebrospinal fluid (Orihuela *et al.*, 2009). The bacteria normally crosses over the blood brain barrier using platelet-activating factor receptor (PAFr)-

mediated endocytosis; however, binding to LRP/LR enhances disease progression (Orihuela *et al.*, 2009). The bacteria rapidly multiplies in the cerebrospinal fluid and causes neuronal damage and meningitis (Orihuela *et al.*, 2009).

Furthermore, LRP/LR is also implicated in neuronal disorders, such as AD and prion disorders. In AD, it is involved in Aβ shedding from amyloid precursor protein to generate neurotoxic $A\beta_{42}$ peptide (Jovanovic *et al.*, 2015). In addition, LRP/LR acts as a receptor for $A\beta_{42}$ to mediate $A\beta_{42}$ endocytosis into the cells (Da Costa Dias *et al.*, 2014). The $A\beta_{42}$ accumulates in the cell thus resulting in $A\beta_{42}$-induced neuronal cytotoxicity in Alzheimer's disease pathogenesis therefore inducing apoptosis of neuronal cells (Da Costa Dias *et al.*, 2013). An additional neurodegenerative disease that LRP/LR has been shown to be involved in prion disorders where it acts as a receptor for PrP^{c} receptor and pathological protease resistant isoform (PrP^{Sc}) receptor to facilitate internalization of both PrP^{c} isoforms to accumulate in the cells leading to progression of prion disorders (Gauczynski *et al.*, 2001). In the cell, normal PrP^{c} is converted to pathological PrP^{Sc}) by other infectious PrP^{Sc} proteins present in the cell and starts to accumulate which eventually results in neurodegeneration and cell death (Panegyres and Armari, 2013).

1.2.3 Role of LRP/LR in aging

Multiple physiological and biological processes are involved in the process of aging including LRP/LR and an enzyme called telomerase. Telomerase catalyzes the synthesis and addition of telomeric repeats (TTAGGG) at 3' end of chromosomes to maintain genomic stability (Blagoev, 2009). Our laboratory has previously shown that LRP/LR interacts with telomerase reverse transcriptase (TERT), a protein that forms part of the catalytic core of telomerase and it is responsible for catalysing the addition of nucleotides to telomere ends (Bellot and Wang, 2013; Otgaar *et al.*, 2017). In fact, a decrease in LRP/LR induces a subsequent decrease in telomerase activity in both normal and tumorigenic cells (Naidoo *et al.*, 2015). In an aging context, the overexpression or elevation of LRP/LR induces a corresponding increase in telomerase activity to impede age-related senescence and apoptosis (Otgaar *et al.*, 2017). Moreover, aging is also associated with shortened telomere length that leads to genomic instability due to limited replicative lifespans and proliferative potential (Blagoev, 2009). When telomeres reach a critically shortened length the cell goes into senescence, a state of aging and halted cell division

before apoptosis. However, when LRP/LR is upregulated in senescing cells this increases telomerase activity to impede aging by elongating the telomeres (Otgaar *et al.*, 2017).

1.2.4 Role of LRP/LR in atherosclerosis

LRP/LR has previously been previously shown to participate in different stages of atherosclerosis. LRP/LR has been shown to mediate cardioprotective effects of epigallocatechin-3-gallate (EGCG), a polyphenol catechin found in green tea EGCG which is an anti-inflammatory, antioxidant and anti-atherogenic compound (Chyu *et al.*, 2004; Holy *et al.*, 2010). In atherosclerosis, EGCG binds LRP/LR on the surface of cells of macrophages and monocytes to mediate anti-inflammatory effects by inhibiting MCP-1 (Li *et al.*, 2017). Furthermore, LRP/LR has been shown to inhibit inflammation by inhibiting the NF- κB signalling pathway (Li *et al.*, 2017). As previously mentioned, NF- κB mediates the induction of pro-inflammatory cytokines using monocytes recruited from the lumen during atherogenesis (Liu *et al.*, 2017). Therefore, in turn the protein helps stabilize the atherosclerotic plaque thus preventing plaque rupture. The receptor also reduces endothelial cell expression of MMP-9 that degrades the fibrous cap and transcription factor that creates a pro-thrombotic environment by impairing phosphorylation of Jun N-terminal kinases involved in gene expression (Holy *et al.*, 2010). Therefore, preventing thrombosis in the arteries which leads to life-threatening cardiovascular diseases. Here, LRP/LR serves as a target receptor that the EGCG utilizes to gain access to cells and carry out its therapeutic effects.

These findings suggest that LRP/LR can be used as a potential treatment for atherosclerosis since it is involved in reducing the advancement of atherosclerosis pathogenesis through mediating cardioprotective effects. Therefore, atherosclerotic cell culture models can be treated with LRP/LR to investigate the anti-inflammatory and anti-atherogenic effect of the receptor. However, the protein needs to be encapsulated for *in vitro* delivery to improve drug delivery and half-life as naked delivery of LRP is not practical.

1.3 Poly (lactic-co-glycolic) acid nanoparticles as a delivery system

PLGA nanoparticles are synthetic copolymers of glycolic and lactic acid monomers that function as delivery systems (Fargnoli *et al.*, 2014). PLGA nanoparticles are used as delivery systems because of targeted drug delivery, biocompatibility and non-cytotoxic biodegradation in organs and cells (Tabatabaei Mirakabad *et al.*, 2014). Unlike conventional drug delivery systems, PLGA

nanoparticles improve the half-life of macromolecular therapeutics such as proteins, peptides and nucleic acid and gene silencing therapeutics such as siRNA and microRNA (miRNA) by shielding the therapeutics from chemical and enzymatic degradation (Gavrilov and Saltzman, 2012; Ding and Zhu, 2018). Due to the hydrophobic nature of PLGA nanoparticles, hydrophobic drugs are distributed on the hydrophobic outer surface and hydrophilic drugs are encapsulated in the core of the nanoparticles. At their targeted site, PLGA nanoparticles are internalized into the cells via clathrin-mediated endocytosis (CME) and fluid phase pinocytosis. CME is the major receptor-mediated endocytosis pathway in mammalian cells mainly used to internalize molecules on the cell surface and surface-bound cargo into vesicles for intracellular uptake (Danhier *et al.*, 2012). Nanoparticles less than 200 nm in size are preferentially internalized into the cells via CME (Sahin *et al.*, 2017). Fluid phase pinocytosis internalization of PLGA nanoparticles is endocytosis independent of the receptor. The cell membrane is invaginated to form endocytic vesicles that internalize drug-encapsulating nanoparticles less than 1000 nm (Sousa de Almeida *et al.*, 2011). Following internalization, the nanoparticles undergo enzymatic and/or non-enzymatic hydrolysis into lactic acid and glycolic acid to release encapsulated therapeutics (Tabatabaei Mirakabad *et al.*, 2014). Lactic acid and glycolic acid are endogenous metabolites and are metabolized through the tricarboxylic acid cycle in the body (Danhier *et al.*, 2012). Therefore, minimal cytotoxicity is associated with PLGA nanoparticle delivery.

As an FDA approved delivery system, PLGA nanoparticles have been used for prolonged administration of vaccines for an effective immune response thereby eliminating the need for boosting administrations (Danhier *et al.*, 2012). PLGA nanoparticles have also been previously used for gene delivery of siRNA and miRNA to mediate RNAi for targeted gene silencing to block metastatic properties of cancer cells (Patil *et al.*, 2010). In cardiovascular disease studies, PLGA nanoparticles have been used to deliver therapeutics for atherosclerosis treatment such as fumagillin antibiotics, PDGF receptor inhibitors and statins (Mir *et al*., 2017). Additionally, PLGA nanoparticles have been used to deliver GW3965, a liver X receptor (LXR) agonist (Chen *et al.*, 2015). LXR protein activates genes that regulate cholesterol and lipid metabolism to inhibit/regress atherogenesis (Leik *et al.*, 2007).

As previously mentioned PLGA nanoparticles are hydrophobic, this is due to the negative charge on their surface therefore resulting in lower intracellular uptake due to the negative charge also

observed on the surface of the cells (Wang *et al.*, 2013). Therefore, modifications of the surface of the nanoparticles with cationic conjugation or encapsulation with hydrophilic polymer or lipids improves intracellular uptake (Lü *et al.*, 2009; Fu and Kao, 2010). Conjugation of polyethylene glycol (PEG) polymer chains or coating of nanoparticles with adsorption enhancers, such as chitosan, increase transport of drugs by opening cellular tight junctions and improves *in vivo* blood half-life (Wang *et al.*, 2013). Therefore, the nanoparticles can be conjugated in the future to improve localised effect and tissue specificity.

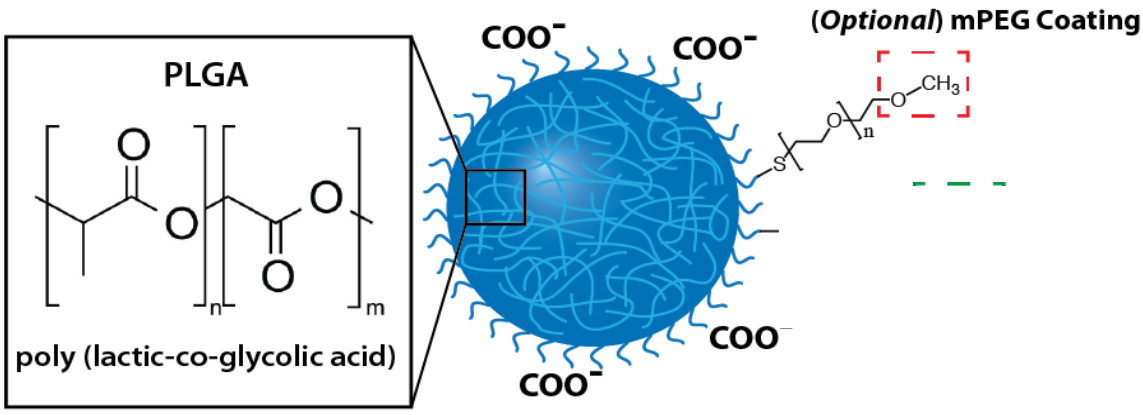

Figure 5: Schematic presentation of PLGA nanoparticle surface charge and coating. The nanoparticles are synthetic copolymers of glycolic and lactic acid monomers with a surface that contains COOH groups which are negatively charged. The negative charge surface allows for conjugation with PEG. Adapted from Luna Nanotech (Toronto, Canada).

Based on the numerous studies and applications of PLGA nanoparticles, PLGA nanoparticles will be used to deliver recombinant LRP to atherosclerotic cell models as a treatment for cardiovascular diseases. The nanoparticles have targeted drug delivery, increased half-life of drugs and non-cytotoxic biodegradation in organs and cells. Therefore, recombinant LRP delivery effects in atherosclerotic models need to be investigated since the protein could potentially function as a therapeutic drug for the treatment of cardiovascular diseases.

1. Rationale

Cardiovascular diseases are heart disorders that affect the heart and/or blood vessels with high morbidity and the world's highest mortality rate. In South Africa, cardiovascular diseases are one of the leading causes of death and account for 17.3% of yearly deaths. As a result of the increasing global economic burden of cardiovascular diseases costs are expected to exceed 1 trillion US dollars by the year 2030. A frequent cause of most cardiovascular diseases is atherosclerosis, a disease characterized by chronic inflammation and the accumulation of fats and cholesterol inside the walls of the arteries. Statins are commonly prescribed drugs for plaque regression and reduction of lipid concentration as a treatment for atherosclerosis. However, cardiovascular diseases still have the highest mortality rate. Therefore, we could benefit from investigating other biomolecules that can serve as a therapeutic intervention to help alleviate morbidity and mortality associated with atherosclerosis such as LRP/LR. LRP/LR is a multi-localized receptor that has been shown to mediate cardioprotective effects in atherosclerosis by inhibiting the acceleration of inflammation and preventing thrombosis in the arteries by stabilizing the plaque. Hence, LRP/LR delivery into cells can be investigated as a potential treatment for atherosclerosis. However, naked LRP treatment is not feasible thus a delivery system is needed. PLGA nanoparticle delivery of therapeutics for treatment of various diseases including cardiovascular diseases is commonplace in nanoparticle delivery studies. Thus, recombinant LRP can be encapsulated into the PLGA nanoparticles as an *in vitro* delivery system to improve half-life and targeted delivery of LRP.

The first aim of this study was to overexpress, purify, and characterize recombinant LRP. The protein was overexpressed using transformed T7 Express Competent *E. coli* cells and purified using cobalt immobilized metal-ion affinity chromatography. Immunological detection of the eluted fractions was performed using western blotting to confirm that the protein was LRP and to also determine its purity. Furthermore, the purity of the purified LRP was assessed using absorbance spectroscopy. The secondary structure and tertiary structure of the protein were characterized using far-UV circular dichroism and intrinsic tryptophan fluorescence, respectively. Lastly, functional characterization of the protein was performed using an affinity binding assay. The second aim of this project focused on encapsulating the protein into PLGA nanoparticles to develop an *in vitro* delivery system. Following synthesis, the morphology and

polydispersity index of the nanoparticles was assessed using scanning electron microscopy and dynamic light scattering, respectively. The release profile of the nanoparticles was performed using a leakage test to ensure that protein is released from the nanoparticles and can carry out its therapeutic functions. The last aim of this project was to assess the PLGA encapsulated recombinant LRP as a treatment for cardiovascular disease. Therefore, CVD was modelled using U937 cells which were differentiated with phorbol 12-myristate 13-acetate to form naive macrophages. The naïve macrophages were treated with 100 µg/ml of oxidized-LDL to create foam cells. Foam cell formation was confirmed using lipid (Oil Red O) staining and light microscopy. Lastly, effective doses of PLGA encapsulated LRP that rescue the cells from atherosclerosis were determined on U937 cells and atherosclerotic cell models using an MTT assay.

2. Aims and Objectives

3.1 Aim

Develop poly(lactic-co-glycolic) acid encapsulated recombinant LRP and evaluate it as a potential treatment for cardiovascular disease.

3.2 Objectives

I. Overexpress, purify, and characterize human LRP.

i. Transform T7 Express Competent *E. coli* bacterial cells with a constructed plasmid pET-11a containing the full length *LRP* gene.
ii. Heterologous expression of recombinant LRP.
iii. Solubilization of recombinant LRP using Triton X-100 detergent to up-scale protein extraction from the membrane.
iv. LRP purification using cobalt immobilized metal ion chromatography.
v. Perform western blotting analysis on elution fractions from purification for immunological detection and confirmation of recombinant LRP.
vi. Structural characterization of recombinant LRP using far-UV circular dichroism and intrinsic tryptophan fluorescence to determine secondary and tertiary structure, respectively.
vii. Functional characterization of the recombinant LRP using affinity binding assay.

II. Encapsulate LRP and characterize encapsulated protein.

i. Encapsulate the recombinant LRP into PLGA nanoparticles using double emulsification and solvent evaporation method.
ii. Characterize the PLGA encapsulated recombinant LRP using scanning electron microscopy, and dynamic light scattering to determine morphology, polydispersity index of the nanoparticles.
iii. Analyse drug release profile of the nanoparticles using a leakage test.

III. Evaluate PLGA nanoparticle encapsulated recombinant LRP as a treatment for cardiovascular disease.

i. Establish cell culture models using U937 cells and differentiate cells into naive macrophages using PMA.
ii. Treat naive macrophages with 100 µg/ml oxidized LDL to produce foam cells.

iii. Assess the effect of encapsulated LRP treatments on U937 cell and foam cell viability using an MTT assay.

3. Methods and Materials

4.1 Expression and purification of LRP

LRP/LR is a multifunctional protein, and it is localized in multiple compartments of the cell. The protein has a 37 kDa laminin receptor precursor protein and undergoes modifications to form the 67 kDa laminin receptor. This study was done using the 37 kDa laminin receptor precursor protein. Recombinant protein expression was employed for protein production in this study. Recombinant protein expression in bacteria is important in expression studies as it yields a significant quantity of the protein of interest (Andersen and Krummen, 2002). The gene of interest was inserted into a plasmid vector and the constructed plasmid was transferred into bacterial cells which were then induced to express the protein of interest. Thereafter, LRP was characterized, and functionalized before downstream experiments in this study.

4.1.1 The recombinant plasmid construct

Plasmids are circular, double-stranded DNA molecules present in bacteria and other microscopic organisms that can replicate independently from the host cell's chromosome DNA. Plasmids are a suitable vector in protein expression due to their stability, affordability, and capacity to produce substantial amounts of protein in a short period of time. The plasmid with the gene insert were purchased from GenScript, New Jersey, USA. The pET-11a plasmid (GenScript, New Jersey, USA) used in this study was 5.7 kilo base pairs (Kbp) in size and the gene of interest was 1088 bp long. The full length of the *LRP* gene sequence (1-295 bp) was inserted into the pET-11a plasmid. The insert contained a Hexahistidine-tag (His-tag), a thrombin cleavage site, and the *LRP* gene. The His-tag was used to assist in the purification of the protein using immobilized metal-ion affinity chromatography (IMAC). A thrombin cleavage site was inserted to separate the His-tag and the recombinant LRP protein to cleave the His-tag for downstream characterization of our protein; however, it was not necessary because characterization of the protein could be performed with the His-tag intact due its small size (~2.5 kDa) that prevents it from interfering with protein structure and function (Booth *et al.*, 2018).

The T7 Express Competent *Escherichia coli* (*E. coli*) cells (New England Biolabs, Massachusetts, USA) were transformed using the constructed pET-11a plasmid. *E. coli* cells were used as the expression host due to their exponential growth (Du *et al.*, 2021). The T7 lac

promoter cassette in the recombinant plasmid was composed of a T7 promoter, T7 terminator, lac operator and a ribosomal binding site. The T7 promoter was used to initiate high expression levels of the gene of interest in the presence of the T7 RNA. Thus, the T7 RNA polymerase expression system was used to produce recombinant protein because it transcribes genes eight times faster (Du *et al.*, 2021). The T7 RNA polymerase is coded for by the expression bacterial cell and its transcription is under the control of the LacUV5 promoter, which is induced by isopropyl β-d-1-thiogalactopyranoside (IPTG) thereby blocking the lac repressor protein encoded by the *lacl* gene (Du *et al.*, 2021). In the absence of IPTG, the lac repressor protein inhibits the expression of the *lac operon* gene to prevent leaky protein expression of LRP and it also inhibits the lacUV5 promoter to prevent T7 RNA polymerase transcription. Moreover, a pBR322 origin of replication is included in the plasmid to allow for a high plasmid copy while reducing leaky protein expression in the absence of an inducer. The plasmid also included an *AmpR* gene which was used for bacterial selection by providing bacterial cells with ampicillin resistance during transformation. The gene encodes for the β-lactamase enzyme which hydrolyses the β-lactam ring in ampicillin, therefore, neutralizing the effect of the antibiotics (Bush, 2018).

4.1.2 Transformation

Transformation is a process whereby bacteria can acquire new genes from free DNA such as plasmids in their environment. In this study, T7 Express Competent *E. coli* cells were transformed with the pET-11a plasmid construct using the heat shock method. Firstly, 2 µl of the plasmid was added to 50 µl of T7 competent cells and incubated on ice for 30 minutes to stabilize cellular lipid membranes. The cells were then heat shocked at 42 °C for 45 seconds to permeabilize the membrane for the uptake of the plasmid and incubated on ice for 5 minutes for recovery. Thereafter, 950 µl of prewarmed (37 °C) sterile Super Optimal broth with Catabolite repression (SOC) media (0.5% (w/v) yeast extract, 2% (w/v) tryptone, 2.5 mM potassium chloride (KCl), 10 mM magnesium chloride ($MgCl_2$), 10 mM (NaCl) and 20 mM glucose) was added to the transformed cells to further assist in cell recovery from heat shock-induced stress. The cells were then incubated in a shaking incubator (230 rpm) for 1 hour at 37 °C for cell growth.

Following transformation, successfully transformed cells were selected by spreading the grown cells onto sterile LB-agar (0.5% (w/v) yeast extract, 1% (w/v) NaCl, 1% (w/v) tryptone, and

1.5% (w/v) agar) plates supplemented with 0.1 mg/ml of ampicillin and allowed to grow overnight at 37 °C. The plates were also spread with untransformed cells, LB-agar, and SOC media as controls. Single colonies were selected from the LB-agar and used to inoculate 100 µl sterile 2x yeast extract-tryptone (YT) media (0.5% (w/v) NaCl, 1% (w/v) yeast extract, and 1.6% (w/v) tryptone) containing 0.1 mg/mL ampicillin to prevent the growth of untransformed cells and contamination. The culture was incubated for 16 hours at 37 °C in a shaking incubator at 230 rpm.

From this culture, 1m glycerol stocks were made in a 1:1 ratio using the overnight culture and 80% glycerol. The glycerol stocks were snap frozen using liquid nitrogen and they were stored for future protein expression at -80 °C. Furthermore, the GeneJet Plasmid Mini-prep Kit (Thermo Fisher Scientific, Massachusetts, USA) was used to isolate plasmids from the overnight culture. Following the protocol, the isolated plasmid was sent for sequencing at Inqaba Biotechnical Industries (Pretoria, RSA) to ensure LRP gene integrity.

4.1.3 Protein expression

Heterologous expression is a technique used to express a foreign gene or part of the gene in a host organism. In this study, LRP was overexpressed using *E. coli* cells to ensure that enough protein was produced for experiments. Stored glycerol stocks were thawed and inoculated into 2x YT media containing 0.1 mg/ml of ampicillin in a 1 in 1000 dilution. The culture was incubated overnight at 37 °C in a shaking incubator (230 rpm) to allow growth. The overnight culture was then diluted 1: 50 with sterile 2x YT media containing 0.1 mg/ml ampicillin and allowed to grow until optical density at 600 nm (OD_{600}) of 0.6 AU was reached. OD_{600} provides information about the growth of bacteria and at 0.6 AU it shows that the cells are in the exponential growth phase which is optimal for induction of expression. Thereafter, the culture was cold shocked for 30 minutes at 4 °C and protein overexpression was induced with 0.3 mM IPTG (Glentham Life Sciences, Wiltshire, UK), after conducting overexpression trials with 0.3 mM and 1.0 mM IPTG concentration. The bacterial cells were subjected to cold shock prior to induction to reduce transcriptional and translational efficiency to stabilize the protein structure of the expressed protein (Rowbury, 2005). The cells were then incubated at 20 °C for 20 hours, while shaking at 230 rpm. The temperature was reduced to prevent the formation of inclusion bodies (Mühlmann *et al.*, 2017). Following incubation, the cells were harvested by centrifugation

at 5000 xg, 4 °C for 30 minutes and resuspended in 50 ml of equilibration buffer (0.01% (w/v) sodium azide (NaN_3), 20 mM tris(hydroxymethyl)aminomethane (tris-HCl), 30 mM imidazole, 500 mM NaCl) per liter of culture. Samples were collected for SDS-PAGE and resuspended cell lysates were stored at -20 °C.

4.1.4 Sodium dodecyl sulphate–polyacrylamide gel electrophoresis

Sodium dodecyl sulphate–polyacrylamide gel electrophoresis (SDS-PAGE) is a technique used to separate proteins according to their molecular weight in response to an applied electric field (Smith, 1984). In this study, SDS-PAGE was used to determine optimal expression conditions of LRP and the size of LRP. The samples were prepared by dilution into sample reducing buffer (4% (w/v) SDS, 3.5 µg/mL bromophenol blue, 10% (v/v) β-mercaptoethanol, 20% (v/v) glycerol and 125 mM Tris-HCl) and denatured at 95 °C for 5 minutes to ensure the protein was linearized and uniformly negatively charged.

The SDS-PAGE gel prepared was composed of a 12.5% acrylamide separating gel (0.05% (w/v) ammonium per sulphate (APS), 0.1% (w/v) SDS, 0.2% (v/v) tetramethyl ethylenediamine (TEMED), 1.08% (w/v) bis-acrylamide, 12.5% (w/v) acrylamide, and 250 mM Tris-HCl) and 4% acrylamide stacking gel (0.005% (w/v) APS, 0.1% (w/v) SDS, 0.2% (v/v) TEMED, 0.36% (w/v) bis-acrylamide, 4% (w/v) acrylamide, 50 mM tris-HCl). The samples were loaded into each well at 10 µl volumes and 3µl of the PageRuler Prestained Protein Ladder (Thermo Fisher Scientific, Massachusetts, USA) was loaded into a separate well. Electrophoresis was carried out in the Mini Protean gel system (Bio-Rad, California, USA) using electrophoresis buffer (0.15% (w/v) SDS, 192 mM glycine, and 250 mM tris-HCl) at 110 V until the dye front had reached 1 cm from the bottom of the gel. Following electrophoresis, the gels were removed from the buffer tank and stained with Coomassie stain solution (0.1% (w/v) Coomassie Brilliant Blue R-250 in 1:5:4 (v/v/v) acetic acid: methanol: dH_2O) for 3 hours in a container. The gels were then destained using destain solution (1:5:4 (v/v/v) acetic acid: methanol: dH_2O) overnight. The gels were imaged using the ChemiDoc™ Imaging System (Bio-Rad, California, USA). The molecular weight of the protein was estimated by calculating the migration distance of the proteins on the gel and plotting a linear curve, where the logarithm of the known molecular weights of the standards was plotted against their relative migration distance (Rf). The Rf values were obtained by using the equation below:

$$R_f = \frac{Distance\ migration\ of\ the\ protein\ (cm)}{Distance\ migration\ of\ the\ dye\ front\ (cm)}$$

4.1.5 Protein solubilization and extraction

In the overexpression trials, it was established that LRP was mostly located in the insoluble fractions due to its localization in the transmembrane region. Therefore, the protein was solubilized using a non-ionic detergent to extract the protein by disrupting the membrane while maintaining protein stability, function, and interactions (Ratkeviciute *et al.*, 2021).

The cell lysates resuspended in an equilibration buffer were thawed in a rotator and 0.1 mg/ml lysozyme (Sigma-Aldrich, Missouri, USA) and 1 mM phenylmethylsulphonyl fluoride (PMSF) (Glentham Life Sciences, Wiltshire, UK) were added to cleave the peptidoglycan membrane and prevent proteolytic degradation of overexpressed protein, respectively. The mixture was incubated at 20 °C for 30 minutes and DNAase 1 (Merck Millipore, Darmstadt, Germany) was added to prevent DNA contamination by fragmenting the bacterial DNA. Thereafter, centrifugation was performed at 18 000 xg for 30 minutes at 4 °C. The supernatant was collected and filtered with a 0.45 µm filter to remove any insoluble matter.

The remaining pellet was resuspended in 14 ml extraction buffer (2% (w/v) Triton X-100, 8 M urea, 50 mM tris-HCl) and incubated for 30 minutes at 20 °C and 4 °C, respectively. Thereafter, the cells were disrupted using a homogenizer and the homogenous solution was centrifuged for 20 minutes, 18 000 xg at 4 °C and the supernatant was collected. The extraction protocol was repeated three times on the pellet. The collected supernatant was filtered with a 0.45 µm filter to remove any insoluble matter.

SDS-PAGE was performed on the collected samples (supernatant) following the protocol in **4.1.4** to determine washes with extracted protein and the gels were imaged ChemiDoc™ Imaging System (Bio-Rad, California, USA).

4.1.6 Immobilized metal-ion affinity chromatography

Affinity chromatography is a separation technique implemented in the purification of biomolecules based on binding affinity of a biomolecule to an immobilized ligand. In immobilized metal-ion affinity chromatography, divalent metal cations cobalt (Co^{2+}), nickel (Ni^{2+}), copper (Cu^{2+}) or zinc (Zn^{2+}) are immobilized onto a stationary phase (Sepharose) and

form covalent bonds with a fusion-tag. The overexpressed protein with His-tags binds to the metal ions in the Sepharose resin columns during IMAC to immobilize it from solution. For protein purification, Co^{2+} and Ni^{2+} metal-ion columns were used to purify LRP from the soluble lysate.

LRP was purified using a 5 ml HiTrap™ IMAC column, 1.6 x 5 cm (Cytiva Life Sciences, Washington D.C, USA) attached to the ÄKTA Prime Liquid Purification System (GE Healthcare Technologies, Illinois, USA) at a flow rate of 5 ml/minutes and pressure limit of 0.3 MPa). The columns were packed with IMAC Sepharose 6 Fast Flow resin (GE Healthcare Technologies, Illinois, USA) and charged with 0.1 M $CoCl_2$ and 0.1 M NiSO4 (Sigma-Aldrich, Missouri, USA). The columns were equilibrated with 5 column volumes of equilibration buffer (0.01% (w/v) NaN_3, 20 mM tris-HCl, 30 mM imidazole, 500 mM NaCl, pH 7.5) to ensure that the protein interacts with the ligand. Thereafter, the supernatant was loaded onto the column and flow through was collected. A salt wash buffer (0.01% (w/v) NaN_3, 20 mM tris-HCl, 50 mM imidazole, 500 mM NaCl, pH 7.5) was passed onto the column to minimize non-specifically bound proteins to the columns and collected. The column was then re-equilibrated with 5 column volumes of equilibration buffer and His-tagged LRP was displaced from the IMAC column using 5 column volumes of elution buffer (0.01% (w/v) NaN_3, 20 mM tris-HCl, 350 mM imidazole, 500 mM NaCl, pH 7.5) and collected.

SDS-PAGE was performed on the collected samples following the protocol in **4.1.4** to determine purity of the collected protein. The gel was imaged using the ChemiDoc™ Imaging System (Bio-Rad, California, USA) and purity was assessed using densitometric analysis on the ImageLab 4.0 software.

4.1.7 Western blotting

The eluted fractions from IMAC purification were resolved on the SDS-PAGE gel following the protocol in **4.1.4** and LRP was detected using western blotting.

Following electrophoresis, the proteins were transferred from the SDS-PAGE gel into polyvinylidene difluoride (PVDF) membranes (Pall corporation, New York, USA) using Trans-blot® Turbo™ Transfer system (Bio-Rad, California, USA). Filter papers were soaked in 1X Transfer buffer (100 ml 10X (30 g tris-HCl, 144 g glycine), 200 ml methanol, 700 ml dH_2O) and

PVDF membranes were soaked in methanol (Associate chemical enterprise (ACE), Southdale, RSA) to activate the membrane. Filter papers were placed on the transfer system followed by the activated membrane. The polyacrylamide gel was then placed onto the PVDF membrane to allow for the transfer of proteins and three more filter papers were placed on top. Transfer of proteins was done using the Trans-blot® Turbo™ Transfer system (Bio-Rad, California, USA) for 30 minutes at 25 V. When the transfer was completed, the membranes were blocked using blocking buffer (3% (w/v) bovine serum albumin (BSA) (VWR Life sciences, Pennsylvania, USA) in 1X Phosphate buffered saline tween (PBST) (0.1% (v/v) Tween 20, 1.8 mM sodium phosphate dibasic (Na_2HPO_4), 2.7 mM mM KCl and 10 mM potassium phosphate monobasic (KH_2PO_4), and 137 mM NaCl) with gentle shaking at room temperature for 1 hour. The membranes were blocked to prevent non-specific binding of primary and secondary antibodies. After blocking, the membranes were incubated with primary antibody Human anti-LRP/LR IgG1-iS18 1:1000 (Affimed, Heidelburg, Germany) diluted in 10 ml 3% (w/v) BSA in 1X PBST with gentle shaking at 4℃ overnight. Following incubation, the membranes were washed with 10 ml 1X PBST five times for 5 minutes each to remove unbound primary antibodies. After the washing, the membranes were incubated with secondary antibody Anti-human IgG-HRP 1:5000 (Abcam, Cambridge, UK) for 1 hour at room temperature in the dark. After incubation, the membranes were washed five times with 1X PBST for 5 minutes each and the proteins were visualized using Clarity™ Western ECL Blotting Substrate (Bio-Rad, California, USA) and the ChemiDoc™ Imaging System (Bio-Rad, California, USA).

4.1.8 Protein characterization

After protein purification, the protein was characterized using absorbance spectroscopy, circular dichroism spectroscopy, and intrinsic tryptophan fluorescence spectroscopy to determine protein purity, secondary structure, and protein folding, respectively. Functional characterization was also done on the protein using the affinity binding assay to assess its functionality after overexpression.

4.1.8.1 Absorbance spectroscopy

Ultraviolet-visible (UV-Vis) absorbance spectroscopy is an analytical technique used to quantify protein concentration, using the Beer-Lambert law, based on the light absorbed by molecules in solution at a specific wavelength. The absorbance of phenylalanine, tyrosine, and tryptophan

amino acid residues due to the aromatic ring at 280 nm (A_{280}) and the molar extinction co-efficient (67 045 $M^{-1}.cm^{-1}$) were used to determine protein concentration. Furthermore, absorbance spectroscopy was used to detect nucleic acid contamination and protein aggregation in the protein samples. Nucleic acids absorb light at 260 nm (A_{260}) due to the resonance structure of nucleic acid bases, purines, and pyrimidines. A $A_{260/280}$ ratio <0.60 is an indicator of minimal nucleic acid contamination in purified protein. The absorbance at 340 nm is an indicator of aggregation in the protein sample.

The protein was first dialyzed against a sodium phosphate buffer (20 mM sodium phosphate, 20 mM tris-HCl) for 20 hours at 4 °C. The protein was then centrifuged at 13 200 rpm for 10 minutes, 4 °C to remove aggregation. The absorbance spectrum was obtained from 240 nm to 340 nm using the Jasco V-630 spectrophotometer (Jasco Inc., Tokyo, Japan), in triplicate. The A_{280} was used to calculate the concentration of LRP using the formular below:

$$c = \frac{A_{280}}{\mathcal{E}.l}$$

c = protein concentration (M)

A_{280} = corrected absorbance at 280 nm

$\mathcal{E}$ = molar extinction coefficient (67 045 $M^{-1}.cm^{-1}$)

l = path length (cm)

4.1.8.2 Circular dichroism spectroscopy

Circular dichroism (CD) is an absorption spectroscopy technique involving circularly polarized light absorption to assess the protein's secondary structure. The peptide bond in the proteins absorbs UV at 180-250 nm, which is known as the Far-UV region. Therefore, far-UV CD was used to estimate alpha-helix, beta-sheet, or the beta-turn conformation of the fraction of the protein due to the distinct CD spectra specific to different secondary structures produced from measuring in the far UV range. The CD spectrum of alpha helical proteins is characterized by a negative band around 208 nm and 222 nm as well as a positive band around 190 nm (Greenfield, 2006). Conversely, β-pleated sheets have a spectrum characterized by a negative peak at 218 nm

and a positive peak at 195 nm, while disordered proteins have negative peaks near 195 nm (Greenfield, 2006).

The secondary structure of LRP is predominantly α-helical therefore CD spectroscopy was performed to confirm the secondary structure of the protein to ensure that it was correctly folded after purification. The protein was first dialyzed against a sodium phosphate buffer (20 mM sodium phosphate, 20 mM tris-HCl) for 20 hours at 4 °C. Following dialysis, the protein was stored at 4 °C. For CD analysis, the protein was prepared by centrifugation for 10 minutes at 13 200 rpm, 4 °C to remove aggregation. Thereafter, the CD spectrum for LRP was measured from 185 nm to 250 nm, in triplicates, using the Jasco J-1500 spectropolarimeter (Jasco, Tokyo, Japan). The spectrum was obtained from averaging 10 accumulations per replicate, 5 nm bandwidth, 2 nm pathlength, and a scanning speed of 200 nm/minute at 20 °C. The samples contained 10 µM of protein which was diluted with Milli-Q® water five times to minimize noise in the background. The CD spectra was corrected by subtracting the absorbance of the buffer which were obtained in millidegrees (mdeg) and normalized to mean residue ellipticity using the equation below:

$$[\Theta]_{MRE} = \frac{\Theta \ x \ 10^6}{C. \ l. \ n}$$

$[\Theta]_{MRE}$ = mean residue ellipticity (deg.cm^2. dmol^{-1}

Θ = recorded signal (mdeg)

C = protein concentration (µM)

l = pathlength (mm)

n = number of residues

4.1.8.3 Intrinsic tryptophan fluorescence spectroscopy

Intrinsic tryptophan fluorescence (ITF) spectroscopy is used to determine the structure, function, and stability of proteins by measuring tryptophan emission. Tryptophan fluorescence uses the ITF of proteins to determine the location of the fluorophore (tryptophan) within its macromolecular structure. A change in fluorescence intensity or emission shift provides

information about the folding/unfolding of the protein, structural rearrangements, or binding of substances. Moreover, tryptophan fluorescence properties depend on the environment in which the amino acid is located, hence this information is used to infer protein conformational changes and protein denaturation (Ghisaidoobe and Chung, 2014).

ITF spectroscopy was used to determine the quaternary structure of LRP by determining the folding of the protein. The protein was first prepared by centrifugation for 10 minutes at 13 200 rpm, 4 °C. The 2 µM protein samples were prepared in the presence and absence of 8 M urea (in triplicates) to compare native and unfolded protein. The samples were incubated with urea for 2 hours at 20 °C and the ITF spectrum was obtained using the Jasco FP-6300 spectrofluorometer (Jasco, Tokyo, Japan) at 20 °C. The excitation wavelengths 280 nm and 295 nm were used to obtain an emission spectrum from 260 nm to 450 nm. Excitation and emission bandwidths of 5 nm and 2.5 nm, respectively, at a scanning speed of 200 nm/minute and a pathlength of 1 cm were used to obtain the spectrum. For native protein samples, the spectrum was corrected by subtracting the spectrum of the buffer. For unfolded protein samples, the spectrum was corrected by subtracting the spectrum of the buffer with 8 M urea.

4.1.8.4 Laminin binding affinity assay

Binding affinity is the strength of the binding interaction between a biomolecule and its ligand. Therefore, binding affinity assays measure the strength of protein binding interaction to a ligand such as another protein, a molecule, or nucleic acids (Pollard, 2010; Hunter and Cochran, 2016). The binding affinity assay was performed in this study to determine the binding of recombinant LRP to its primary ligand, laminin-1 in comparison to a control protein, Glutathione S-transferase of the malarial parasite *Plasmodium falciparum* (PFGST) for functionality.

Millicoat™ Laminin strips (Merck Millipore, Darmstadt, Germany) were blocked overnight with a blocking buffer (0.3% (w/v) NaN_3 and 3% (w/v) BSA in 1X PBS). Following incubation, the plates were incubated with 2 µM LRP for 1 hour at 37 °C to allow the protein to bind to laminin-1. Then the plates were washed three times with a blocking buffer to remove unbound protein. Thereafter, the plates were incubated with 6x-His Tag monoclonal antibody 1: 500 (Invitrogen, Massachusetts, USA) for 2 hours at room temperature and washed three times with blocking buffer to remove unbound HRP- conjugated antibody. The Clarity™ Western ECL Blotting

Substrate (Bio-Rad, California, USA) was added to plates and incubated for 5 minutes. Fluorescence was measured at 490 nm using the VICTOR® Nivo™ Multimode Microplate Reader.

4.2 Encapsulation of LRP and characterization of the encapsulated protein

4.2.1 PLGA nanoparticle synthesis and recombinant LRP encapsulation.

Poly(lactic-co-glycolic) acid nanoparticles were synthesized to encapsulate and deliver recombinant LRP. PLGA nanoparticles were used as delivery systems in this project due to the following properties: targeted drug delivery, biocompatibility, improving drug half-life and non-cytotoxic biodegradation in cells. The nanoparticles were synthesized using double emulsification and solvent evaporation method (McCall and Sirianni, 2013).

Firstly, 100 mg of PLGA (Sigma-Aldrich, Missouri, USA) was dissolved overnight in 2 ml ethyl acetate (Associate Chemical Enterprise (ACE), Southdale, RSA) in glass test tubes to produce smaller and uniform-sized nanoparticles and to improve separation of the particles and prevent them from forming clumps during synthesis. The following day, a double emulsion was formed by adding the polymer solution, containing homogenously dispersed 700 µg/µl LRP, dropwise to 4 ml of constantly agitated 0.3% (w/v) vitamin E- D- α- Tocopherol polyethylene glycol succinate (TPGS) (Sigma-Aldrich, Missouri, USA) using a vortexer (Afrimedics, Johannesburg, RSA). Vitamin E- TPGS is an emulsifying agent used to improve emulsification and encapsulation efficiency of the nanoparticles. Empty PLGA nanoparticles were synthesized as a negative control. The protocol followed all the synthesis steps, but the protein was not added. The double emulsion was sonicated at 40% amplitude using a QSONICA sonicator (Separation Scientific, Roodepoort, RSA) on ice three times for 10 seconds while pausing between each sonication so that the double emulsion can cool off before the next sonication. Thereafter, the emulsion was added to 45 ml of 0.3% (w/v) vitamin E-TPGS solution in a beaker and placed on a magnetic stirrer for 4 hours at room temperature partially covered with foil to facilitate the evaporation of ethyl acetate. The constantly stirred emulsion solution was then moved to a 4 °C cold room overnight to allow the nanoparticles to sufficiently harden without forming clumps due to sedimentation. After the nanoparticles had hardened, they were collected and purified. The nanoparticles were purified for 400-500 nm nanocapsules by first separating larger nanoparticles through pelleting them at 500 xg for 1 minute. The supernatant was transferred to

another falcon and centrifuged at 17 000 xg to purify out smaller nanoparticles to improve cellular uptake. The nanoparticle pellets were resuspended in 1 ml dH_2O using a water bath sonicator. Thereafter, the solution was centrifuged at 17000 xg for 15 minutes and the clear supernatant was discarded. This purification step was repeated three times to collect uniform nanoparticles and to ensure that no vitamin E-TPGS remained. The pellet PLGA nanoparticles were resuspended in 500 µl dH_2O and transferred to a 15 ml centrifuge tube (Corning Inc, New Jersey, USA) to prepare for lyophilization.

The falcon tube was placed in liquid nitrogen to snap-freeze the samples and thereafter, the tubes were covered with parafilm with small holes to facilitate sublimation. The tube was placed in a Freeze-Drying Machine Lyophilizer (Nova Laboratories Ltd, Leicester, UK) for 4 hours and after lyophilization, the particles were stored at -80℃ for long term storage.

4.2.2 PLGA nanoparticle encapsulated LRP characterisation

The PLGA nanoparticles were characterized after purification using scanning electron microscopy (SEM) and dynamic light scattering (DLS) to determine surface morphology and hydrodynamic size, respectively. The nanoparticles needed to be hollow to function as a delivery system for the protein and to be uniform in size. A leakage test was also performed to determine the release profile of the nanoparticles. This was to ensure that the nanoparticles degrade and release the therapeutic LRP.

4.2.2.1 Scanning electron microscopy (SEM)

Scanning electron microscopy was performed at the Wits School of Chemical and Metallurgical Engineering (Johannesburg, South Africa) to confirm surface morphology of PLGA nanoparticles. Firstly, the nanoparticles were placed on a carbon SEM stub to adhere before sputter coating with a single layer of gold palladium (AuPd). The layer of AuPd was used to create a conductive layer of metal to improve stability and imaging of the specimen.

The microscope was vented to release the vacuum and the samples were positioned on the stage. The chamber was vacuumed for 5 minutes or until the vacuum was ready to acquire high resolution images by preventing atmospheric interference. A secondary electron detector was used to detect signals from the electron beam interaction with the surface of the nanoparticles. Secondary electrons were used in high vacuum mode to enhance topographic contrast. A high

voltage index of 12 kV was selected as the accelerating voltage for the electrons. Magnification (21.17 k X), brightness, contrast and beam intensity were set as required. Thereafter, the images were taken, and the surface morphology was analysed.

4.2.2.2 Dynamic light scattering

DLS was used to determine the polydispersity index (PdI) of PLGA nanoparticles. This method determines the hydrodynamic diameter of the nanoparticles from the scattered light intensity based on the Brownian motion theory and Stokes-Einstein equation. The nanoparticle size distribution needs to be narrow as it influences factors such as: cellular internalization, bioavailability of recombinant LRP and blood circulation time to the target.

In a 15 ml falcon tube, 1 mg of encapsulated LRP nanoparticles were resuspended in 10 ml of dH_2O (100 µg/ml). The cuvettes were washed with a detergent solution and ultrapure water and dried using high pressure air. This process ensured that there were no dust particles that scattered light during DLS measurements. DLS analysis was performed three times on the samples (three biological repeats) using a ZetaSizer Nano ZS_{90} (Malvern Panalytical, Malvern, UK) at 25°C to measure the intensity of scattered light. The data was analysed using the Zetasizer Nano software version 3.30 (Malvern Panalytical, Malvern, UK).

4.2.2.3 Drug release profile

Drug release is the process in which drugs move from their initial position in the polymeric system to the polymer's outer surface and then to the release media (Fu and Kao, 2010). In this study, the release profile of LRP from the nanoparticles was important because it showed that the nanoparticles underwent hydrolysis to release LRP from the nanoparticles for the protein to perform its therapeutic function. The drug release of LRP from nanoparticles into solution was analysed using the leakage test.

In a 15 ml falcon tube, 1 mg of encapsulated LRP nanoparticles were resuspended in 10 ml of 1X PBS (100 µg/ml) and 1 ml was aliquoted into Eppendorf tubes. The Eppendorf tubes were incubated in a humidified incubator at 5% CO_2 and 37 °C, in addition to the PBS buffer of pH 7.5, to mimic physiological conditions of living organisms. The NanoDrop® ND-1000 (Thermo Fisher Scientific, Massachusetts, USA) was used to determine the presence of proteins at 280 nm in each sample at time points: 0, 1, 2, 4, 6, 8, 24, 48 and 72 hours.

4.3 Cell culture and PMA-induced differentiation

Human myeloid leukaemia cell line (U937) is a pro-monocytic, suspension cell line that was cultured for experimental procedures in this project. U937 cells are used to study many inflammatory diseases including cardiovascular diseases (Nascimento *et al.,* 2022). These cells can be differentiated into naïve macrophages hence they were used to model atherosclerosis because monocytes and macrophages are involved in atherosclerotic lesion initiation and progression. U937 cells were cultured in Roswell Park Memorial Institute (RPMI) 1640 media (ThermoFisher Scientific, Massachusetts, USA) supplemented with L-glutamine, 1% (v/v) penicillin/streptomycin (Biowest, Nuaillé, France) and 5% (v/v) foetal bovine serum (FBS) (Biowest, Nuaillé, France). The cells were cultured in 250 ml sterile disposable PETG flasks (ThermoFisher Scientific, Massachusetts, USA) in a shaker and incubated at 37 ºC and 5% CO_2 to mimic *in vitro* conditions for optimal growth. The nutrient media was replenished when the nutrients in the media were depleted, shown by a change in the colour of media, and the cells were sub-cultured when they reached ±80% confluency.

Total number of cells per ml was determined for sub-culturing and prior to downstream experimental procedures to seed cells. The cells were washed using 1x phosphate buffered saline (PBS) and 20 µl filtered trypan blue solution (Sigma-Aldrich, Missouri, USA) was added to 20 µl of cell suspension to selectively stain for dead cells in the sample. Thereafter, 20 µl of the sample was loaded onto cell counting slides (Bio-Rad, California, USA) and inserted into the TC20™ Automated Cell Counter (Bio-Rad, California, USA) to determine the number of cells.

Following seeding of U937 cells, phorbol-12-myristate-13-acetate (PMA) (Sigma-Aldrich, Missouri, USA) was used to induce differentiation of U937 cells into naïve (M0) macrophages which are known as unstimulated macrophages (Nascimento *et al.,* 2022). PMA-induced differentiation of U937 cells caused the suspension cells to adhere to the plates. Seeded cells were treated with 25 nM PMA and incubated in a humidified incubator at 37 ºC and 5% CO_2 for 24 hours. The media was aspirated, and new media was added to the plates and further incubated for 48 hours to allow for cell recovery.

4.4 Oxidized LDL treatment and lipid (Oil Red O) staining

Oxidized LDLs are involved in the process of atherosclerosis by inducing the formation of foam cells which are lipid-laden cells. Continual oxidized LDL endocytosis by macrophages accelerates plaque progression and potentiates the inflammatory response. The lipid (Oil Red O) stain kit (Sigma-Aldrich, Missouri, USA) was used to stain and visualize neutral triglycerides and lipids in foam cells. Oil Red O is a fat-soluble dye that dissolves in lipids hence it was used to determine the presence of lipids after oxidation with oxidized LDL to confirm the formation of foam cells.

Naïve macrophages were treated with 100 µg/ml oxidized LDL (Cloud-Clone Corp, Texas, USA) to create atherosclerotic cell culture models which are foam cells (lipid-laden macrophages). Alternatively, oxidized LDL was prepared by exposing 2 mg/ml native LDL to 20 µM copper sulphate ($CuSO_4$) (Sigma-Aldrich, Missouri, USA) and the reaction was incubated for 18 hours at 37℃. The reaction was terminated by adding 0.25 mM EDTA (Sigma-Aldrich, Missouri, USA). M0 macrophages were exposed to 100 µg/ml oxidized LDL for 24 hours. Following this, the media was removed from the dishes and the cells were gently washed twice with 1 ml 1X PBS. To fix the cells to maintain cellular morphology and for dye intake, 1 ml 10% (v/v) formalin (Sigma-Aldrich, Missouri, USA) was added, and the dishes were incubated for 30 minutes to 1 hour. The formalin was aspirated, and the cells were washed twice with dH_2O. To solubilize the Oil Red O stain, 1 ml of 60% isopropanol (Sigma-Aldrich, Missouri, USA) was added to the dishes and incubated for 5 minutes and discarded. The Oil Red O working solution was added to completely cover the cells in each dish and the dishes were incubated for 10-20 minutes to stain neutral lipids and triglycerides. Thereafter, Oil Red O solution was discarded, and the cells were washed 2-5 times with dH_2O to remove excess stain. Thereafter, the cells were covered with dH_2O and were viewed and imaged using the Zeiss Primovert microscope (Zeiss, Jena, Germany).

4.5 3-(4, 5-Dimethylthiazol-2-yl)-2, 5-Diphenyltetrazolium Bromide (MTT) assay to assess cell viability after encapsulated LRP treatment

The effect of encapsulated recombinant LRP treatments on cellular viability of normal and atherosclerosis cell culture models was assessed using the MTT assay. The MTT reaction is a colorimetric reaction dependent on mitochondrial dehydrogenase enzyme which is functional in

the mitochondria of viable cells. Mitochondrial dehydrogenases convert MTT to formazan crystals in viable cells. Thus, it quantifies and assesses cellular viability based on the metabolic activity reflected by viable cells. This assay was performed as an optimization assay to determine the optimum treatment of PLGA nanoparticles for the cells.

The MTT assay was conducted using U937 cells and foam cells. In a 48-well plate, 2×10^4 cells/ml were seeded. For foam cells, the U937 cells were further treated with 25 nM PMA to induce differentiation to M0 macrophages. The cells were incubated in a humidified incubator for 72 hours to induce differentiation and allow the cells to recover. The cells were treated with 75 µg/ml, 100 µg/ml, and 150 µg/ml encapsulated LRP and 100 µg/ml of empty PLGA nanoparticles (control) for 48 hours in a humidified incubator.

Apoptosis-inducing 8 M protocatechuic acid (PCA) (Sigma-Aldrich, Missouri, USA) was used as a positive control and untreated cells were set to 100% viability as the negative control. The experiments were conducted in three biological repeats. After the treatments, 100 µl of 1 mg/ml MTT (Sigma-Aldrich, Missouri, USA) was added to each well and incubated at 37 °C for 2 hours to allow for sufficient MTT metabolism. The media was discarded without disturbing the formazan crystals in foam cells. However, since U937 cells are suspension cells the media was not discarded. Thereafter, the formazan crystals were dissolved using 200 µl dimethyl sulfoxide (DMSO) (Sigma-Aldrich, Missouri, USA) and resuspended. The samples were transferred in three technical repeats to a 96-well plate and absorbance was measured at 570 nm using the VICTOR® Nivo™ Multimode Microplate Reader.

4.6 Statistical analysis

The data collected in this study was statistically analysed using Microsoft Excel (Microsoft Corporation, Washington D.C, USA). Zetasizer Nano software v 3.30 and Image Lab 5.1 (Bio-Rad, California, USA) were used for DLS analysis and analysis of gels and blots, respectively. All the experiments will be conducted in three biological repeats. The error bars will present standard deviation and the Student's t-test will be performed at a 95% confidence interval, where p-values <0.05 will be considered statistically significant ($*p<0.05$, $**p<0.01$, $***p<0.001$).

5. Results

5.1 37 kDa LRP overexpression, purification, and characterization

The main aim of this study was to evaluate PLGA nanoparticle encapsulated recombinant LRP as a treatment for cardiovascular disease. Therefore, LRP was overexpressed, purified, and characterized before encapsulation into nanoparticles. *E. coli* cells were transformed using a pET-11a plasmid containing the 37 kDa LRP gene to express the protein of interest. Thereafter, LRP was purified using IMAC and purity was assessed using SDS-PAGE and absorbance spectroscopy. Structural characterization was performed using western blotting, ITF, and far-UV CD. Lastly, binding affinity assay was conducted to determine functionality of the protein.

5.1.1 Plasmid sequencing

Plasmids were isolated and sent for sequencing at Inqaba Biotechnical Industries (Pretoria, RSA). The protein sequences were then verified using Clustal Omega to verify the insertion of the *LRP* gene into the plasmid. This was done to ensure that there were no mutations within the *LRP* gene in the plasmid in order to correctly produce the protein of interest. Thereafter, Expert Protein Analysis System (ExPASy) (Swiss Institute of Bioinformatics (SIB), Switzerland) was used to translate the gene sequence into an amino acid sequence (Query). The query sequence was aligned with the optimized protein sequence (Reference) using Clustal Omega shown in **Figure 6**. The reference and query sequences had 100% alignment and are indicated by the asterisks between identical residues. Therefore, this confirms that LRP did not undergo mutations and the inserted gene was LRP.

```
Reference       MSGALDVLQMKEEDVLKFLAAGTHLGGTNLDFQMEQYIYKRKSDGIYIINLKRTWEKLLL     60
Query           MSGALDVLQMKEEDVLKFLAAGTHLGGTNLDFQMEQYIYKRKSDGIYIINLKRTWEKLLL     60
                ************************************************************

Reference       AARAIVAIENPADVSVISSRNTGQRAVLKFAAATGATPIAGRFTPGTFTNQIQAAFREPR     120
Query           AARAIVAIENPADVSVISSRNTGQRAVLKFAAATGATPIAGRFTPGTFTNQIQAAFREPR     120
                ************************************************************

Reference       LLVVTDPRADHQPLTEASYVNLPTIALCNTDSPLRYVDIAIPCNNKGAHSVGLMWWMLAR     180
Query           LLVVTDPRADHQPLTEASYVNLPTIALCNTDSPLRYVDIAIPCNNKGAHSVGLMWWMLAR     180
                ************************************************************

Reference       EVLRMRGTISREHPWEVMPDLYFYRDPEEIEKEEQAAAEKAVTKEEFQGEWTAPAPEFTA     240
Query           EVLRMRGTISREHPWEVMPDLYFYRDPEEIEKEEQAAAEKAVTKEEFQGEWTAPAPEFTA     240
                ************************************************************

Reference       AQPEVADWYEGVQVPSVPIQQFPTEDWSAQPATEDWSAAPTAQATEWVGATTEWS  295
Query           AQPEVADWYEGVQVPSVPIQQFPTEDWSAQPATEDWSAAPTAQATEWVGATTEWS  295
                ********************************************************
```

Figure 6: Protein sequence alignment of query and reference sequencing. The plasmid with the LRP gene was isolated and sequenced. The gene sequence was then translated into an amino acid sequence which was then aligned to the reference sequence. There was a 100% alignment between the Reference and Query sequence.

5.1.2 Protein overexpression trials

Since the inserted sequence was confirmed to be LRP, overexpression trials were conducted to determine optimal conditions for overexpressing LRP protein in *E. coli* cells. Two variables were investigated for overexpression: IPTG concentration and time. IPTG was investigated to determine the optimal concentration that induces overexpression of the *LRP* target gene. Time was investigated to identify the optimal time required for overexpression of the *LRP* gene with the highest possible yield. **Figure 7** shows the SDS-PAGE gels of overexpression trials at 0.3 mM and 1.0 mM IPTG concentration and time intervals (4, 6, 8 and 12 hours). In the gels, supernatant (S) is the soluble protein and pellet (P) is insoluble protein. **Figure 7** shows the molecular weight of the overexpressed protein. This was determined from the linear regression model of the logarithm of the protein standards (molecular weight marker) as a function of the standard's R_f.

The LRP protein was overexpressed at 20 °C and 230 rpm at different time intervals after induction with 0.3 mM and 1.0 mM IPTG. Firstly, 1.0 mM IPTG concentration was assessed to induce overexpression of the protein as shown in **Figure 7 A.** However, the yield was low in

both the supernatant and pellet samples in all the different time points as shown in the gel below. A lower concentration of IPTG (0.3 mM) was investigated for the same time points. **Figure 7 B** shows that more protein was overexpressed after 8 hours as shown by the intensity of the bands. However, the protein was in the pellet fraction meaning it was insoluble. Therefore, the protein needed to be solubilized to extract the protein from the pellet fraction. After the overexpression trials, the molecular weight of the bands was determined using a linear regression model which indicated that the protein was ~47 kDa as shown in **Figure 8.** The molecular weight of the overexpressed was unexpectedly higher than the predicted 37 kDa possibly due to post-translational modifications.

A.

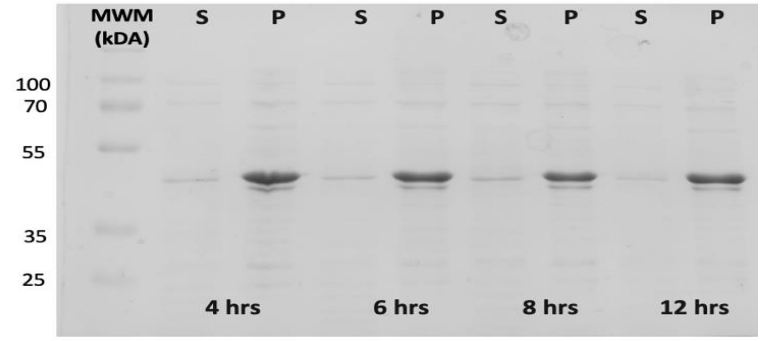

B.

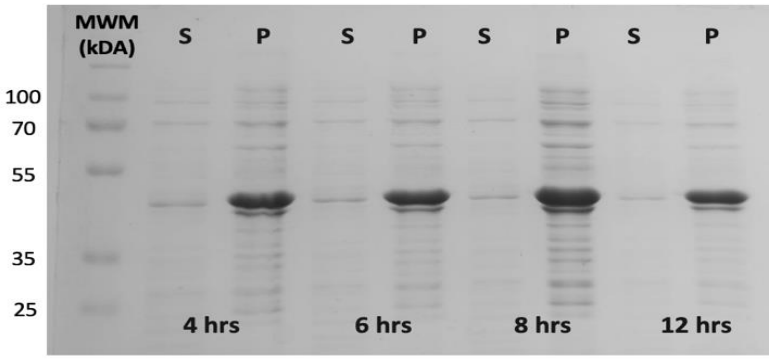

Figure 7: Overexpression trials of human LRP at different IPTG concentrations and time intervals. A. SDS-PAGE gel with the samples for overexpression trials at 1.0 mM IPTG for 4, 6, 8 and 12 hours. B. SDS-PAGE gel with the samples of overexpression trials at 0.3 mM IPTG for 4, 6, 8 and 12 hours. A concentration of 0.3 mM IPTG resulted in more protein being overexpressed in comparison to using 1.0 mM IPTG to induce overexpression. Furthermore, LRP was predominantly overexpressed after 8 hours in the 0.3 mM IPTG condition. MWM: Molecular weight marker, P: Pellet, S: Supernatant.

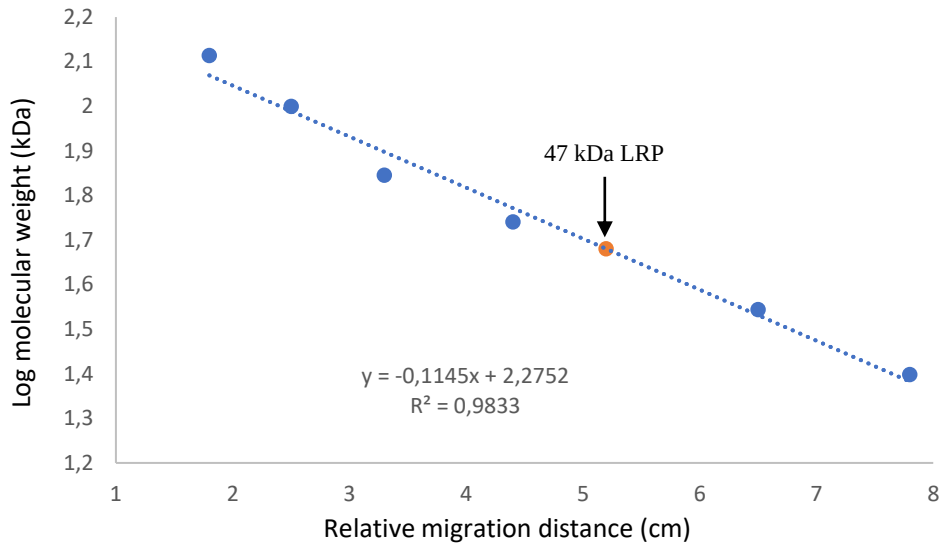

Figure 8: Linear regression model constructed from the standards of known molecular weight. The linear regression model was used to determine the size of the bands on the SDS-PAGE gels in **Figure 5**. The standard curve was constructed using standards of known molecular weight, BLUeye Prestained protein ladder (Merck Millipore, Darmstadt, Germany). The molecular weight of the bands of the target protein, based on their migration distance, correlates with ~47 kDa.

5.1.3 Solubilization of LRP using Triton X-100 detergent

In the overexpression trials, it was established that LRP was mostly located in the insoluble fractions (pellet). As previously mentioned, LRP is a multi-localized protein found in the nucleus, cytosol, and predominantly the membrane. This makes the protein primarily an insoluble protein thus it was solubilized using a detergent 2% (w/v) Triton X-100 (Sigma-Aldrich, USA) detergent. Triton X-100 is a non-ionic detergent that maintains protein stability. Insoluble fractions from overexpression were centrifuged at 18 000 xg for 30 minutes with Triton X-100 thereafter the supernatant containing soluble fractions was collected. Fractions from wash 1 (W1) W1A, W1B, W1F and W1G were poorly solubilized by Triton X-100 as the fractions are poorly seen on the gels in **Figure 9.** Higher fractions of solubilized proteins were predominantly found in Wash 1C to Wash 1E **(W1C-W1E)** as seen in the SDS-PAGE gel in **Figure 9.** This can be seen by the intensity of the bands in the gels. Following the successful solubilization of the protein, the protein was then purified using IMAC.

A.

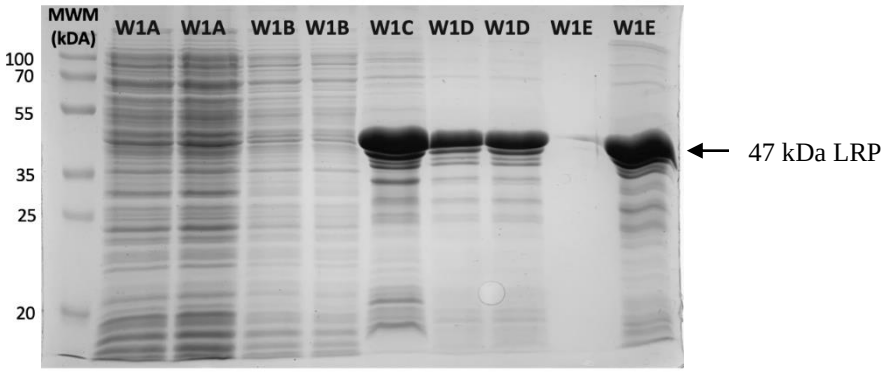

B.

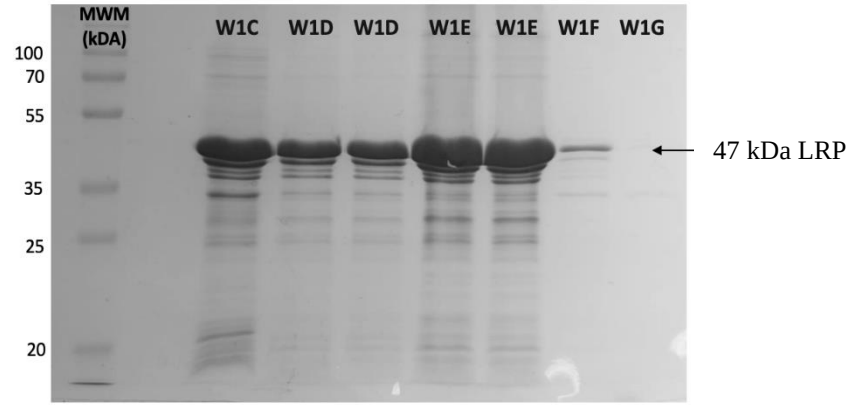

Figure 9: Supernatant fractions of scale-up solubilization of insoluble LRP fractions using Triton X-100. (A) and (B) SDS-PAGE gel with samples after scale-up solubilization of LRP with detergent containing 2% (w/v) Triton X-100 detergent at 18 000 xg for 30 minutes. Higher soluble fractions of LRP were observed in W1C to W1E. MWM: Molecular weight marker, W: Wash.

5.1.4 Protein purification using immobilized metal-ion affinity chromatography

Affinity chromatography is a protein purification technique that was implemented to purify LRP from the soluble protein lysate based on the binding affinity of the biomolecule to the immobilized stationary phase of the column. The affinity tags overexpressed with the protein bind the divalent cations of the stationary phase, therefore, since the overexpressed LRP protein is fused to a His-tag it will bind to metal ions during IMAC to immobilize it from solution. For protein purification two metal-ion columns were used, Co^{2+} and Ni^{2+}, due to their affinity for the His-tag. Ni^{2+} columns are preferred for His-tag protein purification because they provide a higher yield of the target protein and Co^{2+} columns are utilized when the goal is to achieve higher purity.

5.1.4.1 Immobilized nickel-ion affinity chromatography

LRP was first purified using a nickel immobilized metal-ion affinity chromatography column. Ni^{2+} columns are used for His-tag protein purification to obtain a higher yield of the protein of interest due to its high affinity compared to cobalt (Bornhorst and Falke, 2000). The elution profile and SDS-PAGE gels of LRP purification are shown in **Figure 10**. A substantial number of contaminating proteins and LRP unbound to the IMAC column were eluted as shown in the flow through of the elution profile and flow through lane (FT) in the SDS-PAGE gel in **Figure 10 B**. Contaminants that were non-specifically bound were removed using the salt wash buffer resulting in a big peak in the elution profile for salt wash and many bands in the salt wash lane (SW) in the gel in **Figure 10 B**. Therefore, the column had many non-specifically bound proteins which were eluted. The remaining proteins bound to the IMAC column were successfully eluted, as shown by the peak in the elution profile and bands in the gel in the elution lanes (E) using elution buffer. The eluted LRP had a low yield and was not pure, due to the many contaminating bands observed in the elution lanes in **Figure 10 B (lane 7 and 8).**

A.

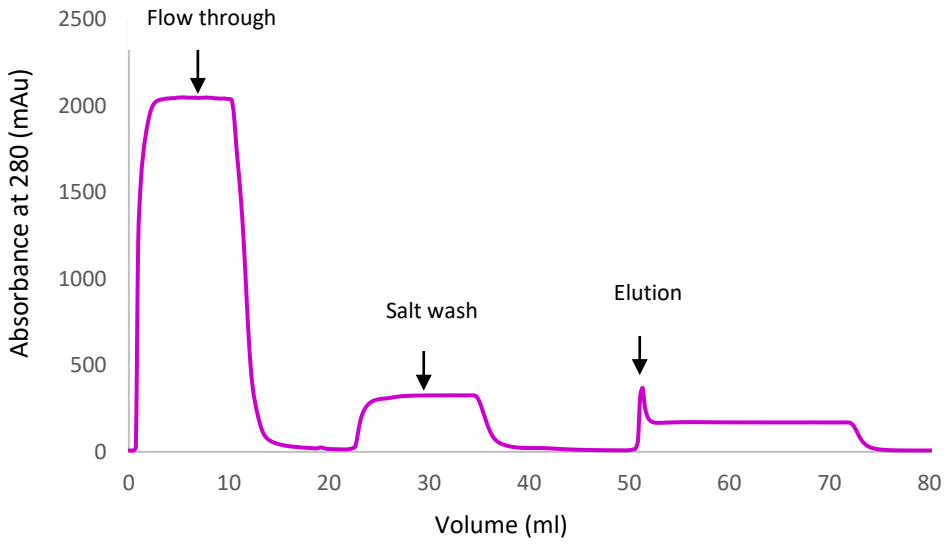

B.

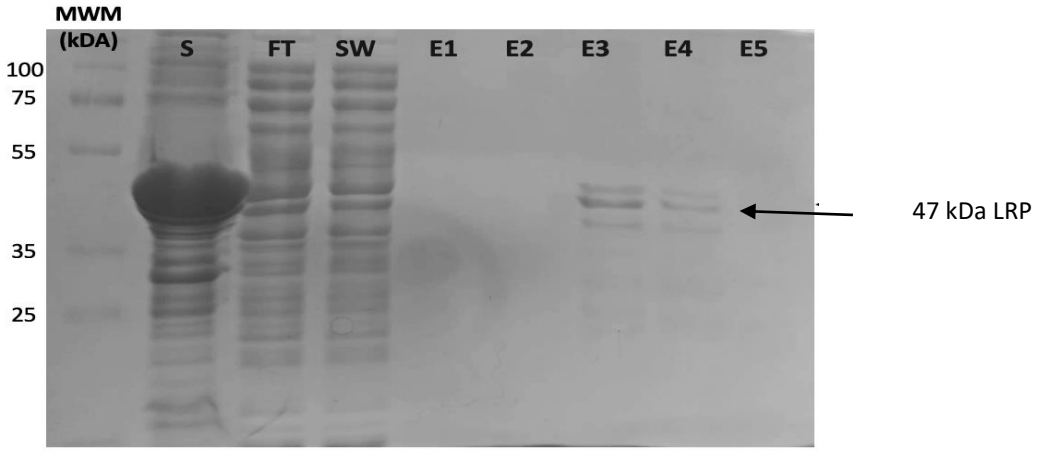

Figure 10: Purification of LRP using nickel immobilized metal-ion affinity chromatography. (A) Elution profile of LRP from nickel immobilized metal-ion affinity chromatography. (B) SDS-PAGE gel with samples from immobilized metal-ion affinity chromatography. E: Elution, FT: Flow through, MWM: Molecular weight marker, S: Supernatant, SW: Salt wash. Many unbound proteins were eluted in the flow through fraction as well as non-specifically bound protein using a salt wash. The contaminants were detected in the FT and SW lane of the gel. The eluted protein from the E lanes was not pure and required subsequent purification due to contaminating bands.

5.1.4.2 Immobilized cobalt-ion affinity chromatography

Due to the low yield and retention of contaminating proteins, Co^{2+} columns were used for His-tag protein purification to obtain protein with a higher purity due to its specificity because it exhibits more specific interaction with the His-tag (Bornhorst and Falke, 2000). Therefore, Co^{2+} IMAC columns were used to improve the purity and yield of purified LRP. **Figure 11** below shows the elution profile and SDS-PAGE gel for the purification of LRP using Co^{2+} IMAC. Unbound contaminating proteins and LRP were eluted as shown in the flow through peak of the elution profile and flow through lane (FT) in the SDS-PAGE gel in **Figure 11 B**. Contaminants that were non-specifically bound were removed using a high salt wash buffer. The salt wash peak in the elution profile (**Figure 11 A)** was small and no contaminating bands were visible in the salt wash lane (SW) of the gel (**Figure 11 B)**. Therefore, non-specifically bound contaminating proteins were of very low concentration. An elution buffer was used to elute protein bound to the column. The remaining proteins bound to the IMAC column were successfully eluted, as shown by the peak in the elution profile and bands in the gel (**Figure 11 B, lane E4/5/6)**. The bands in the elution lanes (E) show LRP and a contaminating band below which may be another isoform of LRP due to post-translational modifications that may occur to the protein. From **Figure 11 B**, we can also see that the protein was purified at a relatively high yield, and this is due to the high specificity with which the His-tags bind Co^{2+} resulting in minimal sample loss. Densitometric analysis was used to assess protein purity and found to be least 85% pure. To further confirm the presence of LRP in the eluted fractions western blotting was performed.

A.

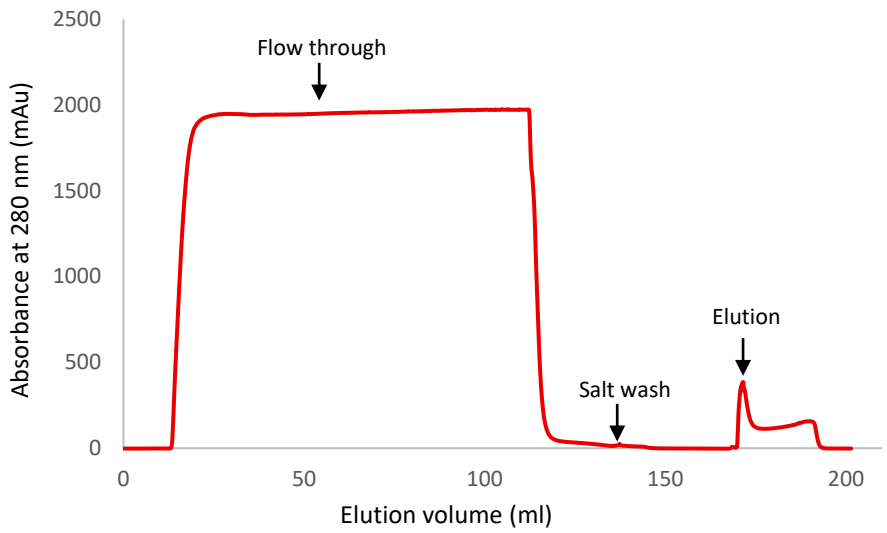

B.

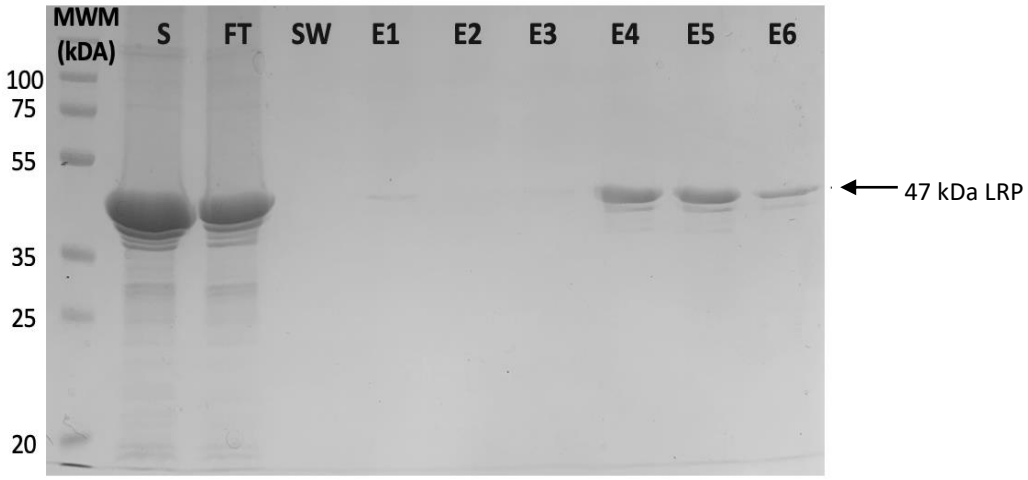

Figure 11: Purification of LRP using cobalt immobilized metal-ion affinity chromatography. (A) Elution profile from cobalt immobilized metal-ion affinity chromatography. (B) SDS-PAGE gel with immobilized metal-ion affinity chromatography samples. Unbound proteins were eluted in the flow through fraction which was detected in the FT lane of the gel. A very low concentration of non-specifically bound contaminating proteins was eluted in the salt wash as they were not detected in the SW lane of the gel. The elution of specifically bound protein was successful as seen in the elution lanes. However, the eluted protein was not completely pure. E: Elution, FT: Flow through, MWM: Molecular weight marker, S: Supernatant, SW: Salt wash.

5.1.5 Western blotting

Western blotting is an analytical technique used to detect, analyse, and quantify proteins of interest in samples. In **Figure 12**, western blotting was performed on elution fractions from cobalt IMAC to confirm the presence of the protein of interest before downstream characterization. LRP was detected in all the elution fractions from Co^{2+} IMAC (**Figure 11 B, lane E4/5/6)** using human anti-LRP/LR IgG1-iS18 (Affimed, Heidelburg, Germany) as shown below. The antibody also detected LRP as a 47 kDa protein mirroring the SDS-PAGE gels banding patterns. The 67 kDa laminin receptor was also detected due to the high sensitivity of the antibodies for the protein and its isoforms.

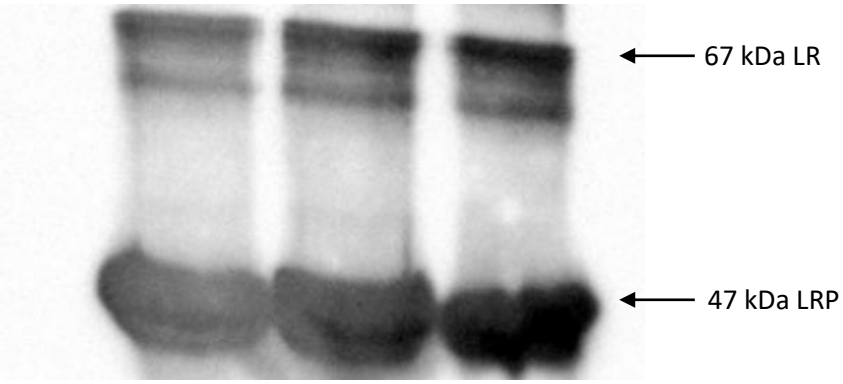

Figure 12: Confirmation of LRP protein in elution fractions from cobalt IMAC using western blotting. Immunoblotting was performed on the purified fractions from the cobalt IMAC. Clarity™ Western ECL Blotting Substrate (Bio-Rad, California, USA) was added to the membranes and the protein was visualized using the ChemiDoc™ Imaging System (Bio-Rad, California, USA). All lanes showed that the protein of interest was present in the elution fractions therefore the protein could be characterized.

5.1.6 Protein purity and concentration assessment using absorbance spectroscopy

After the eluted fractions were confirmed to be LRP, protein purity and concentration were determined. UV-Vis absorbance spectroscopy is an analytical technique used to quantify protein concentration, using the Beer-Lambert law, based on the light absorbed by molecules in solution at a specific wavelength. Furthermore, absorbance spectroscopy was used to detect nucleic acid contamination and protein aggregation in the protein samples. **Figure 13** shows the absorbance spectrum of the LRP protein. The spectrum peaked at 280 nm due to the presence of aromatic amino acids tryptophan, tyrosine, and phenylalanine in the protein. These amino acids absorb UV light at 280 nm. The absorbance at 280 nm in addition to the extinction co-efficient (67 045

$M^{-1}.cm^{-1}$) were used to calculate the concentration of LRP. The extinction co-efficient is a measure of strength of light absorption at a particular wavelength by a chemical substance and was used to calculate protein concentration. The protein concentration was 12.6 µM. Nucleic acid contamination was determined using the A_{260}/A_{280} ratio. Nucleic acids absorb UV light at 260 nm therefore a $A_{260/280}$ = 0.65, suggests that LRP is sufficiently free from contamination by nucleic acids. Moreover, there is a shoulder at 295 nm of the absorbance spectrum due to 10 tryptophan residues present in the protein. The lack of absorbance at 340 nm suggests that little to no aggregation was detected in the protein sample.

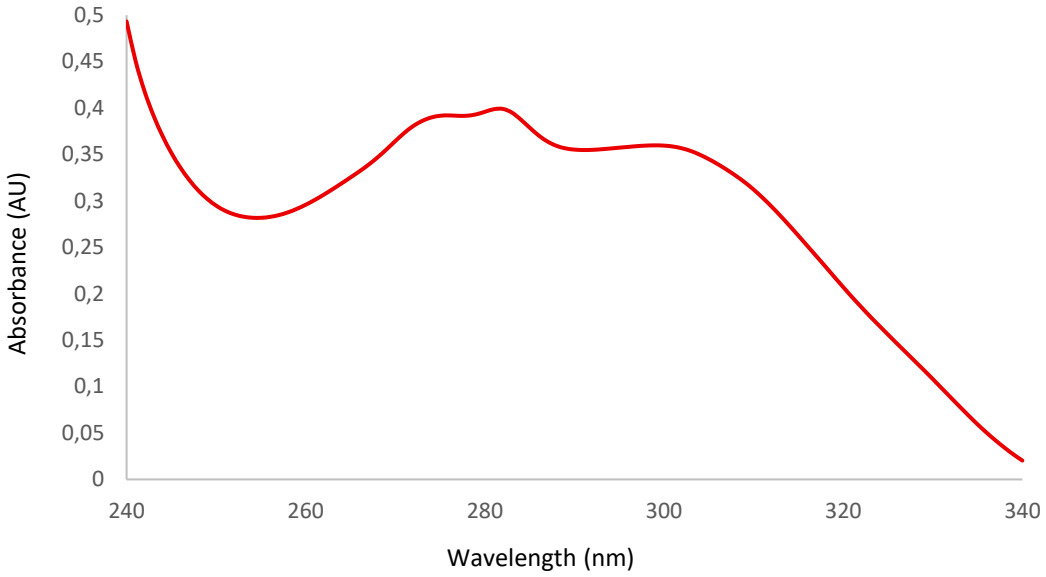

Figure 13: Absorbance spectrum of LRP. The peak at 280 nm was due to the presence of aromatic amino acids tryptophan, tyrosine, and phenylalanine. The absorbance at this wavelength was used to determine the concentration of LRP (12.6 µM) using an extinction co-efficient of 67 045 $M^{-1}.cm^{-1}$. Moreover, the A_{260}/A_{280} ratio was determined to be 0.65 thus suggesting that the protein sample is sufficiently free from contamination by nucleic acids. The shoulder at 295 nm is due to the presence of 10 tryptophan residues in the protein and the lack of absorbance at 340 nm suggests that little to no aggregation was detected in the protein sample.

5.1.6 Structural characterization of LRP

5.1.6.1 Far-UV Circular dichroism

Since LRP was determined to be sufficiently pure and free from nucleic acid contamination, structural characterization could be performed on the protein to determine the secondary and tertiary structure. Circular dichroism was used to determine the secondary structure of the purified protein. **Figure 14** shows the circular dichroism spectra of LRP used to determine secondary structure of the protein. The spectrum was obtained by normalizing the CD signal to mean residual ellipticity (MRE), which accounts for the number of amino acids and protein concentration. The spectrum below shows that the protein contains a peak at 189 nm and a trough at 207 nm which indicates that the protein is predominantly *α-helical*.

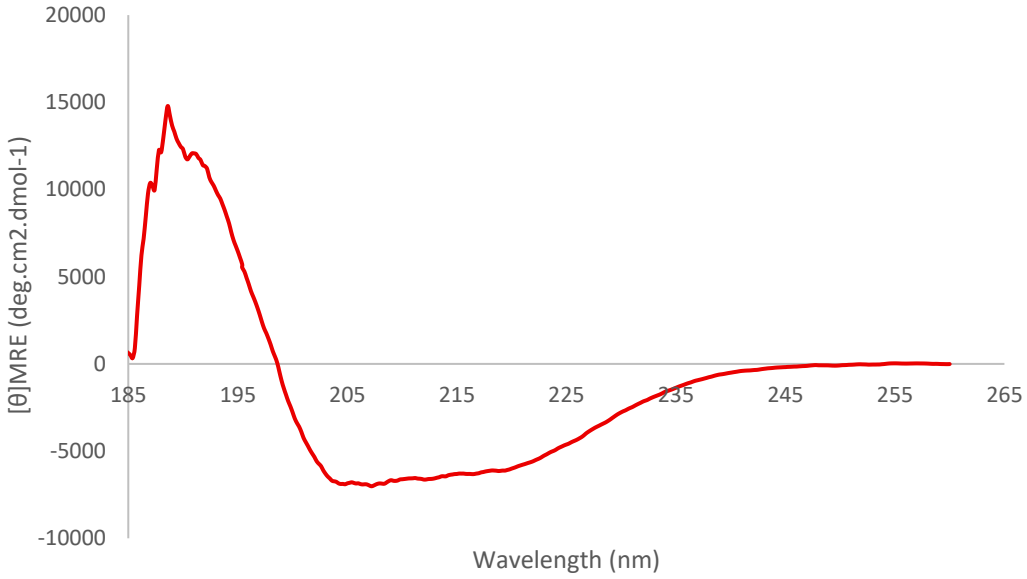

Figure 14: Circular dichroism spectra of LRP to determine secondary structure of the protein. The far-UV circular dichroism spectra were generated by normalizing the circular dichroism signal to mean residue ellipticity (MRE). The MRE takes into account the protein concentration and the total number of amino acids. The spectra indicates that the protein is predominantly α-helical because it contains a trough at 207 nm and peak at 189 nm.

5.1.6.2 Intrinsic tryptophan fluorescence spectroscopy

Following secondary structure characterization, ITF spectroscopy was used to assess protein stability by measuring tryptophan emission. In this study ITF spectroscopy was performed to confirm the folding of LRP in the presence and absence of urea denaturant. **Figure 15** shows the emission spectra of LRP in the absence and presence of 8 M urea denaturant. The spectra were obtained after exciting the tryptophan residues of LRP at 280 nm (shown in blue) and 295 nm (shown in pink). The native spectrum excited at 280 nm has an emission peak at 342 nm for both native and denatured protein. Therefore, there was no shift observed in the emission spectrum of denatured LRP from the native LRP spectrum. However, emission spectra quenching (decrease in emission intensity) was observed from the native LRP spectrum to the denatured LRP spectrum at 342 nm. This was not conclusive that LRP was correctly folded during overexpression hence the tryptophan residues were excited at 295 nm to correct the protein spectra by reducing light scattering. The emission spectrum at 295 nm showed a shift by 5 nm from the native spectrum to the denatured spectrum. This bathochromic shift is observed from 341 nm to 346 nm in the 295 nm emission spectra. Furthermore, a significant decrease in emission intensity is also observed in the emission spectra excited at 295 nm from the native to denatured LRP. As a result, the bathochromic shift and quenching observed upon denaturation demonstrates that LRP was correctly folded during overexpression. Therefore, the tertiary structure of LRP was conserved.

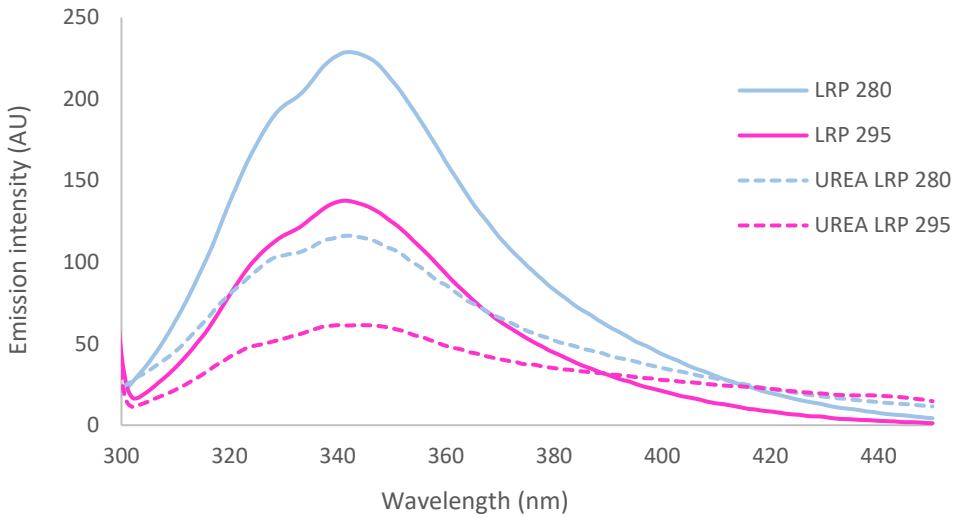

Figure 15: Intrinsic tryptophan fluorescence spectra of LRP in the absence and presence of 8M urea denaturant used to determine tertiary structure. The spectra were obtained after exciting the tryptophan residues of LRP at 280 nm (shown in blue) and 295 nm (shown in pink). The spectra excited at 280 nm only shows quenching between the peaks at 342 nm from native to denatured LRP. The peaks observed in the spectra of LRP excited at 295 nm show a bathochromic shift and quenching from the native to the denatured proteins which meant that our native protein was properly folded.

5.1.7 Functional characterization of LRP

Following structural characterization, functional characterization was performed to ensure that LRP was functional after overexpression. The binding affinity assay measures the affinity between a biomolecule and a ligand. Therefore, a laminin binding affinity assay was performed in this study to determine the binding of recombinant LRP to its primary ligand, laminin-1, to confirm the functionality of the protein. **Figure 16** shows the laminin binding affinity assay results obtained from the fluorescent plate readings. LRP has a relative fluorescence unit of 75914.67 which is two times higher than the control protein PFGST 28163.67. Statistical analysis conducted revealed that the difference in fluorescence was determined to be significant at *p= 0.031674. Therefore, LRP has higher affinity for laminin compared to PFGST which had a low binding affinity with laminin-1 suggesting that the purified LRP protein was functional.

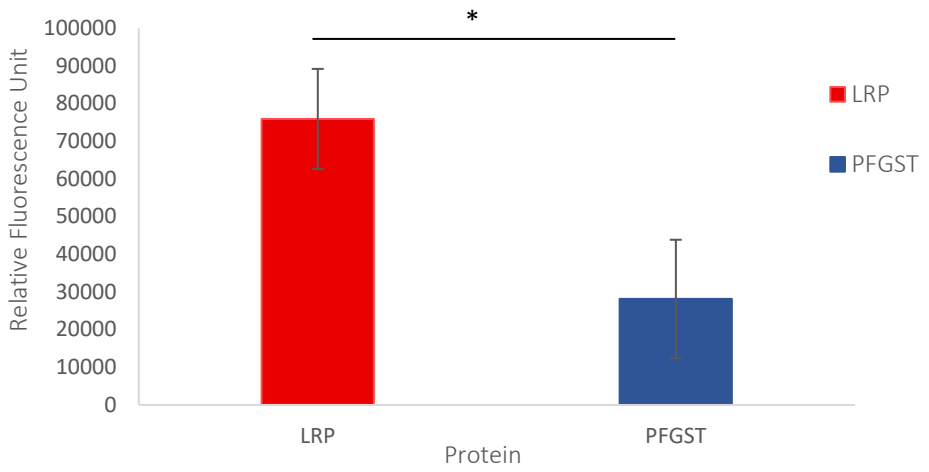

Figure 16: Functional assay to determine the binding affinity of purified LRP for laminin-1. Binding affinity assays determine the strength of the binding interaction between a biomolecule to its ligand. The relative fluorescence unit of binding between LRP and laminin-1 was 75914.67 and for PFGST and laminin-1 was 28163.67. There is significant stronger binding between LRP, and laminin-1 compared to control protein PFGST indicating that the purified LRP was active (*p= 0.031674). Standard deviation is shown by the error bars, n = 3 biological repeats. n/s= not significant, *p <0.05, **p<0.01 and ***p<0.001; Students t-test.

5.2 Encapsulation of LRP into PLGA nanoparticles and characterization of the nanoparticles

Following the successful expression, purification, and characterization of LRP it could be encapsulated into PLGA nanoparticles to develop a potential therapeutic against cardiovascular disease. PLGA nanoparticles were used as a delivery system in this study due to increased half-life and controlled release of the contents. The nanoparticles were synthesized using double emulsion and solvent evaporation method and characterized using SEM, DLS and leakage test to determine morphology, polydispersity index and protein release, respectively.

5.2.1 Morphology and size distribution of the nanoparticles

The protein-based drug was developed by encapsulating the purified protein into nanoparticles. Thereafter, the morphology of the nanoparticles was assessed using scanning electron microscopy as shown in the figure below (**Figure 17)**. The image was taken at a 21.17 kX magnification at a scale bar of 1 µm. **Figure 17** shows that the nanoparticles have a spherical

morphology with varying sizes. Therefore, DLS was performed to determine of the nanoparticles fall within their synthesis size distribution of 200 nm to 400 nm.

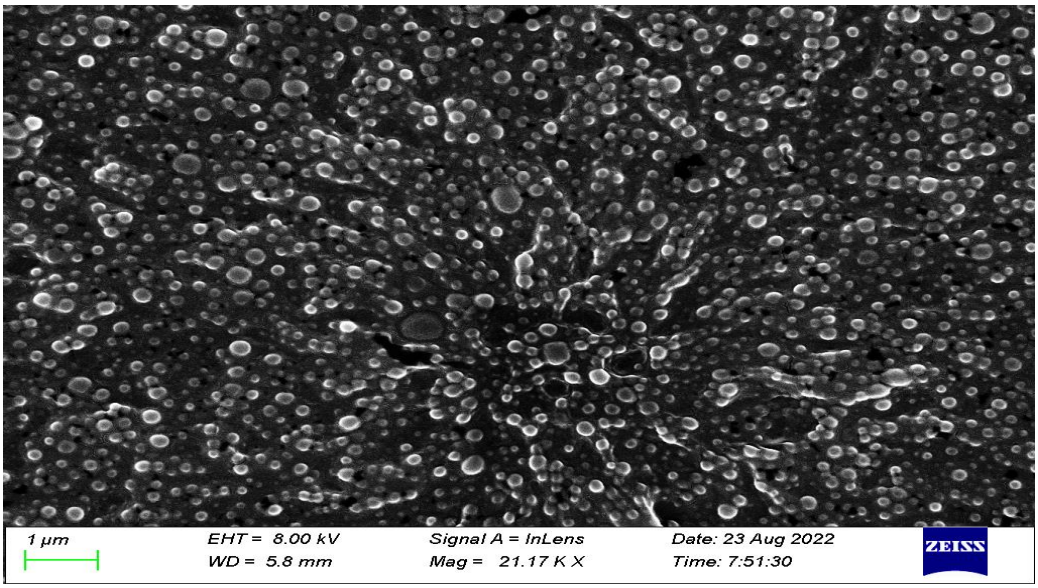

Figure 17: Scanning electron microscope image of PLGA nanoparticles with encapsulated recombinant LRP. The SEM image was taken at 21 kX SEM magnification at a scale bar of 1 µm. The image shows that the nanoparticles synthesized have a spherical morphology. The sample image also shows nanoparticles of varying sizes.

Dynamic light scattering was performed to determine the polydispersity index (PdI) and Z-average size of the nanoparticles which gives insight into the size distribution of the nanoparticles and average diameter of the particles, respectively. A low PdI refers to a smaller size distribution and a large PdI corresponds to a larger size distribution of the particle size (Clayton *et al.*, 2016). The PdI of PLGA nanoparticles encapsulating LRP was determined to be 0.45 and for empty PLGA nanoparticles it was 0.43 as shown in **Figure 18**. A PdI < 0.7 indicates narrow size distribution and a PdI > 0.7 indicates that the nanoparticles have a very broad size distribution. The PdI of the nanoparticles is less than 0.7 therefore the size distribution was narrow. The Z-average size of LRP encapsulating nanoparticles and empty nanoparticles was 221 nm and 857 nm, respectively. The Z-average for LRP encapsulating nanoparticles fell within the desired range of 200-400 nm however, for empty nanoparticles the Z-average size was larger than the expected size range of 200-400 nm. Therefore, LRP encapsulating nanoparticles that were synthesized had a hydrodynamic size that fell within the desired size range of 200-400 nm

with a narrow size distribution. For empty nanoparticles, the nanoparticles had a narrow size distribution, but the hydrodynamic size was 857 nm which was larger than the expected 200-400 nm. The size distribution between the nanoparticle samples was not significantly different (p=0.80). This shows that the nanoparticles have a desired narrow size distribution within their sample group.

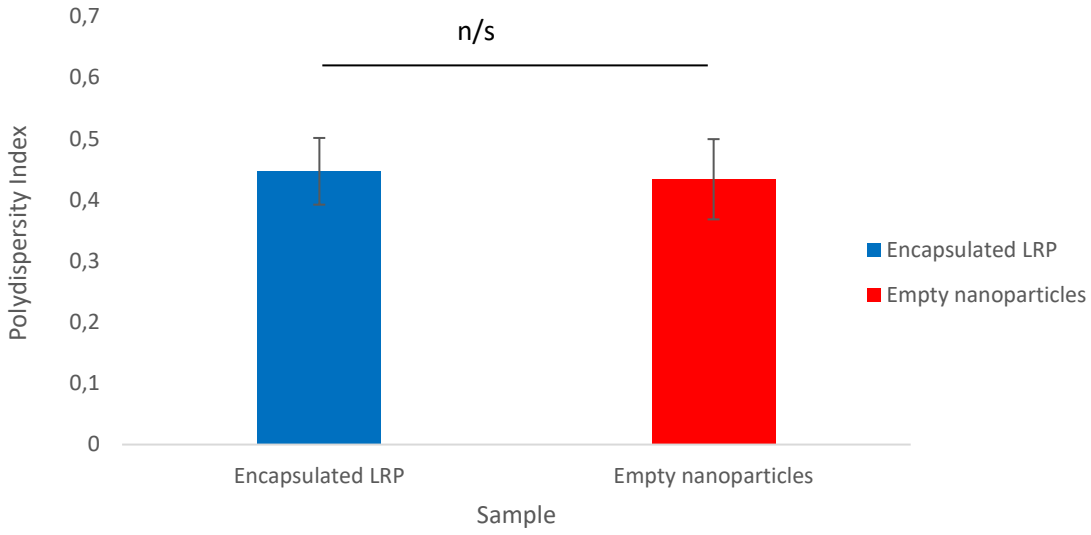

Figure 18: Polydispersity index of PLGA encapsulated LRP and empty PLGA nanoparticles. The figure above shows the polydispersity index of PLGA nanoparticles encapsulating LRP at 0.45 and for empty PLGA nanoparticles at 0.43. The size distribution of the nanoparticles within the sample groups is narrow. The size distribution between the nanoparticle samples was not significantly different (p=0.80). This shows that the nanoparticles have a desired narrow size distribution within their sample group. Nanoparticles encapsulating LRP have the desired 200-400 nm size distribution (Z-average size = 221 nm) and empty nanoparticles have a Z-average of 857 nm. Standard deviation is shown by the error bars, n = 3 biological repeats. n/s= not significant, *p <0.05, **p<0.01 and ***p<0.001; Students t-test.

5.2.2 Release profile of LRP from nanoparticles

The leakage test was performed to determine the release profile of LRP from the PLGA nanoparticles. This was done to ensure that the protein was encapsulated into the nanoparticles during synthesis and hence it can be released when the nanoparticles undergo hydrolysis and act as a therapeutic. **Figure 19** shows the release profile of LRP encapsulated nanoparticles at 100 µg/ml concentration of nanoparticles in the PBS buffer. The absorbance readings peaked at

different time points showing an initial burst release from 0-8 hours followed by a sustained release of the protein after 8 hours which indicates that LRP was successfully encapsulated and released from the nanoparticles. The burst release of LRP is observed at time points 1 and 6 hours with no protein detected at time points 4 and 8 hours. The protein absorbance at these time points was not detected due to aggregation. However, there was a sustained release of the protein after 8 hours. Therefore, the successful encapsulation and release of LRP means that PLGA nanoparticles are a viable delivery system, and the protein can carry out its therapeutic effects in downstream experiments.

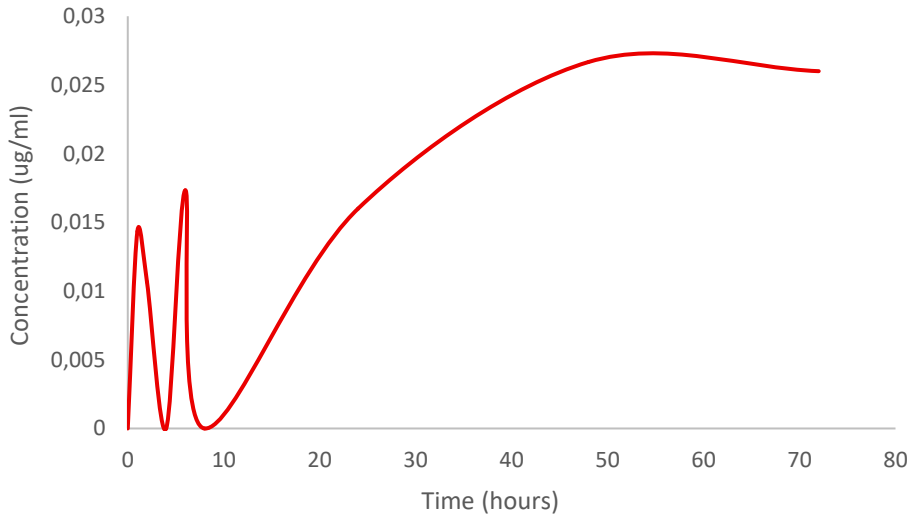

Figure 19: Release profile of encapsulated LRP nanoparticles at a concentration of 100 µg/ml. Absorbance readings of the leak test were taken at 280 nm to detect the presence of the LRP protein in PBS buffer. The readings were taken over a 72-hour period at: 0, 1, 2, 4, 6, 8, 24, 48 and 72 hours. The was a burst release of the protein in the first 8 hours of the experiment. Thereafter, this was then followed by a sustained release of the protein.

5.3 Assessing encapsulated LRP as a treatment for cardiovascular disease

Since it has previously been shown that LRP could be a possible treatment for CVD, we subsequently tested the effect of the encapsulated LRP protein on an atherosclerotic cell culture model. The effect of the treatment on cell viability and protein levels were assessed using an MTT assay and western blot, respectively. However, atherosclerotic cell culture models were first created using PMA differentiation and oxidized LDL treatment on U937 cells.

5.3.1 Cell culture models

U937 cells are a human myeloid leukaemia suspension cell line. This cell line was used because it exhibits monocyte morphology and characteristics and because it can be differentiated into macrophages or dendritic cells depending on the initiators. PMA was used to stimulate adherence of the cells and to differentiate the U937 cells into macrophages. The cells were differentiated for 72 hours at 25 nM PMA concentration. **Figure 20** shows inverted light microscopy images of the morphology and size of U937 cells and PMA-induced differentiated cells at 40x magnification. In **Figure 20 A,** U937 cells are suspension cells and have a smaller size with round morphology. Following PMA induction, the cells become adherent and bigger in size relative to U937 suspension cells as shown in **Figure 20 B**. However, the macrophages still maintain their round morphology.

A.

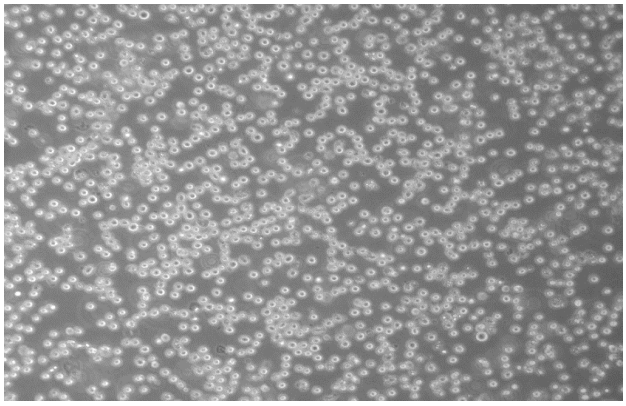

B.

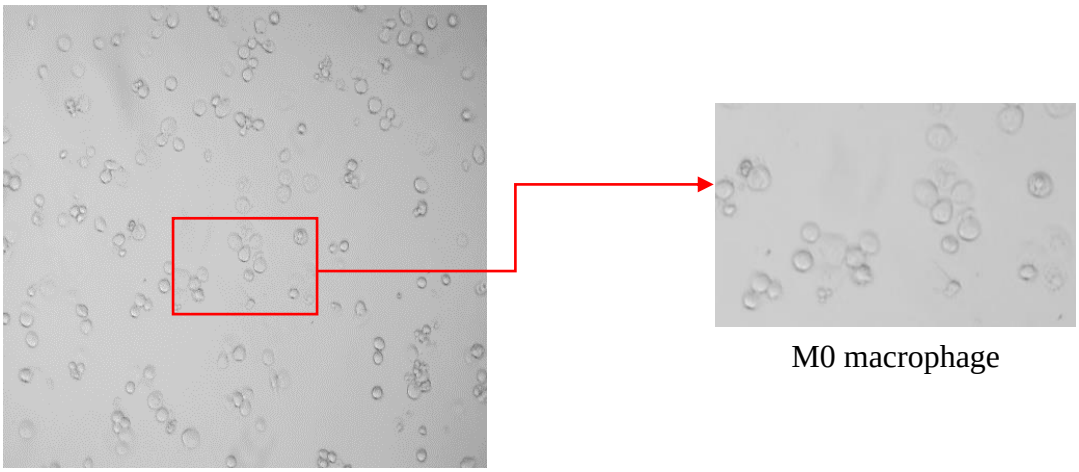

Figure 20: Microscopy image showing the morphology of human myeloid leukaemia cell line (U937) and M0 macrophages under an inverted light microscope (40x). (A) U937 cells are suspension cells, and they have a round morphology and are small as shown. (B) U937 cells after PMA-induced differentiation into M0 macrophages that adhere to the flask and are bigger in size with a round morphology.

5.3.2 Atherosclerotic cell culture model

M0 macrophages were treated with oxidized LDL to create foam cells, which are lipid-laden macrophages to model atherosclerotic cells. Thereafter, oil red staining was performed to confirm that the cells took up the oxidized LDL to form foam cells by using Oil Red O to stain and visualize lipids. **Figure 21** shows an inverted light microscopy image (100x) of foam cells

formed using 100 µg/ml oxidized LDL, this concentration is mostly used in literature (Nagy *et al.*, 1998).

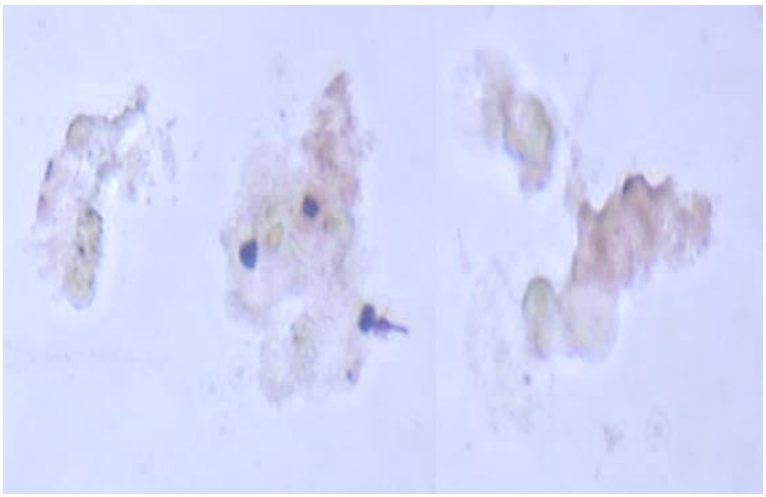

Figure 21: Inverted light microscopy (100x) image of foam cells stained using Oil Red O staining at 100 µg/ml oxidized LDL concentration. The lipids in the cells were stained red by the stain as shown above. The Oil Red O staining confirmed that 100 µg/ml oxidized LDL induced foam cell formation in M0 macrophages.

5.3.3 Cell viability after encapsulated LRP treatment

An MTT assay was used to quantify and assess cellular viability based on the metabolic activity reflected by viable cells. This assay was performed as an optimization assay to determine the optimum treatment of PLGA encapsulated LRP for human myeloid leukaemia cell line (U937). **Figure 22** shows the cell viability of U937 cells and foam cells after treatment with PLGA encapsulated LRP at 75 µg/ml, 100 µg/ml, and 150 µg/ml concentration of nanoparticles. For both cell lines, untreated cells were set to 100% cell viability and data was analysed relative to the untreated cells. In U937 cells, the 75 µg/ml treatment caused a significant 72.77% cell viability increase compared to the untreated cells. The cell viability was also significantly increased at 100 µg/ml by 154.89% compared to untreated cells. Lastly, cell viability was significantly increased by 75.32% for 150 µg/ml treatment. From these results, LRP treatment was determined to increase proliferation of non-atherosclerotic cells. Cellular viability for 100 µg/ml empty nanoparticle treatment was 94.47% and the decrease in cell viability was not significant. Therefore, PLGA nanoparticles not only serve as a viable *in vitro* delivery system but when encapsulating LRP improve cell viability of normal cell lines. Due to the significant effect

of encapsulated LRP treatment on U937 cells, the treatment was investigated on foam cells to determine their ability to rescue diseased cells from the atherosclerotic state.

In foam cells, the 75 µg/ml treatment caused a significant decrease in cell viability by 45.4% compared to the untreated foam cells. The cell viability was also significantly decreased at 100 µg/ml by 61.6% compared to untreated foam cells. Moreover, cell viability was significantly decreased by 38.2% for 150 µg/ml treatment in comparison to the untreated foam cells. Therefore, LRP treatment on foam cells did not increase their cell viability but instead decreased it suggesting that its cardioprotective mechanism may be carried out through apoptosis of the foam cells in the progression of atherosclerosis.

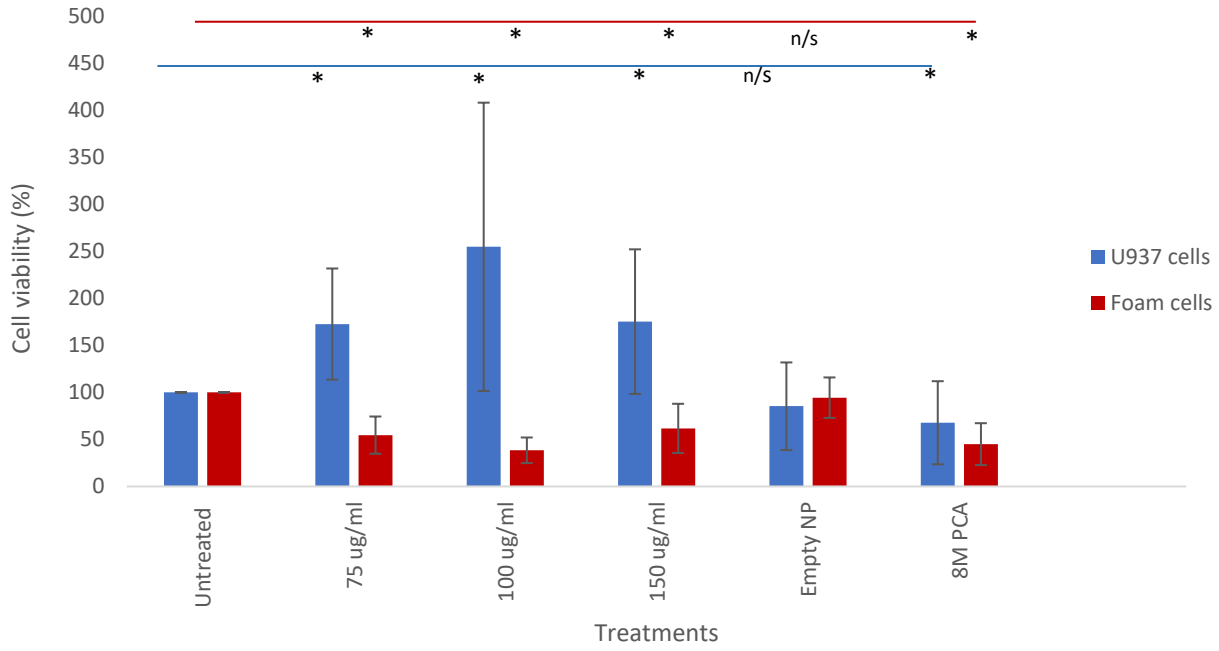

Figure 22: Cell viability of U937 cells and foam cells of LRP encapsulated nanoparticles (75 µg/ml, 100 µg/ml, and 150 µg/ml) and 100 µg/ml empty nanoparticles. Untreated U937 cells (blue) were set to 100% cell viability and data was analysed relative to the untreated cells. For 75 µg/ml treatment, cell viability was significantly increased (*p=0,014680) by 72.77% than the untreated cells. For 100 µg/ml treatment, cell viability was significantly increased (*p=0,017778) by 154.89% relative to untreated cells. Cell viability for 150 µg/ml treatment was 75,32% significantly higher (*p=0,016288) than untreated cells. The decrease for empty nanoparticle treatment was not significant (p=0.290362), cell viability decreased by 5,53%. Untreated foam cells (red) were set to 100% cell viability and data was analysed relative to the untreated cells. The 75 µg/ml treatment caused a significant decrease (*p=0,015919895) in cell viability by 45.4% compared to the untreated foam cells. The cell viability was also significantly decreased (*p= 0,011569922) at 100 µg/ml by 61.6% compared to untreated foam cells. Moreover, cell viability was significantly decreased (*p=0,029834829) by 38.2% for 150 µg/ml treatment in comparison to the untreated foam cells. On the other hand, cell viability for 100 µg/ml empty nanoparticle treatment was decreased by 5.6% with viability at 94.4% confirming that the nanoparticles are a viable delivery system. The decrease in cell viability was statistically not significant (p=0,329877671). For the positive control treatment group (8 M PCA), cell viability was significant decreased (*p=0,038715027) by 55%. Standard deviation is shown by the error bars, n - 3 biological repeats. n/s= not significant *p <0.05, **p<0.01 and ***p<0.001; Students t-test.

6. Discussion

6.1 37 kDa LRP overexpression, purification, and characterization

Isolating pure 37 kDa LRP protein is an important aspect of this research to evaluate how the protein can be used in cardiovascular diseases as a potential treatment. LRP is a multi-localized protein that plays a role in cell migration, adhesion, and migration but it is also involved in several pathological processes including cancer progression, and the internalization of bacteria and viruses. Furthermore, it has been shown to mediate cardioprotective effects hence the project focused on producing LRP. The first part of this project focused on the overexpression, purification, and characterization of the 37 kDa LRP protein to assess its structural and functional integrity.

6.1.1 Expression and purification of LRP

In this study, the full length (1-295 residue) 37 kDa LRP was successfully overexpressed. This was performed using transformed T7 Express Competent *E. coli* with the constructed plasmid. The inserted *LRP* gene was confirmed to be without mutations and 100% aligned to the reference sequence using Clustal Omega. Therefore, the overexpressed protein was coded for by the inserted (reference) sequence as shown in **Figure 6.** Overexpression trials were then conducted to determine optimal conditions for the expression of the protein. IPTG concentration, used to induce gene expression, and time were investigated for overexpression. Firstly, 1.0 mM IPTG concentration was investigated for induction because it is the recommended concentration (Mühlmann *et al.*, 2017). Supernatant and pellet samples were then collected at time points 4, 6, 8 and 12 hours. **Figure 7 A** shows that the expressed protein was at a low yield and found in the pellet. This means that a substantial fraction of the protein was insoluble. Furthermore, due to the low yield obtained at 1.0 mM IPTG a lower concentration of IPTG was investigated for induction. Lower IPTG concentrations ranging from 0 to 0.4 mM have been shown to result in higher induction because it increases the activity and solubility of the protein of interest (Mühlmann *et al.*, 2017). As a result, 0.3 mM IPTG was investigated, and a higher yield of protein was obtained as shown in **Figure 7 B** after 8 hours. Thus, 0.3 mM IPTG was used to induce the overexpression of LRP to produce a higher yield. However, the protein was still insoluble.

Prior to solubilization, a linear regression model (**Figure 8**) was constructed to determine the molecular weight of the overexpressed protein.

The molecular weight was determined to be ~47 kDa which is higher than the expected 37 kDa. According to Barsoum *et al.,* LRP migrates at approximately 37-44 kDa molecular mass on an SDS-PAGE. In addition, the His-tag has a molecular weight of ~2.5 kDa therefore, this can account for the observed 47 kDa molecular mass in **Figure 8.** However, it can also be noted that the addition of the His-tag does not interfere with protein structure and function hence it will not interfere with downstream characterisation of recombinant LRP (Booth *et al.*, 2018).

The transmembrane region of LRP is located between amino acid residues 86-105 (Rao *et al.*, 1983). This region makes the protein primarily an insoluble protein due to its hydrophobicity thus it was solubilized using a non-ionic detergent containing 2% (w/v) Triton X-100. The solubilisation of membrane proteins disrupts the native membrane environment through detergent interaction with the hydrophobic regions of the protein thus forming micelles around the protein (Ratkeviciute *et al.*, 2021). Triton X-100 also maintains protein stability, function and interactions thus it balances the solubilisation efficacy and protein stability and structure (Ratkeviciute *et al.*, 2021). The SDS-PAGE gels in **Figure 9** indicate that higher fractions of solubilized proteins (supernatant) were predominantly found in Wash 1C to Wash 1E (W1C-W1E). Several washes were carried out on the overexpression lysate to maximally extract LRP. The lack of isolated LRP in the SDS-PAGE gel in **Figure 9 A (W1A-W1B)** was a result of the protein not being solubilized into solution yet and as more washes were carried out LRP was then solubilized into solution **Figure 9 (W1C-W1E)** due to the formation of micelles around hydrophobic regions of LRP hence solubilizing it into solution. The protein was completely extracted from the lysates as shown in **Figure 9 (W1-W1G)** by the absence of LRP detection. Due to the presence of contaminating bands, the solubilized protein was then purified using IMAC.

The overexpressed protein had a histidine tag hence it was purified using IMAC. The soluble lysate was purified on a Ni^{2+} and Co^{2+} charged IMAC columns to improve the purity and yield of LRP (Csibra and Stan, 2021). Furthermore, nickel and cobalt matrices are known to tolerate non-ionic detergents to a limited amount (Bornhorst and Falke, 2000). Firstly, the nickel column was

used to purify LRP from the lysate due to its known high affinity for the his-tag compared to cobalt (Bornhorst and Falke, 2000). The lysate was loaded onto the nickel column for purification. However, the eluted fraction was not pure and contained contaminating bands in the eluted fractions (**Figure 10 B (E 3 and 4)**. The impurities in the elution fractions may be due to host cell proteins that contain histidine hence they can bind to the nickel ion charged resin due to its high affinity for histidine (Rubiyana *et al.*, 2015). As a result, these proteins are coeluted with the his-tagged protein resulting in the contamination seen in the gels. Therefore, the column was charged with cobalt instead. Cobalt has a lower binding affinity for the his-tag in comparison to nickel and less non-specific protein binding thus exhibiting more specific interaction with the his-tag (Bornhorst and Falke, 2000). Therefore, it results in higher elution product purity. The soluble protein lysate was loaded on to the column for purification and resulted in less non-specific binding of contaminants (**Figure 11 B (SW)**) and a relatively high yield of his-tag LRP (**Figure 11 B (E4, 5 and 6)**). High protein purity was also observed for the purified protein in **Figure 11 B (E4, 5 and 6)** compared to nickel IMAC.

Densitometric analysis performed on the SDS-PAGE in **Figure 11 B** indicated that the protein was at least 85% pure. A two-step purification method of using affinity chromatography and size exclusion chromatography (SEC) has been previously shown to result in high purity (purity > 90%) and yield (Stressler *et al.*, 2017). SEC is a chromatographic method that separates molecules based on their size and hydrodynamic volume through a gel (Hong *et al.*, 2012). However, it is not suitable for the purification of proteins solubilized using detergents because detergents alter the hydrodynamic conformation, hence migration behaviour, of proteins due to the protein-detergent complex (Kunji *et al.*, 2008). As previously mentioned, detergents stabilize membrane proteins by assembling into micelles by shielding the hydrophobic core in the micelle core and exposing the hydrophilic groups and as a result this alters hydrodynamic volumes of the protein. Hence, even though advisable for secondary purification, SEC is not a suitable technique for LRP purification. Therefore, for LRP purification, cobalt IMAC is preferred compared to nickel IMAC based on its capability to isolate LRP at high purity and relatively high yield.

The samples from the cobalt IMAC were collected and western blotting was performed using the anti-LRP/LR IgG1-iS18 (Affimed, Heidelburg, Germany) to confirm the presence of the protein of interest before downstream characterization. **Figure 12** confirmed that 47 kDa LRP was

purified and the 67 kDa laminin receptor was also detected in the eluted fraction. This is possibly due to the fact that the 67 kDa laminin receptor is derived from the 37 kDa LRP through acylation as a post translational modification that occurs in both eukaryotic and prokaryotic cells (Hentchel and Escalante-Semerena, 2015; DiGiacomo and Meruelo, 2016). Moreover, due to the chemiluminescence detection used during western blotting the high sensitivity results in detection of multiple proteins (Berkelman, 2020). The 67 kDa isoform of LRP was detected due to the high sensitivity of western blotting for low protein concentrations which is better at detection compared to the Coomassie stain (Xiang et al., 2021)

6.1.2 Protein purity and concentration

Following western blotting, further characterization was performed on the purified protein before structural characterization. This was to determine nucleic acid contamination and protein concentration using absorbance spectroscopy. **Figure 13** shows the absorbance spectrum of LRP and from the spectrum, different properties of LRP were determined. The peak observed at 280 nm is due the presence of aromatic amino acids tyrosine, phenylalanine, and tryptophan in LRP. These aromatic amino acids absorb UV light at 280 nm due to the resonance in benzene, phenol, and indole aromatic rings as a result of delocalisation of π-electrons (Reinmuth-Selzle *et al.*, 2022). The absorbance at 280 nm was also used to determine the concentration of LRP using the equation in **4.1.8.1** as 12.6 μM. This concentration of protein was sufficient for subsequent characterization. Furthermore, nucleic acid contamination was determined from the absorbance spectrum using absorbance at 260 and 280 nm. Nucleic acids are known to absorb UV light at 260 nm. Therefore, the A_{260}/A_{280} ratio was used to determine nucleic acid contamination. A A_{260}/A_{280} ratio between 1.8-2.0 is accepted as pure nucleic acid and a lower ratio (A_{260}/A_{280} < 0.6) is considered as a lack of nucleic acid contamination in protein samples (Berglund *et al.*, 2007). A A_{260}/A_{280} ratio of 0.65 was determined indicating that the purified protein was sufficiently free from nucleic acid contamination. The A_{260}/A_{280} ratio for the purified protein sample was slightly higher than the ideal 0.6 and this can be attributed to the trace amounts of Triton X-100 in the sample buffer. Even though the sample was dialysed before absorbance spectroscopy, Triton X-100 in the sample strongly absorbs in the UV region near the analysis wavelength of 280 nm hence it interferes with the A_{260}/A_{280} ratio (Terada *et al.*, 1985). Moreover, there is a shoulder at 295 nm of the absorbance spectrum due to 10 tryptophan residues present

in the protein because the absorbance at 295 nm is exclusively due to tryptophan residues in protein (Bobone *et al.*, 2014). The presence of tryptophan residues in the protein will allow for intrinsic tryptophan fluorescence to determine the tertiary structure of the protein downstream. Absorbance at 340 nm represents protein aggregation therefore, the lack of absorbance at 340 nm suggests that little to no aggregation was detected in the protein sample. Protein aggregation is associated with the loss of protein function hence the protein cannot be assessed using other assays. Therefore, the lack of aggregation in the sample means that the protein purified is functional and can be used for downstream analysis. Therefore, the purified protein was sufficient for downstream characterization.

6.1.3 Structural characterization of LRP

Structural characterization of LRP was important following overexpression and purification of the protein. This was performed to ensure that the secondary and tertiary structure, hence stability of the protein, were not altered. The secondary structure of LRP was assessed using far-UV circular dichroism. The spectrum for the purified LRP (**Figure 14**) showed the CD spectrum of LRP. The spectrum has a peak at 189 nm and a trough at 207 nm. Therefore, this spectrum is indicative of a predominantly α-helical protein. The CD spectrum of alpha helical proteins is typically characterized by a negative band around 208 nm and 222 nm as well as a positive band around 190 nm (Greenfield, 2006). The secondary structure of LRP has been characterized as containing 4 helices in the core of the protein with an N-terminal domain consisting of an α helix (Jamieson *et al.*, 2008). Therefore, this confirms that the purified protein contains the native secondary structure, and the protein was not altered during purification.

LRP was further characterized using ITF to determine the tertiary structure of the purified LRP protein. **Figure 15** shows the emission spectra of LRP in the absence and presence of 8 M urea denaturant to determine if the protein was correctly folded. Urea was used as a denaturant to denature the protein and expose the hydrophobic regions of the protein. The protein was excited at 280 nm and 295 nm because all fluorophores are excited at 280 nm but excitation at 295 nm is exclusive to tryptophan residues in the protein. Quenching (decrease in intensity) and a bathochromic shift which is a change in spectral band position to a longer wavelength (decrease in energy) in the presence of urea are characteristics observed in native that become denatured (unfolded) proteins as an indication of energy transfer (McCubbin and Kay, 1980). Due to the

hydrophobicity of the indole ring in tryptophan residues, when proteins are denatured tryptophan residues are exposed to the polar environment (Palego *et al.*, 2016). Therefore, tryptophan is an ideal residue to study the conformational changes of proteins using spectroscopy and since LRP has 10 tryptophan residues it is a good candidate for ITF spectroscopy (Fontana *et al.*, 1996). Firstly, LRP was excited at 280 nm (blue). There was significant quenching observed at emission wavelength of 342 nm from the native to denatured state of LRP as shown in **Figure 15**. When the protein is in the native state, tryptophan residues are buried in the core thus they are less affected by the presence of quenching water molecules but in denatured proteins (unfolded), the indole rings donate electrons (emission light) to the surrounding water molecules (Möller and Denicola, 2002). Therefore, even though quenching is a good measure of exposed tryptophan residues in proteins it is not sufficient to say that LRP was correctly folded in the native state. Thereafter, LRP was excited at 295 nm (pink) due to selective excitation of tryptophan at this wavelength. The emission spectra for excitation at 295 nm in **Figure 15** shows significant quenching and a bathochromic shift with respect to the native protein. The bathochromic shift was observed from 341 nm to 346 nm in the 295 nm emission spectra. The bathochromic shift is evidence that the tryptophan residues in the native protein were in a hydrophobic environment suggesting that the protein was correctly folded prior to denaturation. Therefore, all the evidence suggests that LRP was correctly folded during overexpression meaning the protein's structure was preserved. As a result, the functionality of the protein could be assessed.

6.1.4 Functional characterization of LRP

Since structural characterization of LRP was conducted and the protein was confirmed to be α-helical and properly folded, functional characterization of LRP was conducted to measure LRP-ligand interaction due to LRPs function as a receptor. Binding assays are conducted to measure molecule interaction, in this study LRP functionality was measured by determining the binding of LRP to laminin-1, its primary ligand. As previously mentioned, the C-terminus domain of LRP has two laminin-binding domains, the peptide G sequence located between 161-180 amino acids and a direct binding region site located between amino acids 205-229 (Castronovo *et al.*, 1991). PFGST was used as a control protein. **Figure 16** shows the relative fluorescence unit of laminin-1 binding to LRP and control protein PFGST. Significantly higher fluorescence was observed between laminin-1 and LRP at 75914.67 in comparison to the binding interaction

between laminin-1 and PFGST at a fluorescence of 28163.67 (*p=0.031674). There is a significant difference in binding because PFGST is a glutathione S-transferase of the malarial parasite *Plasmodium falciparum*. Glutathione S-transferases are enzymes found across different organisms, including mammals, that catalyse the conjugation of glutathione to electrophilic substrates resulting in products that are not toxic to organisms (Hiller *et al.*, 2006). The Glutathione S-transferases proteins have a range of ligands which include pesticides, drugs, hormones, heme and bilirubin therefore the binding observed between LRP and PFGST may be due to non-specific binding (Hiller *et al.*, 2006). Therefore, from these results we could conclude that overexpressed and purified LRP was structural, in addition to its functional characterization, due to its ability to bind to laminin-1 in comparison to PFGST.

Therefore, LRP was successfully overexpressed, purified, and characterized. Purified LRP of high yield and purity (85%) was determined from the SDS-PAGE gel from IMAC purification. The western blot confirmed that the purified protein was the recombinant LRP at 47 kDa and from absorbance spectroscopy the protein was determined to be free from nucleic acid contamination and aggregation. Structural characterization confirmed that the protein was α-helical and properly folded. Binding affinity assay confirmed the protein was functional. Therefore, these results show that the proteins' structure and function was preserved after purification. Therefore, the protein could be encapsulated into PLGA nanoparticles for delivery.

6.2 Encapsulation of LRP into PLGA nanoparticles and characterization of the nanoparticles

The second aim of this study focused on characterization of encapsulated LRP. Therefore, due to the successful characterization of the protein, encapsulation of LRP could be performed for delivery *in vitro*. The nanoparticles were characterized using scanning electron microscopy, dynamic light scattering and leakage test.

6.2.1 Scanning electron microscopy and dynamic light scattering

The double emulsion and solvent evaporation method was used to synthesize the PLGA nanoparticles because it is the most appropriate method to encapsulate hydrophilic drugs such as vaccines, peptides, and proteins (Lü *et al.*, 2009). As a result, in this study LRP was encapsulated into the nanoparticles and the nanoparticles were imaged using SEM to determine the

morphology of the nanoparticles. The method used for synthesis ensures that the synthesized nanoparticles have a spherical morphology. As previously mentioned, a spherical morphology results in maximum encapsulation of drugs (Zhao *et al.*, 2017). Moreover, spherical nanoparticles are also easily degraded due to their higher surface area (Zhao *et al.*, 2017). Furthermore, cells readily endocytose spherical nanoparticles. Therefore, the spherical morphology observed in **Figure 17** was favourable. The image in **Figure 17** also shows that the nanoparticles have varying sizes as they were synthesized between 200-400 nm. Nanoparticles ranging between 10-1000 nm are used for delivery of drugs due to their ability to penetrate vessels and tissue for cellular uptake (Huang and Zhang, 2018). Cellular uptake of nanoparticles with a diameter less than 200 nm and nanoparticles larger than 200 nm is mediated through receptor-mediated endocytosis and phagocytosis, respectively (Huang and Zhang, 2018). The nanoparticles in this study were synthesized between 200-400 nm size range to balance nanoparticle size, cellular uptake and drug loading efficiency (Wang *et al.*, 2013). For increased drug-uptake, nanoparticle size less than 500 nm are favourable due to increased uptake in cells, tissues and organs (Wang *et al.*, 2013; Pala *et al.*, 2020). Furthermore, nanoparticles larger than 1000 nm result in the foreign body reaction. When the foreign body reaction is initiated through inflammation, the immune cells attempt to degrade the foreign material (Carnicer-Lombarte *et al.*, 2021). If the foreign material bypasses this stage, fibroblasts endocytose the nanoparticles to isolate it from circulation. (Carnicer-Lombarte *et al.*, 2021). Therefore, DLS analysis on the nanoparticles was performed to determine the size distribution and hydrodynamic size of the nanoparticles as shown in **Figure 18**. The polydispersity index was used to estimate the homogeneity of particles in solution and Z-average size was used to estimate the average diameter of the nanoparticles. For nanoparticles encapsulating LRP, the PdI was 0.45 and Z-average size was 221 nm. The size distribution of these nanoparticles was narrow with an average size of 221 nm. Therefore, for this sample the nanoparticle size was favourable for cellular uptake and drug loading efficiency. Empty nanoparticles had a narrow size distribution (PdI = 0.43) however the mean average size from the Z-average size analysis was much higher than the expected 200-400 nm size range at 857 nm. Although this is within the 10-1000 nm size range required for cellular uptake it is still high given that the nanoparticles were synthesized using the same protocol. This may be due to large aggregates that formed during lyophilization that sedimented during rehydration of nanoparticles for DLS analysis (Kosinski *et al.*, 2012). As

a result, the Z-average mean from DLS analysis is higher than the expected size but the size distribution is uniform. To correct this, the samples can be sonicated in a water bath sonicator or vortexed to separate the aggregate before DLS. In future studies, PEGylation of the nanoparticles increases hydrophilicity by forming hydrogen bonds between ethers and the solvent (Jokerst *et al.*, 2011). Therefore, in future studies the nanoparticles can be PEGylated so that during rehydration the aggregates are easily disrupted and to enhance cellular uptake.

Following the structural characterization and size distribution of the nanoparticles, the release profile of LRP from the nanoparticles was assessed using a leakage test.

6.2.2 Release profile of LRP from nanoparticles

Determining the drug release profile of a polymer system is important because it provides information about drug release kinetics. Drug release is the process of drug migration from the interior of nanoparticles to the outer surface of the nanoparticles and then the medium (Fu and Kao, 2010). The release profile of PLGA nanoparticles is characterized by an initial burst release phase followed by a zero order phase (Cam *et al.*, 2020). **Figure 19** shows that there was a burst release of LRP from the nanoparticles followed by a zero order (sustained) release after 8 hours. The burst releases observed are the rapid release of LRP associated with the surface of the nanoparticles whereas the low points in the graph are associated with aggregation of the nanoparticles hence there was no protein release (Fu and Kao, 2010). From 8 hours, the PLGA nanoparticles undergo bulk-erosion where the polyester chains undergo degradation through chain scission to release the encapsulated LRP hence the observed sustained release (Burkersroda *et al.*, 2002). As the chain scission occurs, the aqueous solution diffuses inside the matrix and drives the degradation of the nanoparticles and release of the protein from the nanoparticles (Burkersroda *et al.*, 2002). This results in favourable release of the therapeutic *in vitro* and *in vivo* because it will improve targeted drug delivery and lead to a sustained release of LRP over an extended period. Therefore, the release profile of LRP from the nanoparticles is similar to the release profiles observed for PLGA nanoparticles. Furthermore, this proves that LRP was successfully encapsulated and released.

Therefore, the synthesized PLGA nanoparticles encapsulating LRP had favourable characteristics which include a spherical morphology, narrow size distribution with average size of 221 nm. The release profile illustrated that LRP was successfully encapsulated and released

thus PLGA nanoparticles could function as a delivery system. Therefore, the encapsulated protein could be assessed as a potential treatment for cardiovascular disease on an atherosclerotic cell culture model.

6.3 Assessing encapsulated LRP as treatment for cardiovascular disease

The development of the drug was to evaluate it as a potential treatment for cardiovascular disease. Cardiovascular diseases are the world's leading cause of death with atherosclerosis as the most common underlying cause. Therefore, the third aim of this project focused on evaluating the treatment on an atherosclerotic cell culture model developed using PMA and oxidized LDL.

6.3.1 Cell culture models

The cell line cultured in this study was U937 cells which are monocytic suspensions cells characterized by their round morphology as shown in **Figure 20 A.** Depending on the stimuli the cells are differentiated into different cells. In this study, PMA was used to differentiate U937 cells into naïve macrophages as shown in **Figure 20 B.** The cells become adherent and bigger in size relative to U937 cells with macrophages maintaining a round morphology. The differentiation of monocytes to macrophages observed are due to different pathways being activated in the cells. This differentiation occurs through the activation of the NF- κB through the protein kinase C (PKC) pathway (Kuno *et al.*, 2020). PKC is activated by PMA because PMA is an analogue of a strong activator of PKC known as diacyl glycerol (Song *et al.*, 2015). As stated previously, NF- κB activation leads to pro-inflammatory cytokine expression during atherogenesis (Liu *et al.*, 2017). However, the morphological changes and cell adherence are due to activation of the RhoA/Rho-associated protein kinase (RhoA/ROCK) pathway (Kuno *et al.*, 2020). The RhoA/ROCK pathway regulates the cytoskeletal dynamics involved in growth, differentiation, and development of the cells through phosphorylation of downstream targets which include the filament actin (Deng *et al.*, 2019). Hence the cells acquire the ability to adhere to the plates as shown in **Figure 20 B**. The concentration used to differentiate the monocytes was 25 nM PMA for 24 hours due to its ability to maintain cell viability over 80% and maintain a significant percentage of macrophages in the samples after treatment (Kuno *et al.*, 2020). To improve imaging of macrophage to illustrate better morphological changes associated with differentiation, May-Grünwald-Giemsa staining and bright field microscopy could be useful

tools. These techniques would show changes in nuclear morphology, an increase in the cytoplasmic ratio and cytoplasmic vacuolization formation which are morphological changes also associated with macrophages (Kuno *et al.*, 2020). Following naïve macrophage formation, the cells were treated with oxidized LDL to produce foam cells. In fatty streak formation, oxidized LDL endocytosis by macrophages through scavenger receptors leads to foam cell formation (Steinl and Kaufmann, 2015). The foam cells are present from fatty streak formation until thrombosis which is the last stage of atherosclerosis pathogenesis making the cells a good model for this study. Foam cell formation was confirmed using lipid (Oil Red O) staining and light microscopy as shown in **Figure 21**. From **Figure 21**, the foam cells can be seen by red stained fats and triglycerides. Therefore, now that the atherosclerotic cell culture model has been developed, encapsulated LRP could be investigated as a potential treatment for cardiovascular disease.

6.3.2 Cell viability after encapsulated LRP treatment

The monocytic U937 cells and foam cells were treated with encapsulated LRP as a potential therapeutic to determine the optimal effective dose that mitigates atherosclerosis progression. An MTT assay was performed on both cell models to determine the viability of the cells after treatment. The U937 cells were used as a non-atherosclerotic model in comparison to the diseased foam cells. **Figure 22** shows the cell viability of U937 cells and foam cells after treatment with PLGA encapsulated LRP at 75 µg/ml, 100 µg/ml, and 150 µg/ml concentration of nanoparticles. The treatments were investigated on U937 cells to determine the effects of the treatment on cells that are not diseased. Treatment with encapsulated LRP resulted in significant increases on the cellular viability of U937 cells. The 75 µg/ml of encapsulated LRP treatment caused a significant 72.77% cell viability increase compared to the untreated cells. The cell viability was significantly increased at 100 µg/ml and 150 µg/ml by 154.89% and 75.32%, respectively. As a result, this treatment results in increased proliferation of non-atherosclerotic cells because LRP is involved in cellular differentiation, proliferation and survival of cells (Omar *et al.*, 2012; Otgaar *et al.*, 2017; Baichan, 2018). Therefore, the low concentration of encapsulated LRP at 75 µg/ml could be more favourable to prevent excessive proliferation and the development and survival of cancerous cells. Furthermore, since U937 cells are a monocytic cell line and monocytes are recruited to accelerate inflammation and for macrophage formation

in atherosclerosis progression the proliferation of the cell line as a possible side effect should be maintained at low proliferation levels (Crowther, 2005; Steinl and Kaufmann, 2015).

Due to the significant effect of encapsulated LRP treatment on U937 cells, the treatment was investigated on foam cells to determine its therapeutic effect in advanced lesions. The premise of this investigation is based on the proposition that reducing the formation of foam cells, or inducing their removal, might represent an effective therapeutic strategy against the disease (Javadifar *et al.*, 2021). In **Figure 22**, it is shown that the 75 µg/ml treatment caused a significant decrease in cell viability by 45.4%. The cell viability was also significantly decreased at 100 µg/ml and 150 µg/ml by 61.6% and 38.2%, respectively. Since the cell viability of the foam cells was decreased it is suggested that LRP performs its therapeutic effect by inducing the removal of foam cells in early lesion. Even though LRP/LR is a receptor involved in cell survival the treatment had an anti-proliferative effect on foam cells by resulting in decreased viability of the cells. Foam cells can be degraded through the breakdown of the esterified cholesterol and secretion of the cholesterols in the cells through efflux receptors and pathways in a process known as reverse cholesterol transport (Yu *et al.*, 2013). Oxidized LDL in foam cells undergoes esterification for storage and to allow for increased endocytosis of oxidized LDL. Therefore, LRP treatment may be involved in the de-esterification of esterified cholesterol in foam cells to free cholesterol through hydrolysis by cholesterol esterase (Heidrich *et al.*, 2004). This results in efflux of the cholesterol through diffusion or efflux receptors. Transport-mediated efflux of cholesterol occurs through ATP-binding cassette (ABC) transporters (ABCA1 and ABCG1) and scavenger receptor class B type 1 (SR-B1) (Yu *et al.*, 2013). HDL accepts the cholesterol and transports it to the liver for excretion. Therefore, this results in the regression of foam cells slowing down lesion progression. It can also be hypothesized that efferocytosis of the apoptotic cells is enhanced to suppress an inflammatory response in the plaque (Seimon and Tabas, 2009). Efferocytosis in atherosclerosis is the clearance of apoptotic cells by phagocytic cells to suppress a proinflammatory response in the plaque by recognizing “find me” signals (Ge *et al.*, 2022). There is a significant decrease in cellular viability observed at the 75 µg/ml. Therefore, the overall effect would be a reduction in foam cell burden contributing to lesion progression and the size of the plaque (Seimon and Tabas, 2009). A potential target for LRP would be macrophages in early stages of lesion progression. Targeting the macrophages for apoptosis results in rapid phagocytosis of the apoptotic cells slowing down the progression of atherosclerosis to stabilize

the plaque and keeping it small (Neels *et al.*, 2023). The higher efferocytosis rate at this stage is due to macrophages producing less oxidized LDL compared to foam cells (Neels *et al.*, 2023). Furthermore, reverse cholesterol transport in macrophages could provide a more aggressive therapeutic intervention as it will halt progression of macrophages to foam cells thus slowing down atherosclerosis pathogenesis. However, further in-depth research needs to be conducted to properly detail the therapeutic mechanisms and for therapeutic exploration of foam cells. Furthermore, PLGA nanoparticles at 100 µg/ml were determined to be a viable *in vitro* delivery system because cellular viability for cells treated with empty nanoparticles did not significantly decrease. Therefore, PLGA nanoparticles exhibit minimal cytotoxicity in the cells.

7. Conclusion

In conclusion, the first part of this study illustrated that recombinant LRP was successfully overexpressed in *E. coli* cells as a 47 kDa recombinant protein. The recombinant protein was successfully purified using IMAC and characterized to develop the potential treatment for cardiovascular. Structural characterization of the protein confirmed recombinant LRP was predominantly α-helical and correctly folded. Moreover, the laminin-binding assay confirmed the recombinant LRP was functional hence it was encapsulated into PLGA nanoparticles to develop an *in vitro* delivery system for the recombinant protein. Following encapsulation, the nanoparticles were characterized using SEM demonstrating a favourable spherical morphology and DLS showed that the nanoparticles had a narrow size distribution of 221 nm which is advantageous for cellular uptake and drug loading efficiency. Furthermore, the leakage test performed showed that the nanoparticles followed the release profile of PLGA nanoparticles. Where initial bursts were observed followed by sustained release of the protein. The last part of this study focused on assessing the encapsulated protein as a potential treatment for cardiovascular disease. Therefore, an atherosclerotic cell culture model was successfully produced to assess encapsulated LRP. The MTT assay was performed as an optimization assay to determine the concentration of encapsulated LRP treatment with the most therapeutic effect. From this, 75 µg/ml of encapsulated LRP treatment resulted in the most plausible therapeutic effect at a relatively low dose through a possible mechanism of reverse transport of cholesterol and apoptosis of foam cells. Furthermore, empty nanoparticles were determined to be a viable delivery system at 100 µg/ml because they did not result in significant cellular cytotoxicity. In

conclusion, a novel therapeutic was developed for the potential treatment of cardiovascular diseases. The *in vitro* studies implicate that LRP has a role in cardiovascular disease as a result further studies need to be conducted to gain insight into the molecular pathways involved in potential treatment of the disease.

7.1 Future studies

For future studies, crystallization of the 37 kDa LRP full-length protein crystal structure will be an interesting result as only a partial length of the protein has been crystallized by Jamieson *et al.,* 2008 from amino acid residues 1-220. Crystalizing LRP will allow for X-ray diffraction analysis and the X-ray diffraction patterns of the crystal can be used to determine the 3D structure of the full-length protein.

In cell studies, the treatment groups for further studies can be expanded to include untreated U937 cells, untreated M0 macrophages and LRP treated M0 macrophages for proper comparison between the groups to determine the stages at which LRP carries out its therapeutic intervention. M0 macrophages will give us insight into therapeutic interventions at the early stage of lesion progression. The therapeutic efficacy of encapsulated LRP could be assessed by performing the following assays: MTT assay, lipid test, quantitative PCR (qPCR) to determine mRNA expression levels of key proteins involved in atherosclerosis to give information on gene expression. Another beneficial technique that could be conducted is proteomic analysis. From proteomic analysis, expression levels of proteins involved in atherogenesis and rescuing of the cells from atherosclerosis pathogenesis will be identified and the molecular pathways involved in LRP as a potential treatment will be mapped out and compared to the untreated samples. Furthermore, western blotting will be performed to identify the effect of the encapsulated LRP on levels of key proteins involved in atherosclerosis such as LDL, MCP-1, IL-1β, VCAM-1, vWF and tissue factor.

Following adequate *in vitro* analysis, an *in vivo* animal study would be crucial to assess the therapeutic effects of LRP on cardiovascular disease. Physiological tests such as blood pressure, heart rate and lipid profiling can be conducted before and after treatment to assess the effect of the treatment on the physiological state of the animal. Organs would also be harvested to perform

gene and protein quantification utilising qPCR and western blotting to determine expression levels of the proteins identified during the *in vitro* proteomic analysis.

7.2 Study limitations

Further cell studies could not be conducted due to time constraints. If time permitted, MTT assay on a macrophage cell line were going to be performed to determine the effect of the treatment at early stages of the lesion. Moreover, experiments such as western blotting would have been conducted to give insight into levels of LRP after treatment with the encapsulated LRP and to also assess the levels of cardiovascular disease markers. Furthermore, lipid tests would have given insight into the percentage of foam cells after treatment.

8. References

Akache B., Grimm D., Pandey K., Yant S. R., Xu H., Kay M. A. (2006). The 37/67-kilodalton laminin receptor is a receptor for adeno-associated virus serotypes 8, 2, 3, and 9. *Journal of Virology*, 80(19): 9831-9836.

Almeida S. O., Budoff M. (2019). Effect of statins on atherosclerotic plaque. *Trends in Cardiovascular Medicine*, 29(8): 451–455.

Andersen D.C., Krummen L. (2002). Recombinant protein expression for therapeutic applications. *Current Opinion in Biotechnology*, 13(2): 117–123.

Barsoum A. L., Liu B., Rohrer J. W., Coggin J. H., Tucker J. A., Pannell L. K., Schwarzenberger P. C (2009). Production, safety and antitumor efficacy of recombinant Oncofetal Antigen/immature laminin receptor protein. *Biomaterials*, 30(17): 3091-3099.

Basatemur G. L., Jørgensen H. F., Clarke M. C. H., Bennett M. R., Mallat Z. (2019). Vascular smooth muscle cells in atherosclerosis', *Nature Reviews Cardiology*, 16(12): 727–744.

Bellot G. L., Wang X. (2013). Extra-telomeric effects of telomerase (hTERT) in cell death. *Apoptosis*. IntechOpen.

Bennett M. R., Sinha S., Owens G. K. (2016). Vascular smooth muscle cells in atherosclerosis. *Circulation research*, 118(4): 692–702.

Berglund S. R., Schwietert C. W., Jones A. A., Stern R. L., Lehmann J., Goldberg Z. (2007). Optimized Methodology for Sequential Extraction of RNA and Protein from Small Human Skin Biopsies. *Journal of Investigative Dermatology*, 127(2): 349–353.

Berkelman, T. (2020). Fluorescent Western Blotting: High Sensitivity Detection of Multiple Targets. *Current Protocols in Pharmacology*, 88(1): e72.

Blagoev K. B. (2009). Cell proliferation in the presence of telomerase. *PLoS ONE*, 4(2): e4622.

Bobone S., van de Weert M., Stella L. (2014). A reassessment of synchronous fluorescence in the separation of Trp and Tyr contributions in protein emission and in the determination of conformational changes. *Journal of Molecular Structure*, 1077: 68–76.

Bobone S., van de Weert M., Stella L. (2014). A reassessment of synchronous fluorescence in the separation of Trp and Tyr contributions in protein emission and in the determination of conformational changes. *Journal of Molecular Structure*, 1077: 68–76.

Booth W. T., Schlachter C. R., Pote S., Ussin N., Mank N. J., Klapper V., Offermann L. R., Tang C., Hurlburt B. K., Chruszcz M. (2018). Impact of an N-terminal Polyhistidine Tag on Protein Thermal Stability', *ACS Omega*, 3(1): 760–768.

Bornhorst J. A., Falke J. J. (2000). Purification of Proteins Using Polyhistidine Affinity Tags. *Methods in enzymology*, 326: 245–254.

Brophy M.L., Dong Y., Wu H., Rahman H. N. A., Song K., Chen H. (2017). Eating the Dead to Keep Atherosclerosis at Bay. *Frontiers in Cardiovascular Medicine*, 4.

Bush K. (2018). Past and Present Perspectives on β-Lactamases. *Antimicrobial Agents and Chemotherapy*, 62(10): e01076-18.

Burkersroda F., von Schedl L., Göpferich A. (2002). Why degradable polymers undergo surface erosion or bulk erosion. *Biomaterials*, 23(21): 4221–4231.

Bush K. (2018). Past and Present Perspectives on β-Lactamases. *Antimicrobial Agents and Chemotherapy*, 62(10): e01076-18.

Cam M. E., Yildiz S., Alenezi H., Cesur S., Ozcan G. S., Erdemir G., Edirisinghe U., Akakin D., Kuruca D. S., Kabasakal L., Gunduz O., Edirisinghe M. (2020). Evaluation of burst release and sustained release of pioglitazone-loaded fibrous mats on diabetic wound healing: an in vitro and in vivo comparison study. *Journal of The Royal Society Interface*, 17(162), p. 20190712.

Castronovo V., Claysmith A. P., Barker K. T., Cioce V., Krutzsch H. C., Sobel M. E. (1991). Biosynthesis of the 67 kDa high affinity laminin receptor. *Biochemical and Biophysical Research Communications*, 177(1): 177–183.

Chen J., He W., Shen L., Dong H., Yu J., Wang X., Yu S., Li Y., Li S., Luo Y., Sun Y., Qiu H. (2015). The Laminin Receptor Is a Cellular Attachment Receptor for Classical Swine Fever Virus. *Journal of Virology*, 89(9): 4894–4906.

Chyu K., Babbidge S. M., Zhao X., Dandillaya R., Rietveld A. G., Yano J., Dimayuga P., Cercek B., Shah P. K. (2004). Differential Effects of Green Tea–Derived Catechin on Developing Versus Established Atherosclerosis in Apolipoprotein E–Null Mice. *Circulation*, 109(20): 2448–2453.

Clayton K. N., Salameh J. W., Wereley S. T., Kinzer-Ursem T. L. (2016). Physical characterization of nanoparticle size and surface modification using particle scattering diffusometry. *Biomicrofluidics*, 10(5): 054107.

Crowther M. A. (2005). Pathogenesis of atherosclerosis. *Hematology*, 2005(1): 436–441.

Csibra E., Stan, G. (2021). FPCount protocol - Full protocol. Accessed on: 1 February 2024. https://www.protocols.io/view/fpcount-protocol-full-protocol-bztsp6ne.

Da Costa Dias B., Jovanovic K., Gonsalves D., Moodley K., Reusch U., Knackmuss S., Penny C., Weinberg M. S., Little M., Weiss S. F. T. (2013). Anti-LRP/LR specific antibody IgG1-iS18 and knock-down of LRP/LR by shRNAs rescue cells from Aβ42 induced cytotoxicity. *Scientific Reports*, 3: 2702.

Da Costa Dias B., Jovanovic K., Gonsalves D., Moodley K., Reusch U., Knackmuss S., Penny C., Weinberg M. S., Little M., Weiss S. F. T. (2014). The 37kDa/67kDa Laminin Receptor acts as a receptor for Aβ42 internalization. *Scientific Reports*, 4(1): 5556.

Dabagh M., Jalali, P., Tarbell J.M. (2009). The transport of LDL across the deformable arterial wall: the effect of endothelial cell turnover and intimal deformation under hypertension. *American Journal of Physiology - Heart and Circulatory Physiology*, 297(3): H983–H996.

Danhier, F. Ansorena E., Silva J. M., Coco R., Le Breton A., Preatt V. (2012). PLGA-based nanoparticles: An overview of biomedical applications. *Journal of Controlled Release*, 161(2): 505–522.

Deng Z., Jia Y., Liu H., He M., Yang Y., Xiao W., Li Y. (2019). RhoA/ROCK pathway: implication in osteoarthritis and therapeutic targets. *American Journal of Translational Research*, 11(9): 5324–5331.

Department of Health. (2018.) South African Adult Hospital Level Essential Medicines List. Chapter 4: Cardiovascular Conditions. NEMLC Recommendations for Medicine Amendments (2017-2019) Review version 2.0. Accessed on: 20 November 2023. https://knowledgehub.health.gov.za/system/files/elibdownloads/2023-04/Adult%2520Hospital-Cardiovascular%2520NEMLC%2520report%2520for%25202017-9%2520review%2520v2.pdf.

DiGiacomo V., Gando I. A., Venticinque L., Hurtado A., Meruelo D. (2015). The transition of the 37-kDa laminin receptor (RPSA) to higher molecular weight species: SUMOylation OR artifact? *Cellular & molecular biology letters*, 20(4), pp. 571–585.

DiGiacomo V., Meruelo D. (2016). Looking into laminin receptor: critical discussion regarding the non-integrin 37/67-kDa laminin receptor/RPSA protein. *Biological reviews of the Cambridge Philosophical Society*, 91(2): 288–310.

Ding D., Zhu Q. (2018). Recent advances of PLGA micro/nanoparticles for the delivery of biomacromolecular therapeutics. *Materials Science and Engineering: C*, 92: 1041–1060.

Douglas G., Channon K. M. (2014). The pathogenesis of atherosclerosis. *Medicine*, 42(9): 480–484.

Du F., Zhou J., Gong R., Huang X., Pansuria M., Virtue A., Lin X., Wang H., Yang X. (2012). Endothelial progenitor cells in atherosclerosis. *Frontiers in bioscience: a journal and virtual library*, 17: 2327–2349.

Falk E. (2006). Pathogenesis of atherosclerosis. *Journal of the American College of Cardiology*, 47(8): C7–C12.

Falk E., Shah P. K., Fuster V. (1995). Coronary Plaque Disruption. *Circulation*, 92(3): 657–671.

Fargnoli, A.S., Mu A., Katz M. G., Williams R. D., Margulies K. B., Weiner D. B., Yang S., Bridges C. R. (2014). Anti-inflammatory loaded poly-lactic glycolic acid nanoparticle formulations to enhance myocardial gene transfer: an in-vitro assessment of a drug/gene combination therapeutic approach for direct injection. *Journal of Translational Medicine*, 12: 171.

Fatehullah A., Doherty C., Pivato G., Allen G., Devine L., Nelson J., Timson D. J. (2009). Interactions of the 67 kDa laminin receptor and its precursor with laminin. *Bioscience Reports*, 30(2): 73–79.

Fontana L. Rosati L., Sala A., Dobetti L. (1996). Physico-chemical parameters of nitrate esters. A contribution to the choice of a candidate for preclinical development. *Pharmaceutica Acta Helvetiae*, 71(5): 341–343.

Fracassi A., Marangoni M., Rosso P., Pallottini V., Fioramonti M., Siteni S., Segatto M. (2019). Statins and the Brain: More than Lipid Lowering Agents? *Current Neuropharmacology*, 17(1): 59–83.

Fu Y., Kao W. J. (2010). Drug Release Kinetics and Transport Mechanisms of Non-degradable and Degradable Polymeric Delivery Systems. *Expert opinion on drug delivery*, 7(4): 429–444.

Gauczynski S., Peyrin J., Haik S., Leucht C., Hundt C., Rieger R., Krasemann S., Deslys J., Dormont D., Lasmezas C. I., Weiss S. (2001). The 37-kDa/67-kDa laminin receptor acts as the cell-surface receptor for the cellular prion protein. *The EMBO Journal*, 20(21): 5863–5875.

Gavrilov K., Saltzman W.M. (2012). Therapeutic siRNA: Principles, Challenges, and Strategies. *The Yale Journal of Biology and Medicine*, 85(2): 187–200.

Gaziano T., Reddy K.S., Paccaud F., Horton S., Chaturvedi V. (2006). Cardiovascular disease, disease control priorities in developing countries. 2nd edition. The International Bank for Reconstruction and Development / The World Bank. Available at: https://www.ncbi.nlm.nih.gov/books/NBK11767/ (Accessed: 27 April 2022).

Ge Y., Huang M., Yao Y. (2022). Efferocytosis and Its Role in Inflammatory Disorders. *Frontiers in Cell and Developmental Biology*, 10: 839248.

Ghisaidoobe A. B. T., Chung S. J. (2014). Intrinsic Tryptophan Fluorescence in the Detection and Analysis of Proteins: A Focus on Förster Resonance Energy Transfer Techniques. *International Journal of Molecular Sciences*, 15(12): 22518–22538.

Greenfield N. J. (2006). Using circular dichroism spectra to estimate protein secondary structure. *Nature protocols*, 1(6): 2876–2890.

Heidrich J. E., Contos L. M., Hunsaker L. A., Deck L. M., Vander Jagt D. L. (2004). Inhibition of pancreatic cholesterol esterase reduces cholesterol absorption in the hamster. *BMC Pharmacology*, 4: 5.

Hiller N., Fritz-Wolf K., Deponte M., Wende W., Zimmermann H., Becker K. (2006). Plasmodium falciparum glutathione S-transferase—Structural and mechanistic studies on ligand binding and enzyme inhibition. *Protein Science: A Publication of the Protein Society*, 15(2): 281.

Holy E. W., Stampfil S. F., Akhmedov A., Holm N., Camici G. G., Luscher T. F., Tanner F. C. (2010). Laminin receptor activation inhibits endothelial tissue factor expression. *Journal of Molecular and Cellular Cardiology*, 48(6): 1138–1145.

Hong P., Koza S., Bouvier E. S. P. (2012). Size-Exclusion Chromatography for the Analysis of Protein Biotherapeutics and their Aggregates. *Journal of Liquid Chromatography & Related Technologies*, 35(20): 2923–2950.

Horodinschi R., Stanescu A. A., Bratu O. G., Pantea Stoian A., Radavoi D. G., Diaconu C. C. (2019). Treatment with Statins in Elderly Patients. *Medicina*, 55(11): 721.

Huang W., Zhang C. (2018). Tuning the size of poly(lactic-co-glycolic acid) (PLGA) nanoparticles fabricated by nanoprecipitation. *Biotechnology journal*, 13(1): 10.

Hunter S. A., Cochran J. R. (2016). Cell-Binding Assays for Determining the Affinity of Protein–Protein Interactions: Technologies and Considerations. *Methods in enzymology*, 580: 21.

Jamieson K. V., Wu J., Hubbard S. R., Meruelo D. (2008). Crystal structure of the human laminin receptor precursor. *The Journal of Biological Chemistry*, 283(6): 3002–3005.

Jardim T. V., Reiger S., Abrahams-Gessel S., Crowther N. J., Wade A., Gómez-Olivé F. X., Salomom J., Tollman S., Gaziano T. A. (2017). Disparities in management of cardiovascular disease in rural South Africa: data from the HAALSI (Health and Aging in Africa: Longitudinal Studies of INDEPTH Communities) Study. Circulation. *Cardiovascular quality and outcomes*, 10(11): e004094.

Javadifar A., Rastgoo S., Banach M., Jamialahmadi T., Johnston T. P., Sahebkar A. (2021). Foam Cells as Therapeutic Targets in Atherosclerosis with a Focus on the Regulatory Roles of Non-Coding RNAs. *International Journal of Molecular Sciences*, 22(5): 2529.

Jokerst J. V., Lobovkina T., Zare R. N., Gambhir S. S. (2011). Nanoparticle PEGylation for imaging and therapy. *Nanomedicine (London, England)*, 6(4): 715–728.

Jovanovic K., Chetty C. J., Khumalo T., Da Costa Dias B., Ferreira E., Malindisa S. T., Caveney R., Letsolo B., Weiss S. F. T. (2015). Novel patented therapeutic approaches targeting the 37/67 kDa laminin receptor for treatment of cancer and Alzheimer's disease. *Expert Opinion on Therapeutic Patents*, 25(5): 567–582.

Keates A. K., Mocumbi A. O., Ntsekhe M., Sliwa K., Stewart S. (2017). Cardiovascular disease in Africa: epidemiological profile and challenges. *Nature Reviews Cardiology*, 14(5): 273–293.

Khan M. A., Hashim M. J., Baniyas M. Y., Al Suwaidi S. K., AlKatheeri R., Alblooshi F. M., Almatrooshi M. E., Alzaabi M. E. H., Al Darmaki R. S., Lootah S. N. A. (2020). Global epidemiology of ischemic heart disease: results from the global burden of disease study. Cureus, 12(7): e9349.

Khumalo T., Reusch U., Knackmuss S., Little M., Veale R. B., Weiss S. F. T. (2013). Adhesion and Invasion of Breast and Oesophageal Cancer Cells Are Impeded by Anti-LRP/LR-Specific Antibody IgG1-iS18. *PLoS ONE*, 8(6).

Kinoshita K., Kaneda Y., Sato M., Saeki Y., Wataya-Kaneda M., Hoffmann A., Kaneda Y. (1998). LBP-p40 Binds DNA Tightly through Associations with Histones H2A, H2B, and H4. *Biochemical and Biophysical Research Communications*, 253(2): 277–282.

Kosinski A.M., Brugnano J. L., Seal B. L., Knight F. C., Panitch A. (2012). Synthesis and characterization of a poly(lactic-co-glycolic acid) core + poly(N-isopropylacrylamide) shell nanoparticle system. *Biomatter*, 2(4): 195–201.

Kunji E. R. S., Harding M., Butler P. J. G., Akamine P. (2008). Determination of the molecular mass and dimensions of membrane proteins by size exclusion chromatography. *Methods*, 46(2): 62–72.

Kuno S., Srinoun K., Penglong T. (2020). The effects of Phorbol 12-myristate 13-acetate concentration on the expression of miR-155 and miR-125b and their macrophage function-related genes in the U937 cell line. *The Journal of Toxicological Sciences*, 45(12): 751–761.

Landowski T. H., Dratz E. A., Starkey J. R. (1995). Studies of the structure of the metastasis-associated 67 kDa laminin binding protein: fatty acid acylation and evidence supporting dimerization of the 32 kDa gene product to form the mature protein. *Biochemistry*, 34(35): 11276–11287.

Laxton R. C., Hu Y., Duchene J., Zhang F., Zhang Z., Leung K., Xiao Q., Scotland R. S., Hodgkinson C. P., Smith K., Willeit J., Lopez-Otin C., Simpson I. A. Kiechl S., Ahluwalia A., Xu Q., Ye S. (2009). A Role of Matrix Metalloproteinase-8 in Atherosclerosis. *Circulation Research*, 105(9): 921–929.

Leik C. E., Carson N. L., Hennan J. K., Basson M. D., Liu Q., Crandall D. L., Nambi P. (2007). GW3965, a synthetic liver X receptor (LXR) agonist, reduces angiotensin II-mediated pressor responses in Sprague–Dawley rats. *British Journal of Pharmacology*, 151(4): 450–456.

Li Y., Wang H., Fan Y., Shi H., Wang Q., Chen B., Khurwolah M., Long Q., Wang S., Wang Z., Wang L. (2017). Epigallocatechin-3-Gallate Inhibits Matrix Metalloproteinase-9 and Monocyte Chemotactic Protein-1 Expression Through the 67-κDa Laminin Receptor and the TLR4/MAPK/NF-κB Signalling Pathway in Lipopolysaccharide-Induced Macrophages. *Cellular Physiology and Biochemistry*, 43(3): 926–936.

Liu T., Zhang L., Joo D., Sun S. (2017). NF-κB signaling in inflammation. *Signal Transduction and Targeted Therapy*, 2: 17023.

Lü J., Wang X., Marin-Muller C., Wang H., Lin P. H., Yao Q., Chen C. (2009). Current advances in research and clinical applications of PLGA-based nanotechnology. *Expert review of molecular diagnostics*, 9(4): 325–341.

Mackman N. (2004). Role of Tissue Factor in Hemostasis, Thrombosis, and Vascular Development. *Arteriosclerosis, Thrombosis, and Vascular Biology*, 24(6): 1015–1022.

Markin A. M., Sobenin I. A., Grecchko A. V., Zhang D., Orekhov A. N. (2020). Cellular mechanisms of human atherogenesis: focus on chronification of inflammation and mitochondrial mutations. *Frontiers in Pharmacology*, 11. Accessed on: 4 May 2022. Available at: https://www.frontiersin.org/article/10.3389/fphar.2020.00642.

Martos-Rodríguez C. J., Albarran-Juarez J., Morales-Cano D., Caballero A., MacGrogan D., de la Pompa J. L., Carramolino L., Bentzon J. F. (2021). Fibrous Caps in Atherosclerosis Form by Notch-Dependent Mechanisms Common to Arterial Media Development. *Arteriosclerosis, Thrombosis, and Vascular Biology*, 41(9): e427–e439.

Mbazima V., Da Costa Dias B., Omar A., Jovanovic K., Weiss S. F. T. (2010). Interactions between PrP(c) and other ligands with the 37-kDa/67-kDa laminin receptor. *Frontiers in Bioscience (Landmark Edition)*, 15: 1150–1163.

McCall R. L., Sirianni R. W. (2013). PLGA nanoparticles formed by single- or double-emulsion with vitamin E-TPGS', *Journal of Visualized Experiments: JoVE* [Preprint], (82).

McCubbin W. D., Kay C. M. (1980). Acrylamide Fluorescence quenching studies on skeletal and cardiac troponins. *FEBS Letters*, 122(1): 72–76.

Mir M., Ahmed N., Rehman A. ur (2017). Recent applications of PLGA based nanostructures in drug delivery. *Colloids and Surfaces B: Biointerfaces*, 159: 217–231.

Möller M., Denicola A. (2002). Protein tryptophan accessibility studied by fluorescence quenching. *Biochemistry and Molecular Biology Education*, 30(3): 175–178.

Moodley K., Weiss S. F. T. (2013). Downregulation of the Non-Integrin Laminin Receptor Reduces Cellular Viability by Inducing Apoptosis in Lung and Cervical Cancer Cells. *PLoS ONE*, 8(3).

Moreno P. R., Purushothaman K., Sirol M., Levy A. P., Fuster V. (2006). Neovascularization in Human Atherosclerosis. *Circulation*, 113(18): 2245–2252.

Mühlmann M., Forsten E., Noack S., Buchs J. (2017). Optimizing recombinant protein expression via automated induction profiling in microtiter plates at different temperatures. *Microbial Cell Factories*, 16: 220.

Nagy L., Tontonoz P., Alvarez J. G. A., Chen H., Evans R. M. (1998). Oxidized LDL Regulates Macrophage Gene Expression through Ligand Activation of PPARγ. *Cell*, 93(2): 229–240.

Naidoo K., Malindisa S. T., Otgaar T. C., Bernert M., Da Costa Dias B., Ferreira E., Reusch U., Knackmuss S., Little M., Weiss S. F. T., Letsolo B. (2015). Knock-Down of the 37kDa/67kDa Laminin Receptor LRP/LR Impedes Telomerase Activity. *PLoS ONE*, 10(11).

Nascimento C.R. Rodrigues F., Gonzalez M., Rossa J. C. (2022). Comparison of monocytic cell lines U937 and THP-1 as macrophage models for in vitro studies. *Biochemistry and Biophysics Reports*, 32: 101383.

Neels J. G., Gollentz C., Chinetti G. (2023). Macrophage death in atherosclerosis: potential role in calcification. *Frontiers in Immunology*, 14: 1215612.

Nelson J., McFerran N. V., Pivato G., Chambers E., Doherty C., Steele D., Timson D. J. (2008). The 67 kDa laminin receptor: structure, function and role in disease. *Bioscience Reports*, 28(1): 33–48.

Omar A., Reusch U., Knackmuss S., Little M., Weiss S. F. T. (2012). Anti-LRP/LR-Specific Antibody IgG1-iS18 Significantly Reduces Adhesion and Invasion of Metastatic Lung, Cervix, Colon and Prostate Cancer Cells. *Journal of Molecular Biology*, 419(1): 102–109.

Orihuela C. J., Mahdavi J., Thornton J., Mann B., Wooldridge K. G., Abouseada N., Oldfield N. J., Self T., Ala'Aldeen D. A. A., Tuomanen E. I. (2009). Laminin receptor initiates bacterial contact with the blood brain barrier in experimental meningitis models. *The Journal of Clinical Investigation*, 119(6): 1638–1646.

Otgaar T. C., Ferreira E., Malindisa S., Bernert M., Letsolo B. T., Weiss S. F. T. (2017). 37 kDa LRP::FLAG enhances telomerase activity and reduces senescent markers in vitro. *Oncotarget*, 8(49): 86646–86656.

Pala R., Anju V. T., Dyavaiah M., Busi S., Nauli S. M. (2020). Nanoparticle-Mediated Drug Delivery for the Treatment of Cardiovascular Diseases. *International Journal of Nanomedicine*, 15: 3741–3769.

Palego L., Betti L., Rossi A., Giannaccini G. (2016). Tryptophan Biochemistry: Structural, Nutritional, Metabolic, and Medical Aspects in Humans. *Journal of Amino Acids*, 2016: 8952520.

Panegyres P. K., Armari E. (2013). Therapies for human prion diseases. *American Journal of Neurodegenerative Disease*, 2(3): 176–186.

Patil Y. B., Swaminathan S. K., Ma L., Panyam J. (2010). The use of nanoparticle-mediated targeted gene silencing and drug delivery to overcome tumor drug resistance. *Biomaterials*, 31(2): 358–365.

Pollard T. D. (2010). A Guide to Simple and Informative Binding Assays. Molecular Biology of the Cell, 21(23): 4061–4067.

Rao N. C., Barsky S. H., Terranova V. P., Liotta L. A. (1983). Isolation of a tumor cell laminin receptor. *Biochemical and Biophysical Research Communications*, 111(3): 804–808.

Ratkeviciute G., Cooper B. F., Knowles T. J. (2021). Methods for the solubilisation of membrane proteins: the micelle-aneous world of membrane protein solubilization. Biochemical Society Transactions, 49(4): 1763–1777.

Reinmuth-Selzle K., Tchipilov T., Backes A. T., Tscheuschner G., Tang K., Ziegler K., Lucas K., Pöschl U., Fröhlich-Nowoisky J., Weller M. G. (2022). Determination of the protein content of complex samples by aromatic amino acid analysis, liquid chromatography-UV absorbance, and colorimetry. *Analytical and Bioanalytical Chemistry*, 414(15): 4457–4470.

Ritchie H., Roser M. (2019). Causes of death. *Our World in Data* [Preprint]. Available at: https://ourworldindata.org/causes-of-death (Accessed: 23 May 2022).

Rowbury R. J. (2005). Intracellular and Extracellular Components as Bacterial Thermometers, and Early Warning against Thermal Stress. *Science Progress*, 88(2): 71–99.

Rubiyana Y., Santoso A., Batubara I. (2015). Comparison of Immobilized Metal Affinity Chromatography Ni-NTA and Co-TALON for the Purification of Recombinant Human Erythropoietin. Makara Journal of Science, 19(4).

Sahin A., Esendagli G., Yerlikaya F., Caban-Toktas S., Yoyen-Ermis D., Horzum U., Aktas Y., Khan M., Couvreur P., Capan Y. (2017). A small variation in average particle size of PLGA nanoparticles prepared by nanoprecipitation leads to considerable change in nanoparticles' characteristics and efficacy of intracellular delivery. *Artificial Cells, Nanomedicine, and Biotechnology*, 45(8): 1657–1664.

Sato M., Kinoshita K., Kaneda Y., Saeki Y., Iwamatsu A., Tanaka K., Kaneda Y. (1996). Analysis of Nuclear Localization of Laminin Binding Protein Precursor p40 (LBP/p40). *Biochemical and Biophysical Research Communications*, 229(3): 896–901.

Scheiman J., Jamieson K. V., Ziello J., Tseng J., Meruelo D. (2010). Extraribosomal functions associated with the C terminus of the 37/67 kDa laminin receptor are required for maintaining cell viability. *Cell Death & Disease*, 1(5): e42.

Schutte A. E. (2019). Urgency for South Africa to prioritize cardiovascular disease management. *The Lancet Global Health*, 7(2): e177–e178.

Seimon T., Tabas I. (2009). Mechanisms and consequences of macrophage apoptosis in atherosclerosis. *Journal of Lipid Research,* 50: S382–S387

Singh R. B., Mengi S. A., Xu Y.J., Arneja A. S., Dhalla N. S. (2002). Pathogenesis of atherosclerosis: A multifactorial process. Experimental & Clinical Cardiology, 7(1): 40–53.

Song M., Ryoo I., Choi H., Choi B., Kim S., Heo T., Lee J. Y., Park P., Kwak M. (2015). NRF2 Signaling Negatively Regulates Phorbol-12-Myristate-13-Acetate (PMA)-Induced Differentiation of Human Monocytic U937 Cells into Pro-Inflammatory Macrophages. *PLoS ONE*, 10(7): e0134235.

Sousa de Almeida M., Susnik E., Drasler, B., Taladriz-Blanco P., Petri-Fink A., Rothen-Rutishauser B. (2011). Understanding nanoparticle endocytosis to improve targeting strategies in nanomedicine. *Chemical Society Reviews*, 50(9): 5397–5434.

Shay J. W., Bacchetti S. (1997). A survey of telomerase activity in human cancer. *European Journal of Cancer*, 33(5): 787–791.

Singh R. B., Mengi S. A., Xu Y., Arneja A. S., Dhalla N. S. (2002). Pathogenesis of atherosclerosis: A multifactorial process. *Experimental & Clinical Cardiology*, 7(1): 40–53.

Steinl D. C., Kaufmann B. A. (2015). Ultrasound Imaging for Risk Assessment in Atherosclerosis. *International Journal of Molecular Sciences*, 16(5): 9749–9769.

Stressler T., Tanzer C., Ewert J., Claaßen W., Fischer L. (2017). Simple purification method for a recombinantly expressed native His-tag-free aminopeptidase A from Lactobacillus delbrueckii. *Protein Expression and Purification*, 131: 7–15.

Tabatabaei Mirakabad, F. S., Nejati-Koshki K., Akbarzadeh A., Yamchi M. R., Milani M., Zarghami N., Zeighamian V., Rahimzadeh A., Alimohammadi S., Hanifehpour Y., Joo S. W. (2014). PLGA-Based Nanoparticles as Cancer Drug Delivery Systems. Asian Pacific Journal of Cancer Prevention, 15(2): 517–53.

Terada H., Seki H., Yamamoto K., Kametani F. (1985). Quantitative determination by derivative spectrophotometry of Triton X-100 in solubilized preparations of membrane proteins. *Analytical Biochemistry*, 149(2): 501–506.

Varsano N., Beghi F., Elad N., Pereiro E., Dadosh T., Pinkas I., Perez-Berna A. J., Jin X., Kruth H. S., Leiserowitz L., Addadi L. (2018). Two polymorphic cholesterol monohydrate crystal structures form in macrophage culture models of atherosclerosis. *Proceedings of the National Academy of Sciences*, 115(30): 7662–7669.

Wang K. S., (1992). High-affinity laminin receptor is a receptor for Sindbis virus in mammalian cells. *Journal of Virology*, 66(8): 4992–5001.

Wang S., Petzold M., Cao J., Zhang Y., Wang W. (2015). Direct Medical Costs of Hospitalizations for Cardiovascular Diseases in Shanghai, China: Trends and Projections. *Medicine*, 94(20): e837.

Xiang Y., Zheng Y., Liu S., Liu G., Li Z., Dong W. (2021). Comparison of the sensitivity of Western blotting between PVDF and NC membranes. *Scientific Reports*, 11(1): 12022.

Yu X. H., Fu Y. C., Zhang D. W., Yin K., Tang C. K. (2013). Foam cells in atherosclerosis. *Clinica chimica acta; international journal of clinical chemistry*, 424: 245–252.

Yun J., Jin H., Lee Y., Choi E., Carp R. I., Jeong B., Kim Y. (2011). The first report of RPSA polymorphisms, also called 37/67 kDa LRP/LR gene, in sporadic Creutzfeldt-Jakob disease (CJD). *BMC Medical Genetics*, 12(1): 108.

Zhao W., Xiao Z., Zhao S. (2019). The Benefits and Risks of Statin Therapy in Ischemic Stroke: A Review of the Literature. *Neurology India*, 67(4): 983.

Zhao Y., Wang Y., Ran F., Cui Y., Liu C., Zhao Q., Gao Y., Wang D., Wang S. (2017). A comparison between sphere and rod nanoparticles regarding their in vivo biological behavior and pharmacokinetics. *Scientific Reports*, 7(1): 4131.

Zhu Y., Xian X., Wang Z., Bi Y., Chen Q., Han X., Tang D., Chen R. (2018). Research Progress on the Relationship between Atherosclerosis and Inflammation. *Biomolecules*, 8(3): 80.

9. Appendices

Appendix 1: Reagents and materials

i. Associate Chemical Enterprise (ACE), Southdale, RSA: methanol, acetic acid, NaOH.
ii. Merck Millipore, Massachusetts, USA: Tween 20; EDTA; Glycine; KCl; KH_2PO_4; NaCl; SDS; Tris-HCl, Na_2HPO_4, imidazole.
iii. Sigma-Aldrich, Missouri, USA: APS, acrylamide, TEMED, SDS, Triton-X 100; acrylamide, β-mercaptoethanol, bis-acrylamide, tryptone, agar, NaN_3.
iv. Thermo Fisher Scientific, Massachusetts, USA: yeast extract.
v. VWR Life Sciences, Pennsylvania, USA: ethanol.

Appendix 2: Calculations

i. Calculation of molecular weight

$$R_f = 5.25$$
$$\therefore x = 5.25$$

$$y = -0{,}1145x + 2{,}2752$$
$$y = \log(MW) = 1.674075$$
$$MW = \sim 47\ kDa$$

ii. Calculation of protein concentration

$$c = \frac{A_{280}}{\mathcal{E}.l}$$
$$= \frac{0.845}{67045\ x\ 1} x10^6$$
$$= 12.6\ uM$$

Appendix 3: Additional data

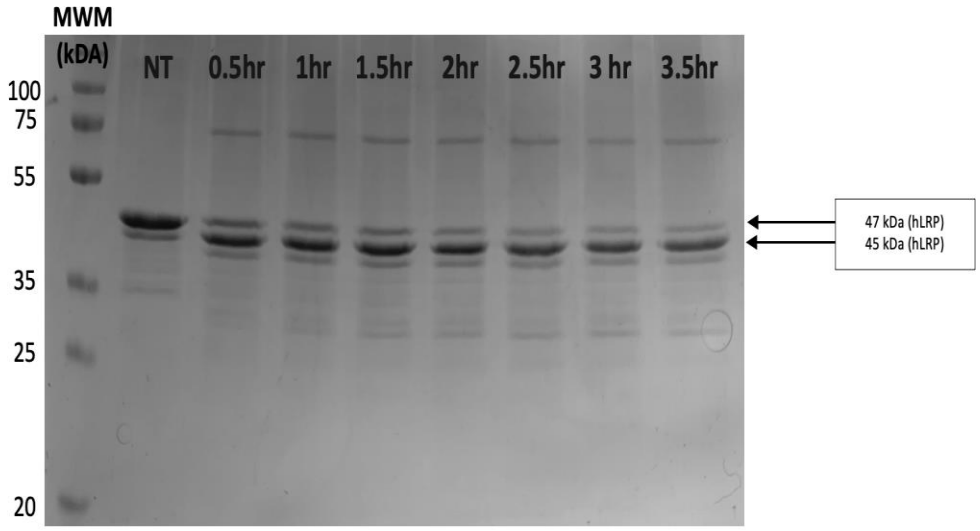

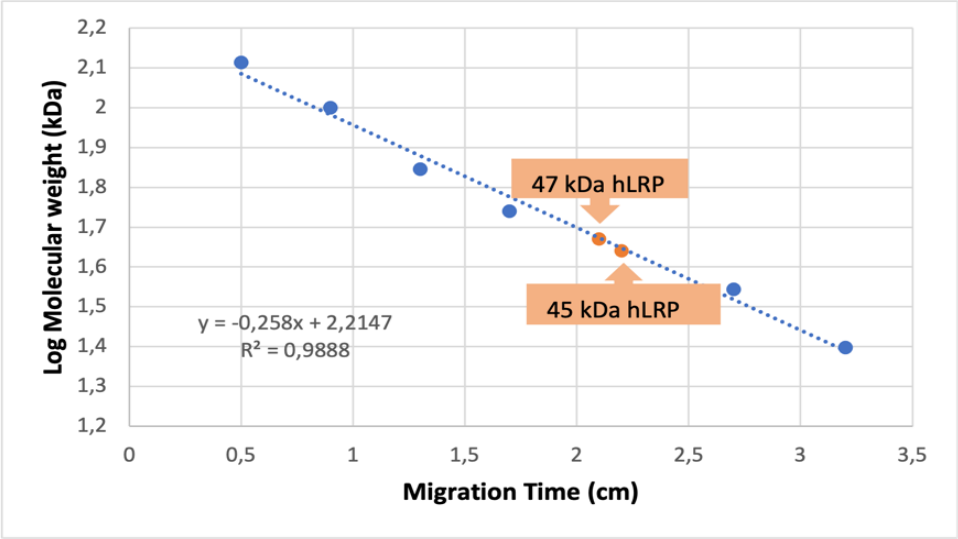

Figure E1: SDS-PAGE gel showing the time dependent thrombin cleavage trials for hLRP and Linear regression model constructed from the standards of known molecular weight. The no thrombin (NT) band illustrates LRP at time 0 hours with no thrombin. As time progresses, the 47 kDa band is cleaved and the intensity of the band is weakened. The band that has migrated down the gel increased in intensity suggesting that the His-tag was cleaved from the 47 kDa protein. The linear regression model was used to determine the size of the bands on the SDS-PAGE gels. The standard curve was constructed using standards of known molecular weight (BLUeye Prestained protein ladder (Merck, Germany)). The molecular weight of the bands of the target protein, based on their migration distance, correlates with 47 kDa and 45 kDa for LRP with the His-tag and without the His-tag, respectively.